

A discrete geometric view on shear-deformable shell models

Dissertation
zur Erlangung des mathematisch-naturwissenschaftlichen Doktorgrades
"Dr. rerum naturalium"
an der Georg-August-Universität Göttingen

vorgelegt von Clarisse Weischedel
aus Lomé / Togo

Göttingen 2012

D7

Referent: Prof. Dr. Max Wardetzky

Koreferent: Prof. Dr. Bernd Simeon

Tag der mündlichen Prüfung: 18.07.2012

Introduction

Les personnes habituées à raisonner au moyen des déplacements infiniment petits pourront, au premier abord, trouver cette méthode indirecte, peut-être même artificielle.

G. Koenigs, Sur l'enseignement de la cinématique,
1912

Thin-walled structures such as plates and shells are abundant in architecture and mechanical engineering, and efficient accurate simulations of these structures have a very long history of research. The most popular approach for this task has been and remains the classical finite element (FE) analysis. This technique, widely-used in the engineering community, gave rise to a large amount of different shell models, whose common focus is quantitative accuracy in the limit of refinement of the involved finite dimensional function spaces. The question underlying this thesis is quite different. Motivated by applications in virtual reality, it is the quest for a shell model that is *qualitatively* accurate already with relatively few degrees of freedom, and thereby suitable for real-time simulations involving large deformations. In other words, we were looking for a shell model that inherently mimics the physical behaviour of a shell, such that it is physically plausible already on coarse meshes.

So much for what we were aspiring at, but the apparent lack of such a model despite the heavy research background, and the various techniques that had been explicitly developed to handle the theoretical and numerical challenges of shell models gave a significant hint that this would not be a free lunch. In particular, it seemed very recommended to find an alternative angle to approach the problem, rather than to follow the strenuous path of finite element analysis. The vote went to discrete differential geometry (DDG). Developed rather recently in the vicinity of computer graphics, this language has appeared very pertinent to formulate models for fast, yet physically credible computations, *e.g.*, for rods and cables [JLLO09, BWR⁺08]. While a framework different from the classical shell analysis was amenable to provide new insights in the geometry of shells, it was still far from certain that it would actually lead us to a suitable or even better model than the existing ones. Thus, this thesis relates how far one can go in the construction of a purely geometric discrete shell model on triangle meshes, and what advantages

this approach provides compared to alternative frameworks.

Right at the beginning of this investigation, a major concern turned out to be the choice of a kinematic shell model suitable for the discrete geometric view. The most popular shell kinematics are the shear-rigid Kirchhoff or Koiter kinematics and the shear-deformable Reissner-Mindlin or Cosserat kinematics, and it appears that setting the priority on theoretical or on practical aspects seems to favour the one or the other of these two formulations. The first chapter is dedicated to discuss this issue. It eventually leads us to adopt a shear-deformable shell model viewed as a mixed penalty formulation of a shear-rigid kinematic model. This choice allows us to benefit from the lower regularity requirements of a mixed formulation while keeping the possibility to recover a Kirchhoff model.

The ease and unambiguity of a discrete formulation strongly depends on the particular smooth formulation one relies on. The vast majority of shell models in finite element methods is based on a coordinate formulation of the smooth kinematics, as this fits the coordinate-based view of FE discretisations and implementations. In the discrete geometric setting however, dealing with coordinates is awkward and defeats the purpose of the whole approach, whose inherent goal is to deal with the geometry itself, not with its representation. Exterior calculus has been found to be an appropriate terminology to this setting (see [DHLM05]), and in Chapter 2 we therefore use this mathematical framework to deduce a coordinate-free deformation energy for an inextensible one-director shell from the 3D elastic energy. While the resulting energy formulation is comparable to the existing index-prone expressions, we are not aware of a similarly concise formulation of this energy. In any case, it will ease the subsequent construction of the discrete geometric model considerably.

In the same chapter, we will present a second formulation of the energy in terms of a differential one-form that will be introduced as 'shear form', and which encodes virtually on its own all the information of the shell. Although we will not use this formulation for our discrete model, writing down the smooth Cosserat model in this unusual form, where shearing is the main ingredient, is of interest in itself.

A fundamental difficulty for discrete approximations of shear-deformable shells is the widely lamented shear locking. Chapter 3 intends to shed light on this phenomenon in the nonlinear setting, by using the clear understanding that has already been achieved for the linearised framework. The gained intuition is then used to motivate the distribution of degrees of freedom on a simplicial mesh, and in particular the positioning of discrete directors on edges. In the end, discrete shearing is defined as a projection of the directors to *rotating* discrete tangent planes on edges. Indeed, it turns out that prescribing discrete tangent planes only partially, in the direction containing the highest order information, practically allows to avoid shear locking without actually increasing the number of degrees of freedom.

Chapter 4 presents a very geometric and little-known piecewise constant dis-

cretisation of quadratic forms on simplicial meshes. This framework, that allows to define discrete quadratic forms by only prescribing their values along edges, is then used to construct discrete first and second fundamental forms. In particular, the resulting membrane and bending energies are proven to be consistent. The construction turns out to provide a geometric reformulation and justification of established piecewise constant approximations for membrane and bending strains from finite elements for shell.

Eventually, by combining the shearing, membrane and bending parts, we obtain the Discrete Cosserat Shell (DCS) model, which perfectly corresponds to the applications we had in mind. This model is described in Chapter 5. Transferred to the finite element framework, this model can be interpreted as a geometric version of the nonlinear shearable shell element TLLL briefly presented by Flores et al. [FOZ95]. However, its geometric deduction allows for a very different reinterpretation of the popular though disputed assumed strain approach used in the formulation of this element. The chapter ends on a selection of numerical benchmarks that validate the model.

The last chapter provides a critical discussion of the DCS model by confronting it with existing low-order shell and plate models, deduced by finite element methods as well as from other discretisation techniques. From there, we will briefly address two more general matters that came up during this work, one questioning the evaluation of shell models, the other discussing the limitations of low-order models for shell simulations.

While adopting a geometric viewpoint, we tried in the course of the construction of the presented discrete model to take into account as many insights and achievements from alternative discretisation methods as possible, in particular from the finite element analysis. The necessary translation task – from one vocabulary to the other and back – made it possible to gain various insights into the geometry behind shell FE by putting techniques such as the MITC formulation for Reissner-Mindlin plates, assumed strain approaches and rotation-free shell elements in a different perspective, and thereby highlight relations and underlying geometric concepts which remained unnoticed or unexplained.

Acknowledgements

I am very indebted to my advisers Max Wardetzky and Joachim Linn for giving me extremely helpful guidance through the labyrinth of shell analysis and shear locking. I also thank them for their patience and their steady encouragement. I would further like to thank Bernd Simeon for accepting to be the co-referee of this thesis on relatively short notice.

Thanks to Alessio Quaglino for jump-starting my C++-coding skills. I thank Keenan Crane for keeping up my motivation with his contagious enthusiasm, and for showing me that coding is a helpful tool rather than an unpleasant duty. I owe Henrik Schumacher for very valuable proof-reading and a care for precision that I doubt I will ever reach. Thanks to Lars, Urs, Uli, and other fellow Ph.D. students and colleagues in Göttingen and Kaiserslautern for asking uncomfortable questions, giving helpful answers, and for keeping me from taking things too seriously.

Most of all, I thank my parents for believing that I can achieve whatever I want.

The work presented in this thesis was funded by a Ph.D. scholarship granted by the Fraunhofer Gesellschaft.

Contents

Introduction	v
1 Choosing a kinematic model	1
1.1 Shear-rigid and shear-deformable shells	1
1.2 Theoretical concerns for shear-deformable shell models	4
1.3 Practical advantages	6
2 Smooth energy formulation	9
2.1 Deduction of a geometric energy formulation	9
2.2 Alternative formulation	16
2.3 Towards a discrete model	18
3 Shear locking and discrete tangent planes	21
3.1 Shear locking in the linear setting	21
3.2 Where to place directors?	30
3.3 Discrete edge normals	31
3.4 Discrete shearing	34
3.5 Consistency	35
4 Discrete fundamental forms	39
4.1 Discrete quadratic forms	39
4.2 Discrete fundamental forms	41
4.3 Consistency	43

4.4	Relation to existing constant strain models	52
5	DCS: A Discrete Cosserat Shell model	57
5.1	Discrete model	57
5.2	A geometric justification of assumed strains	59
5.3	Zero-energy configurations	60
5.4	Numerical validation	63
6	Discussion	69
6.1	Comparison to existing low-order shell models	69
6.2	Limitations	75
	Appendix	79
	List of notations	84
	Bibliography	94

Chapter 1

Choosing a kinematic model

There is no universally accepted basic two-dimensional model of plate stretching or bending.

Richard S. Falk [Fal08]

In this chapter, we motivate our choice of a Cosserat shell model as kinematic foundation for the discrete model. We first introduce the two most popular shell kinematics based on surface theory, namely the shear-rigid Kirchhoff-based model and the shear-deformable Cosserat model. Although the latter seems debatable when it comes to its deduction from 3D elasticity, its lower regularity requirements and its reliability in practice make it an attractive model for the discrete geometric setting. Thus, we compromise by building our discrete model on a Cosserat approach considered as a mixed penalty formulation of a Kirchhoff model, leaving the possibility to constrain it to a shear-rigid model if needed.

1.1 Shear-rigid and shear-deformable shells

The simplest way to describe the deformation of a thin plate or shell, as for example a metal sheet, is to ignore the small extension in a third dimension and reduce its behaviour *completely* to the behaviour of a two-dimensional manifold embedded in \mathbb{R}^3 . Undeformed and deformed configurations are then completely determined by the position of this surface – usually called *mid-surface* – in space. This is the view of the *Kirchhoff*, *Kirchhoff-Love* or *Koiter model* which is based on the *Kirchhoff assumption*:

"normals to the undeformed middle surface move to normals of the deformed middle surface without any change in length" [Koi71].

For moderately thicker structures, as for example a thin rubber plate, this description seems overly simple, as 'something' is likely to happen through the thickness. The *Cosserat*, *Naghdi* or *Reissner-Mindlin* approach softens the Kirchhoff assumption in this respect by introducing additional degrees of freedom. These so called *inextensible directors* can be seen as *generalized* surface normals, which are allowed to deviate from the *true* surface normals of the mid-surface during the deformation, thereby accounting for a transversal shearing of the shell across the thickness (Fig. 1.1).

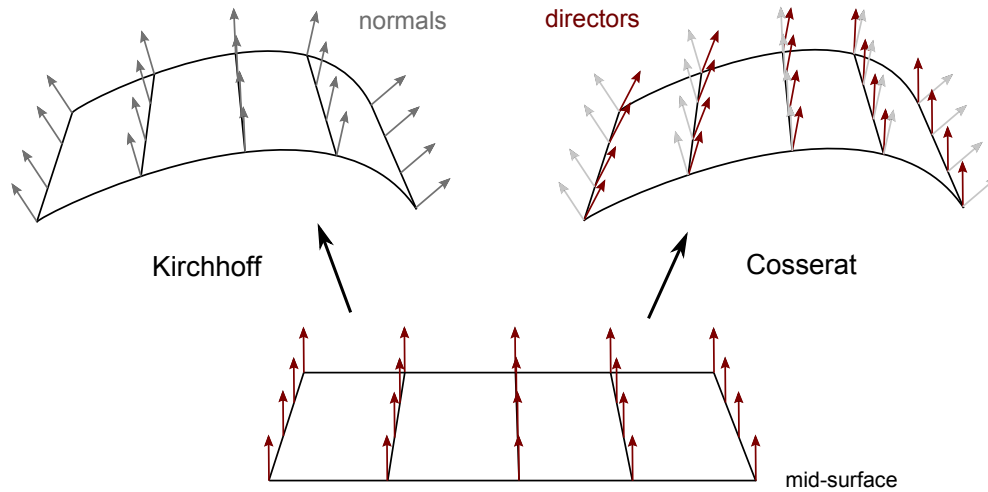


Fig. 1.1 Whereas Kirchhoff-based models describe the shell by the mid-surface and surface normals only, the Cosserat model introduces an additional free director field as a substitute for the normal field

For the construction of the discrete model, we will rely on the tools of *discrete differential geometry*. The underlying concept of this approach is that physical properties are mostly encoded by geometric properties, and that hence it is crucial for the discrete model to mimic the smooth geometry. This essential relation is also well-known in the finite element (FE) community, and was particularly underlined by the landmark work of Arnold, Falk and Winther [AFW09]. Working directly on the discrete geometry, as done in the DDG framework, is a very natural way to be liable to respect this principle.

In practice, this means that the model will be expressed in terms of degrees of freedom directly attached to the combinatorial entities of the simplicial mesh, *i.e.*, to vertices, edges or faces, without explicitly recurring to specific interpolation schemes as is customary in FE. While this method is very efficient for building discrete models that preserve the fundamental properties of its physical prototype, it restricts us to low-order approximations, which are known to be very tenuous, especially for shell modelling. Building the model on shell kinematics that require as little regularity as possible is therefore a first important step to

avoid theoretical and numerical difficulties of the prospective discrete model.

When transitioning to the discrete setting, the kinematic formulation underlying Kirchhoff models is commonly known to bring on the difficulty of having to ensure global C^1 -continuity of the approximating discrete surface in order to avoid what Zienkiewicz [ZT00] calls *kinks*, *i.e.*, the emergence of infinite bending energies. Indeed, in Kirchhoff models, bending strains are encoded by the curvature of the mid-surface, and it is an ubiquitous obstacle in the definition of discrete local curvatures on simplicial meshes that smooth curvatures are given by second order derivatives of the embedding. Accordingly, for piecewise linear approximations of the embedding, second derivatives –if not subject to additional procedures– lead to distributional quantities which cannot be used directly as a meaningful pointwise measure of smooth curvatures.

In order to overcome this problem, it is common practice to treat surface normals as extra degrees of freedom. A mixed penalty formulation of Kirchhoff shells, such as provided by the Cosserat approach, is one variation of this theme: By introducing a free director field as a substitute for the normal field, one obtains curvatures as *first* derivatives of these directors and can thereby work with piecewise linear approximations without imploring regularity issues directly from the start. Although these shear-deformable shell and plate models commonly face the problem of so-called shear locking, the Cosserat model therefore seems to be a more appropriate formulation for a low-order geometric discretisation.

However, in opposition to Kirchhoff models, Cosserat models seem more controversial in view of their theoretical foundation.

Remark. As we want to describe the shell from a differential geometric point of view, we will focus on kinematic formulations essentially based on the differential description of an *embedded two-dimensional manifold*. Various popular shell formulations are in contrast built on the full 3D model. We will not consider such kinematics and refer to [YSMK00] for an overview of different popular frameworks for shell modelling. Notice that one of these formulations also goes under the name of 'Cosserat model', or 'micropolar model'. It is based on a 3D description that associates an $SO(3)$ -frame with each particle of the considered solid to encode strains and stresses (*e.g.*, [NJ09]). Although both approaches are founded on the work of the brothers Eugène and François Cosserat from 1896 [CC96], they need to be carefully distinguished. In this thesis, the Cosserat model will always designate a *shear-deformable geometrically nonlinear shell model*.

For a comprehensive discussion of the history, the achievements and the challenges in shell modelling we refer to the very informative introduction of Bischoff *et al.* in [BBWR04].

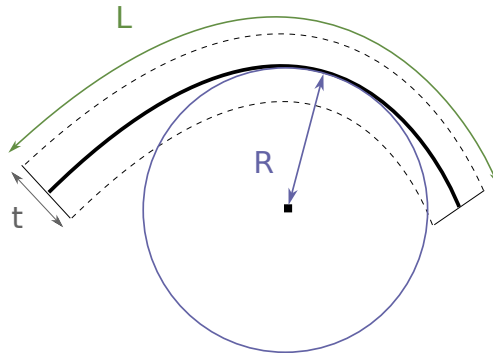
1.2 Theoretical concerns for shear-deformable shell models

There are mainly two approaches to justify the deduction of 2D shell models from 3D elasticity. On the one hand, one can use an asymptotic expansion of the 3D equations and neglect terms that are small by the a priori assumptions. This goes under the name of *asymptotic analysis* and is the subject of a large literature, mostly on the engineering side [Ber09, CL96, GKN93]. On the other hand, there is a more rigorous mathematical view that looks at the Γ -convergence of the minimizers of the elastic energy when t tends to 0 by different rates and under different boundary conditions.

Both of these points of view suggest that the Cosserat model with its inextensible directors is built on an artificial distinction of entities entering with the same order of magnitude in the 3D kinematics. Its justification with respect to the 3D model appears to rely on very particular assumptions on the considered geometry and boundary conditions.

1.2.1 Asymptotic analysis

The classical way of deducing shell models is to expand the 3D elastic energy into a Taylor series in terms of relative thickness t/L and curvature radii t/R , where t is the thickness of the shell, L the diameter of the surface and R its smallest curvature radius. From this, by relying on model assumptions involving the geometry and the considered deformation of the shell, terms that are 'small' are neglected, leading to different shell kinematics.



In this setting, Kirchhoff models can be seen as an approximation of the 3D model of order $\mathcal{O}(t/L, t/R)$, and the Cosserat model as a higher order approximation of $\mathcal{O}((t/L)^3, (t/R)^2)$ [Ber09]. Notice however that the latter relies on the assumption on the geometry of the shell that

$$L \ll R,$$

i.e., that the length of the geometry is much smaller than the curvature radius. Already if $L \sim R$ or even slightly larger (which happens even for moderate curvatures), the shearable model becomes incoherent, as it drops the terms $(t/R)^3$ but keeps the terms $(t/L)^3$ which are of the same order.

Moreover, although this straightforward asymptotic deduction is –as Berdichevsky states– "methodologically convenient", it is not suitable to rigorously describe the limit behaviour of the 3D elastic energy when the thickness t tends to zero, as it cannot capture the correlation between quantities that enter at different orders of t .

1.2.2 Γ -convergence

Properly defining Γ -convergence is out of the scope of this thesis. For our purposes, it is sufficient to understand that, in contrast to classical asymptotic analysis, it provides a notion of convergence that allows to examine asymptotic behaviours when a problem involves quantities vanishing at different rates. Such a tool is necessary for the analysis of the asymptotic behaviour of minimizers of the 3D shell energy for $t \rightarrow 0$. Indeed, depending on the boundary conditions, parts of this energy scale like t or t^3 , whereas the volume of the shell always scales like t (see, *e.g.*, [LR96]).

For *plates*, it was thereby shown that *asymptotically* there are only two possible behaviours. In one case, the plate turns into an elastic membrane, where all deformations are responded by a metric distortion (stretching). In the other case, the plate basically behaves like a thin metallic sheet, that can only be bent but not stretched, and the energy corresponds to the original Kirchhoff model (in particular with respect to the material parameters) [FJM02]. Hence, at least for plates, *no other asymptotic regime is possible*, such that the assumption of a shear-deformable shell has no right of being in this setting. The same is however true for plates that can both stretch *and* bend, which underlines that these results are to be understood as asymptotic behaviours and cannot solve the question of which physical models are practically sound or not.

However, it seems that at least the assumption of the director to be *inextensible* is delicate to justify rigorously. Friesecke et al. [FJM02] show that the order by which the directors can be distorted from the normals, which is accounted for in the Cosserat model, is of the same order as the stretching along these directors, which is explicitly *not* accounted for by the assumed inextensibility.

This result is supported by the asymptotic analysis carried out by LeDret and Raoult in [LR00] where they compare the asymptotic limit model of the 3D nonlinear shell energy and the Cosserat energy for different assumptions. They show that the limit energies only coincide when the director field is left completely unconstrained.

Paroni, Podio-Guidugli and Tomassetti describe in [PPGT06] how to obtain

the Reissner-Mindlin plate model, which is the linearised pendant of the Cosserat model (see Chapter 3), as the Γ -limit of certain 3D energy functionals under specifically chosen assumptions. It particularly relies on the fact that the 3D energy features *certain* second-order terms, which fits to the already conveyed picture that a shear-flexible model which does not allow for through-the-thickness stretching lies in an intermediate approximation regime.

1.3 Practical advantages

While from a purely theoretical point of view the Cosserat model seems debatable, it has very strong practical advantages that makes it attractive for actual computations.

On the one hand, the wide use of this model in engineering practice face that it actually *does* give a better approximation for moderately thick plates compared to the shear-rigid Kirchhoff shell models.

In the linear setting, this can be rigorously verified. For a square plate under small uniform load, there are analytic solutions available for 3D kinematics, the Kirchhoff model and for the Reissner-Mindlin model [SRR69]. It is thereby possible to evaluate the error coming from the model assumptions exclusively, disregarding any further discretization errors. Figure 1.2 shows the relative error of the Kirchhoff solution and the Reissner-Mindlin solution with respect to the analytic 3D solution for different thickness values t . It clearly shows that for moderately large t , the error of the Kirchhoff model is relatively large, whereas the Reissner-Mindlin model stays surprisingly accurate.

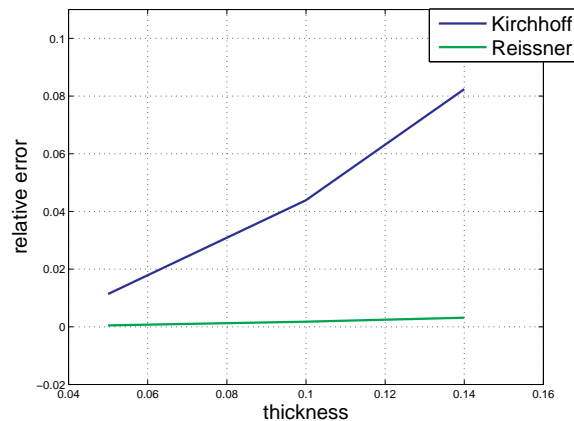


Fig. 1.2 Error of the analytic Kirchhoff solution and the analytic Reissner-Mindlin solution with respect to the analytic 3D solution, for a clamped square plate of edge length 1 for increasing thickness t .

On the other hand, as already mentioned in Section 1.1, by measuring bending

by the change of directors instead of the change of normals, the shear-deformable Cosserat model involves only first order derivatives of its variables and makes it thereby possible to approximate these variables with piecewise linear functions without further ado.

Eventually, we decided that the practical accuracy and the computational advantages of the Cosserat shell outweigh the theoretical concerns that we will however keep in mind. In particular, we will interpret the Cosserat model as a mixed formulation of the Kirchhoff model by treating the additional shearing term as either a penalty term (Cosserat) or a constraint (Kirchhoff), and thereby keep the option to restrict the model to a shear-rigid model.

Remark. Another compromise between the convenience of the low regularity and the indications of the theoretical results would be to use a model based on *extensible* directors. However, this approach excludes the use of a plane strain assumption and therefore requires a more involved constitutive model.

Chapter 2

Smooth energy formulation

Interestingly, notions that pertain to differential geometry per se [...] appear most naturally in the derivation [...] of three-dimensional elasticity and shell theory.

Philippe G. Ciarlet [Cia05]

A crucial step in the construction of a discrete geometric model is to formulate the adopted smooth kinematic model in terms of differential geometric entities. In this objective, this chapter provides an asymptotic deduction of such an expression for the Cosserat shell energy. The proposed formulation only involves coordinate-free differential quantities of the undeformed and deformed mid-surfaces, namely the respective first fundamental forms, \bar{I} and I , *generalized* second fundamental forms, \bar{II} and II_n , and a differential one-form σ_n encoding shearing, that we call the *shear form*. Eventually, we obtain the very concise formula

$$\mathcal{W} = \frac{1}{2} \int_{\bar{\mathcal{S}}} \left(\frac{t}{4} \|I - \bar{I}\|_M^2 + \frac{t^3}{12} \|II_n - \bar{II}\|_M^2 + t\kappa G |\sigma_n|^2 \right) d\bar{A}$$

that will be described in detail below.

Additionally, in Section 3, we present an alternative formulation of the deformation energy that reduces the model to variations of the shear form σ_n .

2.1 Deduction of a geometric energy formulation

In this section, we start from a kinematic description of an elastic deformation of an inextensible one-director shell in 3D, and deduce its energy in terms of fundamental forms of the mid-surface. As already suggested by the last chapter, the proper rigorous deduction of a 2D shell model from a 3D shell description keeps being an arduous topic of research [Mar08, FJM06].

We do not aim to contribute to this question. Instead, we will follow the deduction of the *inextensible one-director* model as formulated by Simo and Fox [SF89]. In particular, we adopt their smallness assumptions and constitutive relations. Several different kinematic formulations for shearable shells are available, and we chose to follow this particular one for its geometric taste and its popularity in the engineering community. In contrast to the original work however, we will use a very different vocabulary by relying on the framework of exterior calculus. While this approach is rather unusual for shell models, it allows us to deduce very naturally a coordinate-free energy formulation.

For further more classical deductions of the Cosserat shell energy from 3D elasticity by asymptotic analysis, we refer to [Ber09, Mar08].

2.1.1 3D kinematics

Definition 2.1. A *configuration of a shell* or simply a *shell* $\mathcal{S} = (\mathcal{S}, n, t)$ is a triple composed of an *embedded* two-dimensional differentiable manifold \mathcal{S} (the mid-surface), a differentiable *unit* vector field $n : \mathcal{S} \rightarrow \mathbb{S}^2$ (the inextensible director field) mapping to the unit sphere \mathbb{S}^2 , and a constant thickness $t \in \mathbb{R}$.

Let $\bar{\mathcal{S}} = (\bar{\mathcal{S}}, \bar{n}, t)$ be the undeformed configuration of a shell. We will assume that the undeformed reference configuration is always unsheared, *i.e.*, directors and normals of the undeformed mid-surface $\bar{\mathcal{S}}$ coincide. Throughout, barred quantities will refer to the undeformed configuration.

Definition 2.2. A *deformation of a configuration of a shell* is a map

$$\begin{aligned} \Phi = (\phi, \underline{n}) : \bar{\mathcal{S}} \times \left[-\frac{t}{2}, \frac{t}{2}\right] &\rightarrow \mathbb{R}^3 \\ (x, \xi) &\mapsto \phi(x) + \xi \underline{n}(x) , \end{aligned}$$

such that ϕ is a diffeomorphism onto its image and $\underline{n} : \bar{\mathcal{S}} \rightarrow \mathbb{S}^2$ is a differentiable unit vector field. The resulting *deformed configuration* is then given by

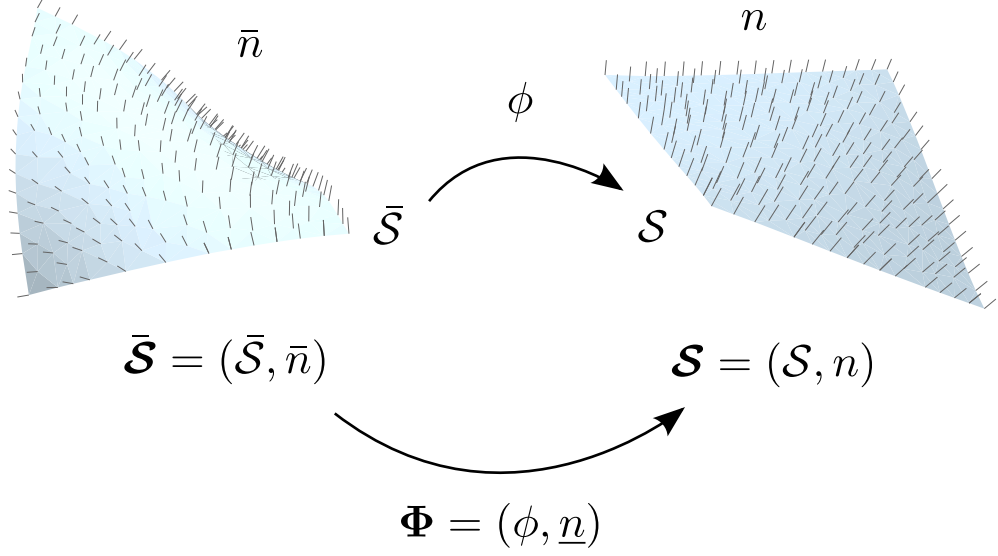
$$\mathcal{S} = (\mathcal{S} := \phi(\bar{\mathcal{S}}), n := \underline{n} \circ \phi^{-1}, t) .$$

Thus \underline{n} is the *pullback* of the deformed director field n to the undeformed mid-surface.

Next, we introduce the fundamental differential entities that will appear in the elastic energy.

Definition 2.3. Let $v, w \in T\mathcal{S}$ be tangent vector fields on a shell's mid-surface \mathcal{S} . The first fundamental form I of \mathcal{S} is given by

$$I(v, w) = \langle v, w \rangle ,$$



where $\langle \cdot, \cdot \rangle$ stands for the euclidean metric in \mathbb{R}^3 that is inherited by \mathcal{S} as a submanifold. We call *generalized second* and *generalized third fundamental forms with respect to a director field n* on \mathcal{S} the symmetric quadratic forms given by:

$$\begin{aligned}
 II_n(v, w) &= \frac{1}{2} (\langle dn(v), w \rangle + \langle v, dn(w) \rangle) \\
 III_n(v, w) &= \langle dn(v), dn(w) \rangle,
 \end{aligned}$$

where d denotes the (metric-free) Cartan outer derivative [Spi98].

We use a subscript n to distinguish these generalized second and third fundamental forms from their classical counterparts of surface theory with whom they coincide when the director field n is equal to the unit surface normal.

Definition 2.4. We call the *shear form* of a shell the one-form σ_n associated with the projection of the director n to the tangent space of the mid-surface through

$$\begin{aligned}
 (\sigma_n)_p &: T_p \mathcal{S} \rightarrow \mathbb{R} \\
 v &\mapsto \langle n(p), v \rangle
 \end{aligned}$$

for all $p \in \mathcal{S}$.

When n corresponds to the surface normal, the shear form σ_n clearly vanishes.

These geometric entities are defined for any configuration of a shell, regardless of a specific deformation. In order to derive a deformation energy, it is convenient to consider them on a fixed reference surface, which we choose to be the mid-surface of the undeformed configuration. Specifically, for a deformed shell

(\mathcal{S}, n, t) , obtained by a deformation (ϕ, \underline{n}) , such that $\mathcal{S} = \phi(\bar{\mathcal{S}})$ and $n = \underline{n} \circ \phi^{-1}$, we consider the pullbacks:

$$\begin{aligned}\phi^* I(\bar{v}, \bar{w}) &= \langle d\phi(\bar{v}), d\phi(\bar{w}) \rangle \\ \phi^* II_n(\bar{v}, \bar{w}) &= \frac{1}{2} (\langle dn(d\phi(\bar{v})), d\phi(\bar{w}) \rangle + \langle d\phi(\bar{v}), dn(d\phi(\bar{w})) \rangle) \\ \phi^* III_n(v, w) &= \langle dn(d\phi(\bar{v})), dn(d\phi(\bar{w})) \rangle \\ \phi^* \sigma_n &= \sigma_n \circ d\phi ,\end{aligned}$$

with $\bar{v}, \bar{w} \in T\bar{\mathcal{S}}$. In the following, we will mostly be working on the undeformed shell and consider these pullbacks, such that, if not stated otherwise, we will abuse notation and omit the pullback operator ϕ^* .

Let (\mathcal{S}, n, t) be a deformed shell. For simplicity, let assume there exists a smooth embedding $x : \mathbb{R}^2 \rightarrow \mathbb{R}^3$ of \mathcal{S} (the arguments can easily be extended to the general case, when \mathcal{S} is described by a differentiable atlas). Every point X of the three-dimensional structure $\Phi(\bar{\mathcal{S}} \times [-t/2, t/2]) \subset \mathbb{R}^3$ occupied by the shell in space can be represented by

$$X := x + \xi n ,$$

with $\xi \in [-t/2, t/2]$. The metric tensor of Ω writes

$$\begin{aligned}\mathbf{C}_{(x,\xi)} &:= dX^\top dX \\ &= (dx + \xi dn + d\xi n)^\top (dx + \xi dn + d\xi n) \\ &= dx^\top dx + \xi(dx^\top dn + dn^\top dx) + \xi^2 dn^\top dn \\ &\quad + d\xi(dx^\top n) + (n^\top dx)d\xi + d\xi^2 n^\top n .\end{aligned}$$

As we assume the director n to have unit length, the last term simplifies to $d\xi^2$. In the other terms we easily recognize the generalized fundamental forms of the mid-surface as well as the shear form, leading to

$$\mathbf{C}_{(x,\xi)} = I + 2\xi II_n + \xi^2 III_n + (d\xi \sigma_n + \sigma_n d\xi) + d\xi^2 .$$

As signalized before, we consider the pullbacks of the deformed fundamental forms, hence all the operators involved in this expression are defined on the undeformed shell.

In the same vain, on the unsheared ($\sigma_n = 0$) undeformed configuration $(\bar{\mathcal{S}}, \bar{n}, t)$, the undeformed metric $\bar{\mathbf{C}}$ writes

$$\bar{\mathbf{C}} = \bar{I} + 2\xi \bar{II} + \xi^2 \bar{III} + d\xi^2 .$$

Notice that we consider the fundamental forms, which are quadratic forms on the two-dimensional tangent space $T\bar{\mathcal{S}}$, as semi-definite quadratic forms on $T_{s,\zeta}(\bar{\mathcal{S}} \times [-t/2, t/2]) \cong T_s \bar{\mathcal{S}} \times \mathbb{R}$ by extending them constantly on $[-t/2, t/2]$. We similarly extend the differential one-forms σ_n and $d\xi$ through

$$\begin{aligned}\sigma_n(v, \tau) &:= \sigma_n(v) \\ d\xi(v, \tau) &:= d\xi(\tau)\end{aligned}$$

for all $(v, \tau) \in T_s \bar{\mathcal{S}} \times \mathbb{R}$.

2.1.2 Elastic energy

The elastic energy of the deformation Φ is determined by the change of metrics:

$$\mathbf{E} := \frac{1}{2}(\mathbf{C} - \bar{\mathbf{C}}) .$$

Focussing on deformations with large rotations but small strains, we will assume a Saint-Venant-Kirchhoff material and use a linear material law. We denote by $\|\cdot\|_{\mathbf{M}}$ the material norm corresponding to the chosen linear material law, hence for a symmetric tensor \mathbf{A} defined on the undeformed shell, we set

$$\|\mathbf{A}\|_{\mathbf{M}}^2 := \text{tr}(\mathbf{A}^\top \mathbf{M} \mathbf{A}) ,$$

where \mathbf{M} is some appropriate material tensor. We extend this norm canonically to a metric $\langle \cdot, \cdot \rangle_{\mathbf{M}}$ by setting

$$\langle \mathbf{A}, \mathbf{B} \rangle_{\mathbf{M}} := \text{tr}(\mathbf{A}^\top \mathbf{M} \mathbf{B})$$

for symmetric tensors \mathbf{A}, \mathbf{B} .

Applied to the elastic strain tensor \mathbf{E} , this norm encodes the density of the potential elastic energy of the deformation. The resulting deformation energy \mathcal{W} of the shell is then given by the integral of $\|\mathbf{E}\|_{\mathbf{M}}^2$ over the undeformed configuration $\bar{\mathcal{S}} \times [-t/2, t/2]$:

$$\mathcal{W} := \frac{1}{2} \int_{-t/2}^{t/2} \int_{\bar{\mathcal{S}}} \|\mathbf{E}\|_{\mathbf{M}}^2 d\bar{A}_\xi d\xi .$$

For offset surfaces of $\bar{\mathcal{S}}$ at a distance ξ , Steiner's formula [Ste81] provides the expression of the area element as

$$d\bar{A}_\xi = (1 - 2\xi\bar{H} + \xi^2\bar{K})d\bar{A} ,$$

where \bar{H} and \bar{K} are the mean and Gauss curvature of the undeformed mid-surface $\bar{\mathcal{S}}$. Hence the energy splits into

$$\mathcal{W} = \frac{1}{2} \int_{\bar{\mathcal{S}}} \left(\underbrace{\int_{-t/2}^{t/2} \|\mathbf{E}\|_{\mathbf{M}}^2 d\xi}_{E_1} - 2\bar{H} \underbrace{\int_{-t/2}^{t/2} \|\mathbf{E}\|_{\mathbf{M}}^2 \xi d\xi}_{E_2} + \bar{K} \underbrace{\int_{-t/2}^{t/2} \|\mathbf{E}\|_{\mathbf{M}}^2 \xi^2 d\xi}_{E_3} \right) d\bar{A} . \quad (2.1)$$

Developing 2.1 in powers of ξ yields a messy expression with terms up to order 7. To simplify this expression, we use that the one-form $d\xi$ is constant and equal to 1, that scalar products of $d\xi\sigma_n$ and fundamental forms vanish, and that odd powers of ξ cancel when integrated over the *symmetric* thickness $[-t/2, t/2]$.

Remark. For the last simplification we need to use that the considered mid-surface of the shell actually lies centred in between the top and bottom surfaces of the shell, otherwise several more terms have to be carried along.

Especially the shearing term of the metric tensor \mathbf{E} which, for $(v, \tau), (w, \rho) \in T\mathcal{S} \times \mathbb{R}$, writes

$$d\xi(v, \tau)\sigma_n(w, \rho) + \sigma_n(v, \tau)d\xi(w, \rho) = d\xi(\tau)\sigma_n(w) + \sigma_n(v)d\xi(\rho)$$

reduces to

$$\sigma_n(w) + \sigma_n(v) ,$$

and for simplicity we will denote its norm by $\|2\sigma_n\|_{\mathbf{M}}$.

Eventually, for E_1 we get

$$E_1 = \frac{1}{4} \left(t(\|I - \bar{I}\|_{\mathbf{M}}^2 + \|2\sigma_n\|_{\mathbf{M}}^2) + \frac{t^3}{3} \|II_n - \bar{II}\|_{\mathbf{M}}^2 + \frac{t^3}{6} \langle I - \bar{I}, III_n - \bar{III} \rangle_{\mathbf{M}} + \frac{t^5}{80} \|III_n - \bar{III}\|_{\mathbf{M}}^2 \right) .$$

Developing E_2 yields

$$E_2 = \frac{1}{4} \left(\frac{t^3}{3} \langle I - \bar{I}, II_n - \bar{II} \rangle_{\mathbf{M}} + \frac{t^5}{20} \langle II_n - \bar{II}, III_n - \bar{III} \rangle_{\mathbf{M}} \right) .$$

For E_3 , we obtain

$$E_3 = \frac{1}{4} \left(\frac{t^3}{12} \left(\|I - \bar{I}\|_{\mathbf{M}}^2 + \|2\sigma_n\|_{\mathbf{M}}^2 \right) + \frac{t^5}{80} \left(4 \|II_n - \bar{II}\|_{\mathbf{M}}^2 + 2 \langle I - \bar{I}, III_n - \bar{III} \rangle_{\mathbf{M}} \right) + \frac{t^7}{518} \|III_n - \bar{III}\|_{\mathbf{M}}^2 \right) .$$

2.1.3 Parametrization-free Cosserat energy

The reduction from the 3D elastic energy to a simpler 2D shell energy by asymptotic analysis relies on smallness assumptions that tend to make several terms of the 3D energy neglectable. The main assumption is inherent to shell models per se, namely that the ratio thickness/length τ is small

$$(\text{A}_{\text{thick}}) \quad \tau := \frac{t}{L} \ll 1 .$$

As mentioned in the previous paragraph, in order to justify the use of a linear material law, we also need to assume that the deformation only involves small membrane strains, and more specifically *small* with respect to the thickness ratio τ . This corresponds to

$$(\text{A}_{\text{mem}}) \quad \varepsilon_m := \|I - \bar{I}\|_{\mathbf{M}} \ll \tau .$$

To simplify notations, we will assume that the problem is scaled such that the thickness t is equal to the ratio thickness/length, thus $t := \tau$. If we use (A_{thick}) and only retain terms of order lower than $\mathcal{O}(t^4)$, the terms in the energy (2.1) become

$$\begin{aligned} E_1' &:= \frac{1}{4} \left(t(\|I - \bar{I}\|_{\mathbf{M}}^2 + \|2\sigma_n\|_{\mathbf{M}}^2) + \frac{t^3}{3} \|II_n - \bar{I}\bar{I}\|_{\mathbf{M}}^2 \right. \\ &\quad \left. + \frac{t^3}{6} \langle I - \bar{I}, III_n - \bar{I}\bar{I}\rangle_{\mathbf{M}} \right) \\ E_2' &:= \frac{1}{4} \left(\frac{t^3}{3} \langle I - \bar{I}, II_n - \bar{I}\bar{I}\rangle_{\mathbf{M}} \right) \\ E_3' &:= \frac{1}{4} \left(\frac{t^3}{12} (\|I - \bar{I}\|_{\mathbf{M}}^2 + \|2\sigma_n\|_{\mathbf{M}}^2) \right). \end{aligned}$$

If we further assume (A_{mem}) and neglect terms of order $\mathcal{O}(t^3\varepsilon_m) \leq \mathcal{O}(t^4)$, we can drop E_2' and what remains of E_1' and E_3' is:

$$\begin{aligned} E_1'' &:= \frac{1}{4} \left(t(\|I - \bar{I}\|_{\mathbf{M}}^2 + \|2\sigma_n\|_{\mathbf{M}}^2) + \frac{t^3}{3} \|II_n - \bar{I}\bar{I}\|_{\mathbf{M}}^2 \right) \\ E_3'' &:= \frac{1}{4} \left(\frac{t^3}{12} \|2\sigma_n\|_{\mathbf{M}}^2 \right). \end{aligned}$$

For the whole energy, this leads to:

$$\mathcal{W} = \frac{1}{2} \int_{\bar{\mathcal{S}}} \left(\frac{t}{4} \|I - \bar{I}\|_{\mathbf{M}}^2 + \frac{t^3}{12} \|II_n - \bar{I}\bar{I}\|_{\mathbf{M}}^2 + \frac{1}{4} (t + \bar{K} \frac{t^3}{12}) \|2\sigma_n\|_{\mathbf{M}}^2 \right) d\bar{A}.$$

Interestingly, we observe that the shearing stiffness seems to depend on the Gauss curvature \bar{K} of the undeformed configuration. In particular, for developable surfaces, the term $\bar{K} \frac{t^3}{12} \|2\sigma_n\|_{\mathbf{M}}^2$ vanishes. To drop this term in the general case and actually recover an expression similar to the one in [SF89], we will further have to assume that this Gauss curvature is smaller than the thickness t , as then we can again argue that $\bar{K}t^3$ is of order $\mathcal{O}(t^4)$ and can be neglected. Hence we add the assumption

$$(A_{\text{gauss}}) \quad \bar{K} \leq \tau = t.$$

Cosserat energy By adapting the 3D material norm to a plane strain assumption, we finally obtain the deformation energy of a homogeneous, isotropic, inextensible one-director shell, comparable to the energy proposed in [SF89]:

$$\mathcal{W} = \frac{1}{2} \int_{\bar{\mathcal{S}}} \left(\frac{t}{4} \|I - \bar{I}\|_{\mathbf{M}}^2 + \frac{t^3}{12} \|II_n - \bar{I}\bar{I}\|_{\mathbf{M}}^2 + t\kappa G |\sigma_n|^2 \right) d\bar{A}. \quad (2.2)$$

The deduced 2D material norm $\|\cdot\|_{\mathbf{M}}$ is then given by

$$\|\cdot\|_{\mathbf{M}}^2 := \frac{E}{(1-\nu^2)} (\nu \text{tr}(\cdot)^2 + (1-\nu) \text{tr}(\cdot^2)).$$

The deduced material constant $G = \frac{E}{2(1+\nu)}$ is the shearing modulus, and κ is the shear correction factor.

Remarks.

1. We will not discuss the justification of using a linear material law for applications with large deformations and small strains. A deduction of material tensors and laws, and a discussion of when they are appropriate can be found in, *e.g.*, [Ogd97].

2. The shear correction factor is introduced to compensate higher order effects of the shear stresses through the thickness that appear when these stresses get larger. The particular choice of this factor with respect to the material tends to be important only for laminated plates and shells. For homogeneous, isotropic plates with a Poisson ratio of approximately 0.3, κ is usually set to $\frac{5}{6}$. Though seemingly a crude trick to rescue the model although the model assumptions break down, it works surprisingly well in practice. See [BDS93] and [DAT10] for further discussions on this topic.

3. Notice that this energy formulation can easily be extended to non-homogeneous and non-isotropic materials by use of an appropriate material norm $\|\cdot\|_M$, or by directly adapting $\|\cdot\|_M$ and an additional norm that encodes an anisotropic shear behaviour.

Kirchhoff energy If we assume the deformed directors to coincide with the surface normals of the deformed mid-surface, expression (2.2) similarly provides a compact energy formulation for the shear-rigid shell model respecting the Kirchhoff assumption, comparable to classical formulations, *e.g.*, [Cia05]:

$$\mathcal{W}_{\text{Kirchhoff}} = \frac{1}{2} \int_{\bar{\mathcal{S}}} \left(\frac{t}{4} \|I - \bar{I}\|_M^2 + \frac{t^3}{12} \|II - \bar{II}\|_M^2 \right) d\bar{A} .$$

Here II denotes the pullback of the *classical* second fundamental form of the deformed mid-surface.

2.2 Alternative formulation

In this section, we will present a formulation for the bending and shearing parts of the Cosserat energy in terms of the shear form, which provides a very different view on shearable shell models. Although this formulation will not be used in the remainder of the thesis, we present it here as we believe that this view is amenable to provide new tools for a rigorous analysis of shear-deformable models in the nonlinear case.

As before, let $\bar{\mathcal{S}} \subset \mathbb{R}^3$ be the embedded undeformed configuration of the mid-surface of a shell $(\bar{\mathcal{S}}, \bar{n}, t)$ of thickness t , and let \mathcal{S} be the deformed configuration

of $\bar{\mathcal{S}}$ under a deformation ϕ .

In the following, we will be dealing with both the shear form on the deformed surface as well as with its pullback, such that in the latter case the pullback operator ϕ^* will be written explicitly.

The vector fields v, w will denote commutative local tangent vector fields on \mathcal{S} . We distinguish by \cdot^+ and \cdot^- the symmetric and antisymmetric part of a bilinear form respectively.

To obtain the bending energy of \mathcal{S} in terms of σ_n , we need to look at its covariant derivative $\nabla\sigma_n$ which is defined as

$$(\nabla_w\sigma_n)(v) = \nabla_w(\sigma_n(v)) - \sigma_n(\nabla_w v) .$$

$\nabla\sigma_n$ will be considered as a (in general non-symmetric) bilinear form

$$\nabla\sigma_n : (v, w) \mapsto \nabla_w\sigma_n(v)$$

that can be decomposed orthogonally with respect to the metric $\langle \cdot, \cdot \rangle$ in its symmetric and its antisymmetric part:

$$\nabla\sigma_n = (\nabla\sigma_n)^+ + (\nabla\sigma_n)^- .$$

Lemma 2.1. *The generalized second fundamental form II_n of \mathcal{S} is the symmetric part of $\nabla\sigma_n$. Its pullback can be expressed through*

$$\phi^* (\nabla\sigma_n)^+ = \nabla(\phi^*\sigma_n)^+ - \langle \text{Hess } \phi, \underline{n} \rangle .$$

Remark. As the covariant derivative is symmetric if and only if σ_n is closed [Pet06], this means in particular that for closed shear forms, covariant derivative of the shear form and generalized second fundamental form coincide.

Proof. The generalized second fundamental form on \mathcal{S} is given by

$$II_n(v, w) = \frac{1}{2}(\langle dn(v), w \rangle + \langle v, dn(w) \rangle) .$$

For $\nabla\sigma_n$ we have

$$\begin{aligned} \nabla\sigma_n(v, w) &= \nabla_w(\sigma_n(v)) - \sigma_n(\nabla_w v) \\ &= \nabla_w \langle n, v \rangle - \langle n, \nabla_w v \rangle \\ &= \langle dn(w), v \rangle \end{aligned}$$

so $(\nabla\sigma_n)^+ = II_n$.

Let $\bar{v}, \bar{w} \in T\bar{\mathcal{S}}$ be tangent vectors to the undeformed mid-surface $\bar{\mathcal{S}}$, and let again be $\underline{n} = \phi^*n$ the pullback of the deformed director field. For the pullback of the shear form, we then get

$$\begin{aligned} \nabla(\phi^*\sigma_n)(\bar{v}, \bar{w}) &= \langle (\nabla_{\bar{v}}d\phi)(\bar{w}), \underline{n} \rangle + \langle d\phi(\bar{w}), d\underline{n}(\bar{v}) \rangle \\ &= \langle \text{Hess } \phi(\bar{v}, \bar{w}), \underline{n} \rangle + \langle d\phi(\bar{w}), d\underline{n}(\bar{v}) \rangle \end{aligned}$$

thus

$$\langle d\phi, d\underline{n} \rangle = \phi^* \nabla \sigma_n = \nabla(\phi^* \sigma_n) - \langle \text{Hess } \phi, \underline{n} \rangle .$$

□

Alternative Cosserat energy The elastic energy of the deformed Cosserat shell (2.2) for an isometric deformation can hence be written in terms of the shear form as

$$\begin{aligned} W(\mathcal{S}) &:= \frac{1}{2} \int_{\mathcal{S}} \frac{t^3}{12} \|(\phi^* \nabla \sigma_n)^+\|_M^2 + t\kappa G |\phi^* \sigma_n|^2 d\bar{A} \\ &= \frac{1}{2} \int_{\mathcal{S}} \frac{t^3}{12} \|(\nabla(\phi^* \sigma_n))^+ - \langle \text{Hess } \phi, \underline{n} \rangle\|_M^2 + t\kappa G |\phi^* \sigma_n|^2 d\bar{A} . \end{aligned}$$

2.3 Towards a discrete model

We presented two different formulations of the Cosserat energy, both relying on coordinate-free differential operators whose smooth properties are well-known. On our way to a discrete model, the next step is to find discrete pendants to these entities which mimic, if not all their smooth properties, at least those properties that are substantial for the regarded problem. Depending on the considered quantities and involved operators, this task can be more or less challenging.

In this view, we will build our discrete shell model on the energy formulation (2.2), involving quadratic forms and one-forms rather than the formulation of the energy in terms of derivatives of the shear form.

Although the latter seems more elementary, it involves a covariant derivative, whose geometric discretisation is more delicate and would require a satisfying theory of discrete connections. Though a fascinating question, this would carry us too far away from the very practical question we had in mind, and we refer to [Nov03, LMW04, CDS10] for work in this direction. Moreover, trying to discretise a Hessian defeats the motivation of using a Cosserat model in order to avoid higher order derivatives.

In contrast, the main players in the first energy formulation are differential one-forms and quadratic forms, who have a rather simple structure and clear properties that can be mimicked in the discrete setting. This will be the topic of the next two chapters.

Linear elasticity and geometrically nonlinear shells Throughout the thesis, we will keep relating different aspects of the geometrically nonlinear Cosserat model to concepts of linearised plate analysis. Linear elasticity aims to describe *small* deformations and therefore only considers a first order approximation of the elastic model. This linearisation restricts the range of practical applications,

and the resulting discrete models are in particular not suited for the simulation of large deformations of shells like the ones we have in mind.

However, the finite element analysis available in the linear framework provides a very good understanding of the underlying phenomena and the fundamental correlations of the smooth formulation that should be respected. It can therefore be used as a reliable guide to avoid unnecessary discretization issues.

Chapter 3

Shear locking and discrete tangent planes

One needs to recognize that different physical quantities have different properties, and must be treated accordingly.

Mathieu Desbrun *et al.* [Bob08]

In order to define a discrete shell model, we need to determine how to describe the discrete mid-surface and the discrete director field. In the DDG setting, the canonical choice to approximate the mid-surface is an embedded two-dimensional simplicial mesh, and the position of the discrete surface is usually described by the positions of the vertices of this mesh. For the director field however, there is *a priori* no intuitive choice of whether to attach it to vertices, edges or faces.

Discrete shearable shell models are known to be prone to so-called *shear locking* which, in finite element analysis, is usually due to an incompatibility of the approximating finite-dimensional spaces. In order to get an indication of how to place directors in a way to avoid such incompatibilities, the first section of this chapter will demonstrate the phenomenon of shear locking for the linear Reissner-Mindlin plate model where it is relatively well understood. In the second section, we use these insights to eventually put the discrete directors on edge midpoints. The definition of a discrete shear form then leads us to an unusual though very beneficial definition of edge-based discrete tangent planes.

3.1 Shear locking in the linear setting

An often used heuristic to explain locking is that *bending induces shearing* when it should not. Indeed, in the Cosserat energy (2.2), the weights attached to shearing

and bending contributions are essentially

$$c_{shear} := \frac{5t}{6} \frac{E}{2(1+\nu)} \quad \text{and} \quad c_{bend} := \frac{t^3}{12} \frac{E}{(1-\nu^2)} = \frac{t^2}{5(1-\nu)} c_{shear} .$$

This means that as soon as $\frac{t^2}{5(1-\nu)}$ is considerably smaller than 1, which happens quickly when the thickness t is small, shearing is much more penalized than bending. Thus if bending induces shearing, much more energy is needed for the deformation, and the deflections predicted by the model are smaller than they should.

3.1.1 Shear locking for the Timoshenko beam

Shear locking is not proper to shearable plates, but already occurs in shear-deformable beams, so called *Timoshenko beams*. We will briefly describe this case to prepare the more involved situation of shear locking of the Reissner-Mindlin plate.

Let $w : [0, L] \rightarrow \mathbb{R}$ denote the scalar vertical displacement of the centreline of a beam of length L , and $\theta : [0, L] \rightarrow \mathbb{R}$ the scalar rotation of the director (Fig. 3.1). Both scalar functions are assumed to be weakly differentiable, *i.e.*, lie in the Sobolev space $H^1([0, L])$. We will further denote by $\|\cdot\|_{L^2([0, L])}$ the usual L^2 -norm of the considered domain.

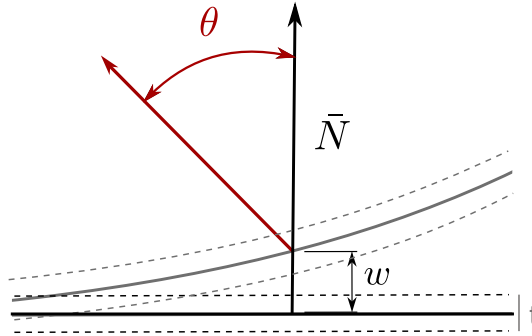


Fig. 3.1 The variables of the Timoshenko beam model are scalar displacements w and scalar rotations θ . \bar{N} denotes the undeformed surface normal.

The deformation energy of a Timoshenko beam of length L and thickness t is then given by

$$W_{beam} = \frac{1}{2} \left(\underbrace{\int_0^L (\theta')^2 dx}_{\text{bending}} + t^{-2} \underbrace{\int_0^L (\theta - w')^2 dx}_{\text{shearing}} \right) .$$

Similarly to the Cosserat shell energy, this energy is composed of a bending part and a shearing part (the membrane part is neglected because we are in the linearised setting). For a simpler presentation, the problem is scaled such that no material coefficients appear.

A possible way to discretise this problem which is very well known to lead to locking is to split the interval $[0, L]$ in segments of length h and approximate both variables by piecewise linear, continuous functions. On a segment $[x_i, x_i + h] \subset [0, L]$ let for instance

$$\begin{aligned} w_h(x) &:= ax + b \\ \theta_h(x) &:= \alpha x + \beta, \end{aligned}$$

with $a, b, \alpha, \beta \in \mathbb{R}$. Then the shearing part can be bounded by

$$\begin{aligned} \int_{x_i}^{x_i+h} (\theta_h - w'_h)^2 dx &= \int_{-h/2}^{h/2} (\alpha x + (\beta - a))^2 dx \\ &\geq \int_{-h/2}^{h/2} (\alpha x)^2 dx \\ &= \frac{h^2}{2} \int_{x_i}^{x_i+h} \alpha^2 dx. \end{aligned}$$

The inequality holds independently of α and β because we integrate over a *symmetric* domain.

The last expression can be written as

$$\frac{h^2}{2} \int_{x_i}^{x_i+h} \alpha^2 dx = \frac{h^2}{2} \int_{x_i}^{x_i+h} (\theta')^2 dx,$$

and by summing over all intervals, we obtain a lower bound for the shearing part in terms of the bending part

$$\|(w'_h - \theta_h)\|_{L^2([0,L])} \geq \frac{h}{\sqrt{12}} \|\theta'\|_{L^2([0,L])}.$$

From this inequality, we see that for positive h , the shearing part cannot be zero as long as the bending part does not vanish. More generally: if the discrete spaces containing $\text{grad } w_h$ and θ_h do not overlap sufficiently to allow $\|\theta_h - \text{grad } w_h\|_{L^2([0,L])}$ to vanish unless both components are zero, then bending induces shearing, and the model locks.

For more details on shear locking for the Timoshenko beam and for an analytic description of locking in general, we refer to Braess [Bra01]. A further insightful intuition on shear locking in terms of a *shear gap* is given by Bletzinger *et al.* in [BBR00].

3.1.2 Shear locking for the Reissner-Mindlin plate

For shear-deformable Reissner-Mindlin plates, the interactions of the involved function spaces are more challenging than for the Timoshenko beam.

The Reissner-Mindlin plate problem

Let $\{e_1, e_2, e_3\}$ be an orthonormal basis in \mathbb{R}^3 , and let the mid-surface $\bar{\mathcal{S}}$ of the undeformed plate lie in the plane spanned by $\{e_1, e_2\}$. In the Reissner-Mindlin model, the deformation Φ of the plate is assumed to have the form

$$\Phi : (x, y, z) \mapsto \begin{pmatrix} x \\ y \\ z \end{pmatrix} + \begin{pmatrix} z\theta_1(x, y) \\ z\theta_2(x, y) \\ w(x, y) \end{pmatrix} \in \mathbb{R}^3 .$$

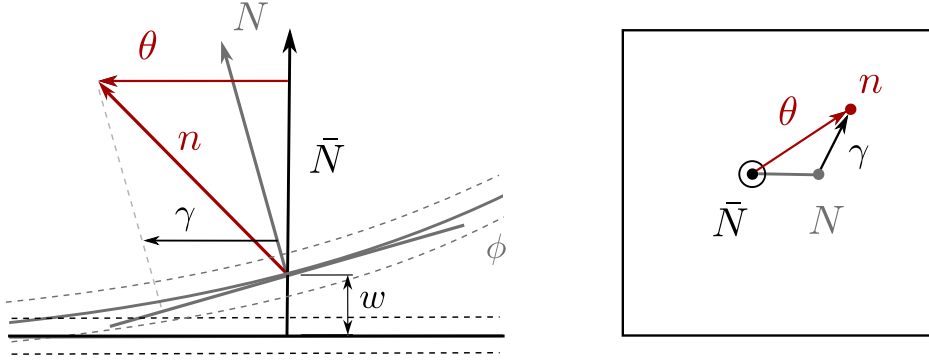


Fig. 3.2 Lateral and top view of the deformation of a Reissner-Mindlin plate. The involved variables are: scalar displacements w , vector-valued rotations θ , vector-valued shearing γ .

The involved variables are again scalar *vertical* or *transversal displacements* $w \in H^1(\bar{\mathcal{S}})$ of the mid-surface, and a vector field $\theta \in \mathbf{H}^1(\bar{\mathcal{S}}) := [H^1(\bar{\mathcal{S}})]^2$ of so-called *infinitesimal rotations* measuring how far and in which direction directors deviate from undeformed normals (see Fig. 3.2). The Reissner-Mindlin deformation energy of a plate of thickness t , under some external force f , is then given by

$$\mathcal{W}_{RM} = \frac{t^3}{2} a(\theta, \theta) + \frac{t}{2} \|\theta - \text{grad } w\|_0^2 - t^3(f, w) \quad (3.1)$$

where a is the bounded, coercive symmetric bilinear form defined as

$$\begin{aligned} a : \mathbf{H}^1(\bar{\mathcal{S}}) \times \mathbf{H}^1(\bar{\mathcal{S}}) &\rightarrow \mathbb{R} \\ (\theta, \tau) &\mapsto \frac{E}{(1-\nu^2)} (\nu \text{tr}(\varepsilon(\theta)) \text{tr}(\varepsilon(\tau)) + (1-\nu) \text{tr}(\varepsilon(\theta) \cdot \varepsilon(\tau))) . \end{aligned}$$

As usual in linear elasticity, the differential operator ε gives the symmetric part of the derivative of a function in $\mathbf{H}^1(\bar{\mathcal{S}})$.

Before entering the details, let us give a proper definition of shear locking for Reissner-Mindlin plates.

Definition 3.1. A discretisation of the Reissner-Mindlin model is called *shear locking free* if the discrete solution (w_h, θ_h) converges uniformly in thickness t , $t > \xi > 0$, to the smooth solution (w, θ) . It is said to suffer shear locking otherwise.

Remark. In engineering literature, shear locking is often tacitly defined as a deterioration of the convergence rate when t gets smaller, which is not equivalent, but captures the most current appearance of shear locking.

A straightforward discretisation of this energy is very likely to lead to shear locking, especially for low-order approximations, because of the incompatibilities between the discrete function spaces used to approximate w and θ , just as in the case of the Timoshenko beam.

Many techniques have been proposed to overcome this difficulty, including the introduction of bubble functions [AF89], penalty terms [Lov04], and reduced integration [AT95], and although mostly theoretically justified, such regularizations tend to occlude an intuitive understanding of the discrete model. Also, most of these approaches are specifically adapted to a single discrete formulation.

A more systematic analysis that provides a general recipe to construct locking-free Reissner-Mindlin plate elements was proposed by Brezzi, Bathe, Fortin and Stenberg [BFS91, BBF89]. As it provides valuable insight in the nature of shearing and shear locking, we will describe this approach in more detail, following closely the exposition by Braess in [Bra01].

How to prevent shear locking

The first step of this method is to reformulate the smooth equation as a mixed formulation. More precisely, an additional *shearing* vector field

$$\gamma = t^{-2}(\theta - \text{grad } w) \in \mathbf{L}^2(\bar{\mathcal{S}}) := [L^2(\bar{\mathcal{S}})]^2$$

is introduced and (3.1) is restated in a weak and mixed formulation as

$$\begin{aligned} a(\theta, \psi) + (\text{grad } v - \psi, \gamma)_0 &= (f, v)_0, & \forall (v, \psi) \in H^1(\bar{\mathcal{S}}) \times \mathbf{H}^1(\bar{\mathcal{S}}) \\ (\text{grad } w - \theta, \eta)_0 - t^2 (\gamma, \eta)_0 &= 0, & \forall \eta \in \mathbf{L}^2(\bar{\mathcal{S}}). \end{aligned} \quad (3.2)$$

As a next step, the analysis of this equation is simplified by splitting it into more familiar problems. To do so, one first notices that γ lies in the Sobolev space $H(\text{rot}, \bar{\mathcal{S}})$, i.e., $\text{rot } \gamma \in L^2(\bar{\mathcal{S}})$, because $\text{rot grad } w = 0 \in L^2(\bar{\mathcal{S}})$ and $\text{rot } \theta \in L^2(\bar{\mathcal{S}})$.

Moreover, it holds $H(\text{rot}, \bar{\mathcal{S}}) \subset \mathbf{L}^2(\bar{\mathcal{S}})$, such that, if $\bar{\mathcal{S}}$ is simply connected, we can use the Helmholtz-decomposition of $\mathbf{L}^2(\bar{\mathcal{S}})$ and write γ as

$$\gamma =: \text{grad } r + \text{curl } q$$

with $r \in H^1(\bar{\mathcal{S}})$ and $q \in H^1(\bar{\mathcal{S}})/\mathbb{R}$.

If we substitute this expression in the previous system (3.2), some simple manipulations allow to split the latter into a Stokes' equation and two Poisson equations:

Find $r \in H^1(\bar{\mathcal{S}})$ such that

$$(\text{grad } r, \text{grad } v)_0 = (f, v)_0, \quad \forall v \in H^1(\bar{\mathcal{S}}) .$$

Then find $(\theta, p) \in \mathbf{H}^1(\bar{\mathcal{S}}) \times L^2(\bar{\mathcal{S}})$ such that

$$\begin{aligned} a(\theta, \psi) - (\text{rot } \psi, q)_0 &= (\text{grad } r, \psi)_0, & \forall \psi \in \mathbf{H}^1(\bar{\mathcal{S}}) \\ -(\text{rot } \theta, p)_0 - t^2 (\text{curl } q, \text{curl } p)_0 &= 0, & \forall p \in L^2(\bar{\mathcal{S}}) . \end{aligned}$$

Finally, find $w \in H^1(\bar{\mathcal{S}})$ with

$$(\text{grad } w, \text{grad } z)_0 = (\theta, \text{grad } z)_0 - t^2(f, z)_0, \quad \forall z \in H^1(\bar{\mathcal{S}}) .$$

Remark. We denote by $\text{curl} : L^2(\bar{\mathcal{S}}) \rightarrow \mathbf{H}^1(\bar{\mathcal{S}})$ the differential operator that is *adjoint* to $\text{rot} : \mathbf{H}^1(\bar{\mathcal{S}}) \rightarrow L^2(\bar{\mathcal{S}})$ with respect to the L^2 -metric.

This reformulation of the Reissner-Mindlin equation in well-studied Poisson and Stokes problems considerably simplifies the task of identifying sufficient properties to avoid the locking problem.

Consider a finite element discretisation of the Reissner-Mindlin model, where $W_h \subset H^1(\bar{\mathcal{S}})$ denotes the finite-dimensional function space approximating scalar displacements, Θ_h is a finite-dimensional vector space lying in $\mathbf{H}^1(\bar{\mathcal{S}})$ approximating rotations of the directors, and $\Gamma_h \subset \mathbf{L}^2(\bar{\mathcal{S}})$ stands for the finite-dimensional space approximating shearing.

We further introduce a *reduction operator*

$$R : \mathbf{H}^1(\bar{\mathcal{S}}) \rightarrow \Gamma_h$$

and slightly alter the initial Reissner-Mindlin energy in a way to obtain the following discrete problem:

Find $(w_h, \theta_h) \in W_h \times \Theta_h$ and $\gamma_h \in \Gamma_h$ such that

$$\begin{aligned} a(\theta_h, \psi) + (\text{grad } v - R\psi, \gamma_h)_0 &= (f, v)_0, & \forall (v, \psi) \in W_h \times \Theta_h & \quad (3.3) \\ (\text{grad } w_h - R\theta_h, \eta)_0 - t^2 (\gamma_h, \eta)_0 &= 0, & \forall \eta \in \Gamma_h . \end{aligned}$$

Let further be $Q_h \subset L^2(\bar{\mathcal{S}})$ an additional discrete function space, whose role will become clear shortly. Then we can formulate the following 5 conditions on $W_h, \Theta_h, \Gamma_h, Q_h$ and on the reduction operator R :

The *shear-locking-free* properties (Brezzi, Bathe, Fortin 1989):

(P1) $\text{grad } W_h \subset \Gamma_h$.

(P2) $\text{rot } \Gamma_h \subset Q_h$.

(P3) Θ_h, Q_h is suitable for a Stokes' problem (inf-sup-compatible):
There exists $\varepsilon > 0$ such that

$$\inf_{q \in Q_h} \sup_{\theta \in \Theta_h} \frac{(\text{rot } \theta, q)_0}{\|\theta\|_1 \|q\|_0} \geq \varepsilon . \quad (3.4)$$

(P4) The diagram

$$\begin{array}{ccc} \mathbf{H}^1(\Omega) & \xrightarrow{\text{rot}} & L^2(\Omega) \\ R \downarrow & & \downarrow P \\ \Gamma_h & \xrightarrow{\text{rot}} & Q_h \end{array}$$

commutes, for $P : L^2(\bar{\mathcal{S}}) \rightarrow Q_h$ being the L^2 -projection.

(P5) $W_h \xrightarrow{\text{grad}} \Gamma_h \xrightarrow{\text{rot}} Q_h$ is an exact sequence, *i.e.*, $\ker \text{rot} = \text{im grad}$.

These conditions were first listed and investigated by Brezzi, Bathe and Fortin [BBF89], and they basically guarantee that the discrete spaces mimic the smooth setting sufficiently for the problem-splitting described above to go through. Indeed, the following theorems show how the conditions allow

- (a) the existence of a discrete Helmholtz-Hodge decomposition of Γ_h , such that the discrete problem can be rewritten analogously to (3.2), and
- (b) the well-posedness of the involved Poisson and the Stokes equations.

Theorem 1 (Brezzi, Bathe, Fortin 1989). *If (P1), (P2) and (P5) are satisfied, then*

$$\Gamma_h = \text{grad } W_h \oplus \text{rot } Q_h$$

yields an L^2 -orthogonal decomposition.

Therefore, we can split the discretised equation (3.3) in an analogous way to (3.2) into two Poisson equations and a generalized Stokes problem.

The property (P4), sometimes called the commuting diagram property, makes sure that the Poisson problems are well-posed. The involved discrete Stokes' problem writes

$$\begin{aligned} a(\theta_h, \psi) - (\text{rot } \psi, q_h)_0 &= (\nabla r, \psi)_0, & \forall \psi \in \Theta_h \\ -(\text{rot } \theta_h, p)_0 - t^2 (\text{curl } q_h, \text{curl } p)_0 &= 0, & \forall p \in L^2 . \end{aligned}$$

From property (P3) it follows by usual analysis of Stokes' problems, that the discrete problem is inf-sup-stable.

Theorem 2 (Braess, Peisker 1992). *Let*

$$A_t((\theta_h, q_h), (\psi, p)) := a(\theta_h, \psi) + (\operatorname{rot} \psi, q_h)_0 - (\operatorname{rot} \theta_h, p)_0 - t^2 (\operatorname{curl} q_h, \operatorname{curl} p)_0 .$$

If the couple (Θ_h, Q_h) satisfies (P3), then there exists $\alpha > 0$ independent of t and h such that for all $(\theta_h, q_h) \in (\Theta_h, Q_h)$ it holds

$$\sup_{\substack{\psi \in \Theta_h \\ p \in Q_h}} \frac{A_t((\theta_h, q_h), (\psi, p))}{\|\psi\|_0 + \|p\|_0 + t \|\operatorname{curl} p\|} \geq \alpha (\|\theta_h\|_1 + \|p_h\|_0 + t \|\operatorname{curl} p_h\|_0) .$$

See [PB92] for a proof of both theorems.

Searching for a lowest-order locking-free Reissner-Mindlin element

These conditions can now be used to search for a locking-free Reissner-Mindlin plate element which involves at most piecewise linear approximation spaces, as in terms of degrees of freedom this is the maximum a DDG model naturally provides.

On the triangular mesh K_h of the discrete plate, with maximum edge length h , and triangular faces T_{K_h} , we consider the following finite-dimensional function spaces

$$M^0 = \{f \in H^1(\mathcal{S}_h) \mid f|_T \text{ constant } \forall T \in T_{K_h}\}$$

$$M_0^1 = \{f \in H^1(\mathcal{S}_h) \mid f|_T \text{ linear } \forall T \in T_{K_h}, f \text{ continuous and vanishes} \\ \text{on the boundary}\}$$

$$M_{nc}^1 = \{f \in L^2(\mathcal{S}_h) \mid f|_T \text{ linear } \forall T \in T_{K_h}, f \text{ continuous on edge midpoints}\}$$

$$RT_0 = \{f \in L^2(\mathcal{S}_h) \mid f|_T \begin{pmatrix} x \\ y \end{pmatrix} = \begin{pmatrix} a \\ b \end{pmatrix} + c \begin{pmatrix} y \\ -x \end{pmatrix}, a, b, c \in \mathbb{R}, \forall T \in T_{K_h}\} .$$

The spaces M^0 and M_0^1 are the usual constant and piecewise linear Lagrange finite element spaces. M_{nc}^1 are the Crouzeix-Raviart elements, which are linear over each triangle and continuous at edge-midpoints. RT_0 denotes the *rotated* lowest-order Raviart-Thomas vector fields. These are piecewise linear vector fields whose edge-tangential projection is constant on each edge and continuous between triangles. These last two spaces are non-conforming, *i.e.*, they are not contained in $H^1(\mathcal{S})$.

The possible combinations of spaces that satisfy the inf-sup-condition (3.4) have been thoroughly investigated before, and in particular it is well-known that combinations of conforming constant or piecewise linear finite spaces are not suitable candidates. However, if we soften the requirements to allow for a non-conforming approach, we can find at least one couple of such spaces, namely $((M_{nc}^1)^2, M^0)$ [CR73].

Moreover, the rotated lowest-order Raviart-Thomas space has a discrete Helmholtz decomposition

$$RT_0 = \text{grad } M_0^1 \oplus \text{curl } M^0 .$$

Hence there *is* a triple of spaces that is able to mimic the Helmholtz decomposition and the inf-sup stability required for the Reissner-Mindlin-problem, namely:

$$W_h = M_0^1 , \quad \Theta_h = (M_{nc}^1)^2 , \quad \Gamma_h = RT_0 . \quad (3.5)$$

By their non-conformity, these finite dimensional spaces fail however to satisfy condition (P4).

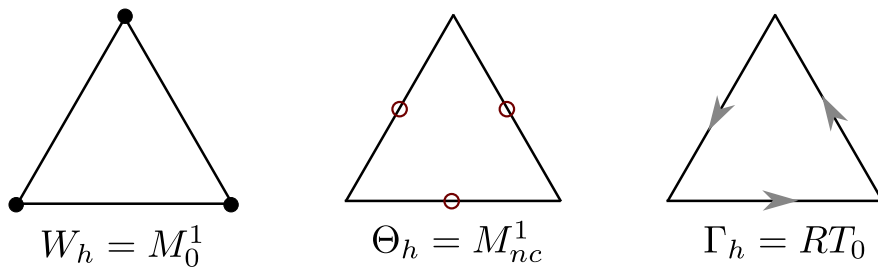


Fig. 3.3 FE-scheme of the low-order Reissner-Mindlin plate element proposed by Oñate, Zarate and Flores in [OZF94].

This triple corresponds to a Reissner-Mindlin plate element proposed by Oñate, Zarate and Flores in [OZF94]. Arnold and Falk carried out a convergence analysis of this element in [AF97] and proved a convergence order of $\max(t^2, h^2)$ where t is the thickness of the plate and h the mesh size. This convergence order is unusual and actually prevents classical convergence for fixed thickness t while h tends to zero, and in particular this element is *not locking-free* in the sense of Definition 3.1.

However, it still seems to be the best compromise we can get while sticking to a piecewise linear discretisation, as it is sufficiently suitable for applications involving thin structures on relatively coarse meshes, which corresponds to the purpose we had in mind. In such applications it holds $h \gg t$ and the convergence order comes down to $\mathcal{O}(h^2)$. Moreover, this shell element is not locking in the engineering sense given that the convergence rate gets *better* for t getting smaller.

Remarks.

1. The fact that shearing is approximated by a Raviart-Thomas space perfectly agrees with the view of shearing as a differential one-form. Indeed, Raviart-Thomas spaces are equivalent to the discrete Whitney forms [Whi57], which are the discrete pendant to one-forms in terms of the de-Rham complex [AFW09].

2. In the convergence analysis by Arnold and Falk it appears that this plate element does not achieve uniform convergence because of the additional consistency error introduced by the non-conforming approximation of the rotations Θ .

3. Our quest for a lowest-order locking-free plate element focused on satisfying propositions (P1)–(P5). However, alternative characterizations of 'locking-free' seem similarly unable to overcome the lack of degrees of freedom, as the provenly shear locking free element of lowest order that we are aware of is the model proposed by Arnold and Falk [AF89], which uses nonconforming piecewise linear displacements $W_h = M_{nc}^1$, and piecewise constant shearing $\Gamma_h = M^0$, but needs to augment the piecewise linear rotations by a cubic bubble B_3 , thus $\Theta_h = M_0^1 \oplus B_3$.

3.2 Where to place directors?

As directors are involved in both shearing and bending, their positioning on the discrete mesh requires particular care in order to avoid shear locking. This is where we can make use of the insights of the linear setting. Indeed, it seems a reasonable requirement for a nonlinear shell model to be suitable for small displacements, *i.e.*, for linearised problems. Hence, our discrete Cosserat shell model should also be as suitable as possible for the Reissner-Mindlin plate setting, which means that it should recover the Reissner-Mindlin element (3.5) that we identified as the best lowest-order model we could get regarding the applications we are aiming at. In this objective, the correspondences between the linear and the nonlinear model provide a strong hint of where to place the degrees of freedom.

The position of the vertices will, for small deformations, be encoded by scalar vertical displacements. Hence, if we want to recover conforming piecewise linear approximations for the latter, it is natural to use a conforming piecewise linear approximation of vertex positions. This agrees with simply using the vertices as degrees of freedom as suggested by the DDG approach.

To relate rotations and directors, let us remind the deformation of the plate $\bar{\mathcal{S}}$ in the Reissner-Mindlin model

$$\Phi : \begin{pmatrix} x \\ y \\ z \end{pmatrix} \mapsto \begin{pmatrix} x \\ y \\ z \end{pmatrix} + \begin{pmatrix} z\theta_1(x, y) \\ z\theta_2(x, y) \\ w(x, y) \end{pmatrix} .$$

If in the nonlinear setting we assume the deformation to be small enough that only vertical displacements w appear, the deformation has the form

$$\Phi : \begin{pmatrix} x \\ y \\ z \end{pmatrix} \mapsto \underbrace{\begin{pmatrix} x \\ y \\ z \end{pmatrix}}_{\phi(x, y, z)} + \begin{pmatrix} 0 \\ 0 \\ w(x, y) \end{pmatrix} + z\underline{n}(x, y, z) .$$

The rotations $\theta : \bar{\mathcal{S}} \rightarrow \mathbb{R}^3$ are assumed to be small, such that the unit director field \underline{n} can be approximated by

$$\underline{n} \cong \bar{N} + \theta ,$$

where \bar{N} is the normal of the undeformed mid-surface. This gives us the relation between directors and rotations (see Fig. 3.2).

Similarly, the pullback of the surface normal \underline{N} of the deformed configuration writes approximately

$$\underline{N} \cong \bar{N} + \text{grad } w .$$

By substituting \bar{N} by $\underline{N} - \text{grad } w$, we obtain as shear form

$$\underline{\sigma}_n(v) = \langle \underline{N} - \text{grad } w + \theta, d\phi(v) \rangle = \langle (\theta - \text{grad } w), d\phi(v) \rangle .$$

It follows that the shearing field $\theta - \text{grad } w$ is indeed the linearisation of the projection $\underline{n}^{\text{tan}}$ of the director onto the tangent plane of the deformed mid-surface.

Hence, in the linearised setting, the directors will provide both the rotations and the shearing vector field. The corresponding finite function spaces M_{nc}^1 and RT_0 both carry their degrees of freedom on edges, such that there is a strong motivation to attach directors to edges.

Moreover, in the smooth setting, shearing was described as a one-form. If we want to mimic this structure and treat discrete shearing as a discrete one-form, edges are again the natural place to associate shearing with, independently of what is happening in the linear setting.

Now that we established that –in view of the the linear setting– directors should be attached to edges, the next question arises: If shearing is the projection of directors to tangent planes, how to define tangent planes –or equivalently normals– on edges?

3.3 Discrete edge normals

In order to investigate a definition of discrete normals on edges that is suitable for our model, we will consider a simplicial mesh that is inscribed to a smooth surface.

Definition 3.2. Let \mathcal{S} be a smooth embedded surface with normal field N , and let \mathbb{K} be an embedded simplicial surface. We say that \mathbb{K} is *closely inscribed* to \mathcal{S} if the vertices of \mathbb{K} all lie on \mathcal{S} and if the *shortest distance map* $\psi : \mathcal{S} \rightarrow \mathbb{K}$ defined by

$$\psi(x) = x - \lambda(x) \cdot N(x) ,$$

with a scalar function $\lambda : \mathcal{S} \rightarrow \mathbb{R}$, is bijective.

In that case, we call the inverse $\pi := \psi^{-1} : \mathbb{K} \rightarrow \mathcal{S}$ the *normal projection onto* \mathcal{S} (see Fig. 3.4).

The seemingly most straightforward choice to define normals on a triangle mesh is to use piecewise constant triangle normals. However, for a triangular mesh closely inscribed to a smooth surface (Fig. 3.4), the quality of the approximation of these normals strongly depends on the approximated smooth geometry \mathcal{S} as

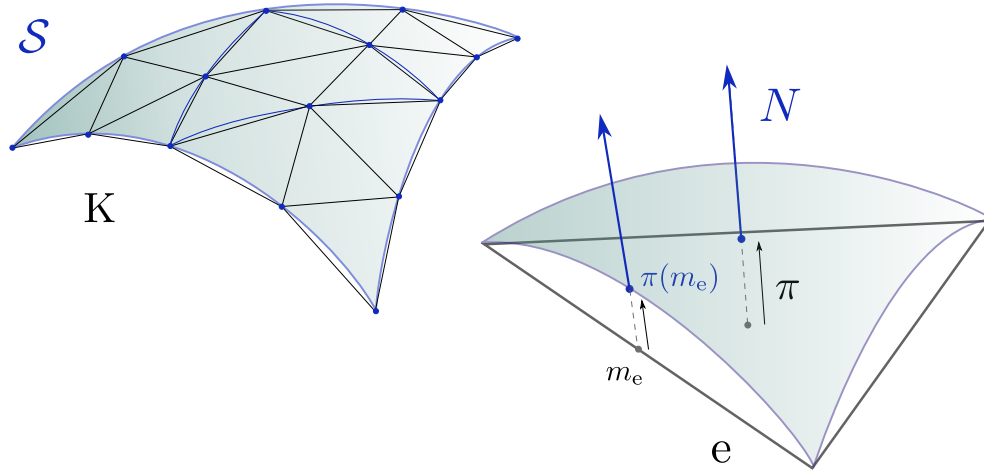


Fig. 3.4 A simplicial mesh closely inscribed to a surface. The bijection π projects points of the mesh K to the surface \mathcal{S} along the surface normal N .

well as on the quality of the triangular mesh K , namely the local curvature of \mathcal{S} , the local distance from K to \mathcal{S} , and on the angles of the triangular faces of K [MT04].

Moreover, trying to improve this approximation by averaging these face normals on vertices or edges will not help. Meek and Walton [MW00] showed by asymptotic analysis that the arithmetic mean of triangle normals on a discrete mesh enclosed to a smooth surface can approximate the surface normal still only up to $\mathcal{O}(h)$:

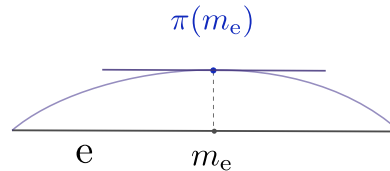
Lemma 3.1 (Meek, Walton 2000). *For non-uniform data, the unit vector parallel to the arithmetic mean of unit normals of the triangular faces around a point approximates the unit normal to the surface at that point to accuracy $\mathcal{O}(h)$.*

Numerical experiments indicate that the same holds for an average of area- and angle-weighted triangle normals.

In contrast, if we desist from triangle normals and focus on *edges*, it is easily observed that these approximate, *at their midpoint*, tangent vectors, and thereby *one* direction of the corresponding tangent plane, up to second order, independently of the shape of the triangles.

Lemma 3.2. *Let K be a simplicial mesh closely inscribed to a sufficiently smooth surface \mathcal{S} . Let $\pi : K \rightarrow \mathcal{S}$ by the bijective normal projection onto the surface. Let e be an edge and m_e its midpoint. Then e approximates a tangent vector of the tangent plane $T_{\pi(m_e)}\mathcal{S}$ up to second order.*

Indeed, it is well-known that for a planar curve, a central finite difference approximation at *the midpoint* gives a second order approximation of the tangent vector at that point. Hence, if we consider the curve resulting from the intersection of the surface \mathcal{S} with any plane containing the edge, at its midpoint the edge approximates the tangent vector to this curve up to second order.



Given that the smooth surface normal in $\pi(m_e)$ is orthogonal to the approximated tangent vector, we obtain that one of the unit vectors orthogonal to the edge approximates (again at the edge midpoint) the smooth normal up to second order. In actual computations, we will not know the exact position of this particular normal vector, such that all we know about it is that it is attached to the *edge midpoint* and *orthogonal to the edge*. Therefore, we will only use this *incomplete* information to fix the discrete normal and its corresponding tangent plane, without imposing any further –possibly overly restrictive– assumed knowledge about it.

Remarks.

1. Note that this partial construction of discrete normals can only be realized on edges. On faces as well as on vertices, there is in general no distinguished direction that approximates the tangent plane more accurately than another.
2. An alternative way to get a second order approximation of smooth normals is to construct a quadratic fit to the vertices of a triangle flap (a triangle and its three neighbours) and compute its normal field. However, this construction is very sensitive to vertex positions and valence, as discussed in [Zor05, RGZ07].

The Kirchhoff limit

Yet another way to characterize shear locking is the inability of the shear-deformable model to provide a satisfying Kirchhoff model when shearing is constraint to vanish, *i.e.*, when directors are constrained to coincide with normals.

In that case, bending will again be evaluated through the change of discrete normals, and if normals are defined by the vertex positions only, curvature will be given by second derivatives of piecewise linear functions. Hence we run back into the high regularity requirements of the Kirchhoff model that we tried to avoid in the first place by choosing a kinematic shell model based on a mixed formulation. This emphasizes the close connection between locking and the definition of the discrete normals used to evaluate the shearing part.

The above definition of normals is not based on the position of the vertices only,

but contains a rotation around the edge as an additional degree of freedom. It is thereby more likely to provide a consistent notion of curvature, and indeed, such a definition of normals has already been used successfully for Kirchhoff plates and shells, namely in the so-called Morley triangle and its nonlinear generalizations. The relation of our model to these elements will be discussed in more detail in the next chapter, where we define discrete curvatures and bending.

3.4 Discrete shearing

Conceptually, our construction of tangent planes introduces an additional degree of freedom which is the angle of the discrete edge normal with respect, for example, to the angle bisecting edge normal. *Practically*, however, this degree of freedom is already determined by the director.

Indeed, during the computation, the discrete configuration will be determined by the principle of least energy, meaning that we will minimize the total energy to find the position of the vertices and the directors. The same holds for the additional degree of freedom in the definition of the discrete tangent plane. Hence, as these tangent planes only enter in the shearing energy, the actual *tangent plane on an edge* e is the plane that

- (i) contains the edge e , and
- (ii) minimizes the length of the projection of the director onto this plane.

The minimization (ii) only involves the position of the directors, hence the position of the tangent planes is already fixed in terms of the position of the directors: no more degree of freedom is left.

Lemma 3.3. *The discrete tangent plane satisfying (i) and (ii) is such that the projection of the director onto this plane is the projection on the corresponding unit edge \hat{e} itself (Fig. 3.5).*

Condition (i) leaves the potential plane only the freedom to turn around the edge axis. It is clear that any position of this plane different from the one described in the lemma would induce an additional contribution along a direction normal to e , increasing the length of the projected director.

The normal corresponding to this tangent plane is the unit vector orthogonal to e and lying in the plane spanned by the edge and the director.

Discrete tangential projection Thus we set as discrete tangential projection of the director:

$$\mathbf{n}^{\text{tan}} := \langle \mathbf{n}, \hat{e} \rangle \hat{e} . \quad (3.6)$$

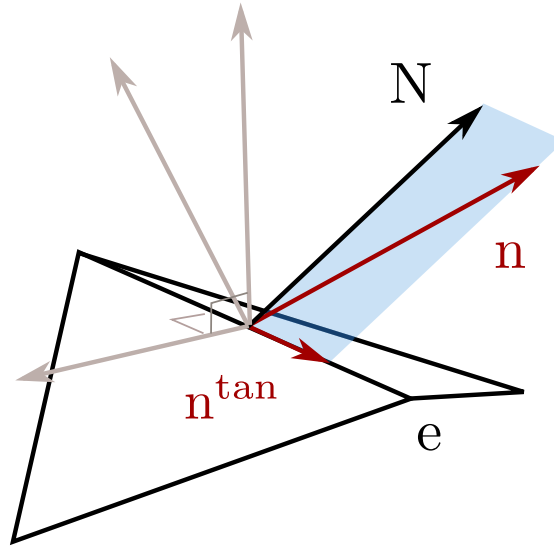


Fig. 3.5 Gray arrows represent admissible edge normals. The edge normal N inducing the smallest discrete tangential projection n^{tan} of the director n is the one lying in the same plane as the edge and n .

It was already underlined that we consider shearing as a one-form. We want to mimic this structure by defining discrete shearing by a discrete one-form. Such forms, so-called *Whitney one-forms*, are defined by one value per edge, such that this edge-wise projection of discrete directors to discrete tangent planes is sufficient to determine the shear form completely. The discrete shear form, denoted by s is hence uniquely defined through

$$s(\hat{e}_i) := \langle n_i, \hat{e}_i \rangle .$$

3.5 Consistency

Whitney one-forms are known to yield an approximation of an interpolated smooth one-form that is *consistent* of order h . By consistent, we mean that if we approximate a smooth surface by a series of closely inscribed discrete surfaces (Def. 3.2), with mesh size $h \rightarrow 0$, whose piecewise constant normal fields converge to the smooth normal field, then the discrete energy recovers the smooth energy in the limit of refinement. In our case, the discrete shear form *does not* sample the exact shear form. Instead it samples a one-form defined by the projection of the smooth director in specific directions of the smooth tangent plane. However, this is sufficient for the consistency of the discrete shear form.

Proposition 3.1. *The discrete shear form s and the smooth shear form σ_n satisfy*

$$\left| \int_{\mathcal{S}} \|\sigma_n\|^2 dA - \int_{\mathcal{K}} \|s\|^2 dA \right| \leq Ch ,$$

where C is a positive constant independent of h .

Proof. Let us consider a triangle T of \mathcal{K} with edges e_i . We will view an edge as a parametrized path $e_i : [0, |e_i|] \rightarrow \mathcal{K}$ on \mathcal{K} . Let further $\zeta_i := \pi \circ e_i$ be the image of this path on \mathcal{S} .

The de-Rham map R that provides the link between a smooth one-form σ_n on $\pi(T)$ and a discrete Whitney one-form on T is defined by a Whitney interpolation of the values

$$R\sigma_n(\zeta_i) = \int_{\zeta_i} \sigma_n ds .$$

In contrast, the discrete shear form s was defined by a Whitney interpolation of the edge values $s(\hat{e}_i) = \langle n_i, \hat{e}_i \rangle$. First, we have that

$$R\sigma_n(\zeta_i) = s(e_i) + \mathcal{O}(h^2) . \quad (3.7)$$

Indeed, let $\dot{\zeta}_i$ be the tangent field to ζ_i on \mathcal{S} . Then $R\sigma_n(\zeta_i)$ can be expressed in terms of the director field n as

$$R\sigma_n(\zeta_i) = \int_{\zeta_i} \langle n, \dot{\zeta}_i \rangle ds .$$

A constant approximation of the integral in m_i' yields

$$R\sigma_n(\zeta_i) = \langle n(m_i'), \dot{\zeta}_i(m_i') \rangle |\zeta_i| + \mathcal{O}(h^2)$$

where $|\zeta_i|$ is the length of the path ζ_i . By definition of ζ_i and $\dot{\zeta}_i$, and again by a simple finite difference approximation, we have $\dot{\zeta}_i = d\pi(\hat{e}_i) = \hat{e}_i + \mathcal{O}(h^2)$. Thus, we get

$$\begin{aligned} R\sigma_n(\zeta_i) &= \langle n(m_i'), \hat{e}_i \rangle |\zeta_i| + \mathcal{O}(h^2) \\ &= s(\hat{e}_i) |\zeta_i| + \mathcal{O}(h^2) . \end{aligned}$$

With $|\zeta_i| = |e_i| + \mathcal{O}(h^2)$ and the linearity of s we obtain the statement.

From (3.7) we can now deduce the approximation by measuring the error introduced by a Whitney interpolation W of the edge values $\{s(e_i)\}_i$. Notice that the definition of Whitney interpolation requires barycentric coordinates. On the smooth surface \mathcal{S} the choice of such coordinate functions can be delicate. For our purposes –as we only consider the interpolation elementwise– we make use of the bijective normal projection π between the piecewise flat surface \mathcal{K} and \mathcal{S} to use the well-defined barycentric coordinates of the corresponding flat triangle.

As π is sufficiently regular, we can then apply approximation results of a Raviart-Thomas interpolation (e.g., [AADL11]), which corresponds to a Whitney interpolation on flat triangles.

We obtain

$$\|\sigma_n - s\|_{\infty, T} = \|\sigma_n - WR\sigma_n\|_{\infty, T} + \mathcal{O}(h^2) = \mathcal{O}(h) .$$

Triangle inequality and integration over the corresponding surfaces yields the statement of the proposition (see also the proofs of Section 4.3 for further details about the error made by the transition through π).

□

Chapter 4

Discrete fundamental forms

For triangular elements it is remarkable that many formulations contain awkward procedures while deriving the element stiffness matrix.

Kai-Uwe Bletzinger *et al.* [BBR00]

In this chapter, we describe a very useful though little-known geometric pattern for defining discrete quadratic forms on triangle meshes. This cast is then used to define discrete fundamental forms, which are in particular shown to lead to consistent membrane and bending energies. Moreover, the geometric derivation of these discrete energies allows to set well-established piecewise constant finite element strain measures in a common framework and underline their geometric character.

4.1 Discrete quadratic forms

In the smooth setting, first and second fundamental forms are symmetric quadratic forms on the tangent space of the considered surface. Such a quadratic form on \mathbb{R}^2 , say Q , is uniquely defined by three values that can be provided by its evaluation either on a basis $\{e_i, e_j\}$ through

$$Q(e_i, e_i), Q(e_j, e_j), Q(e_i, e_j),$$

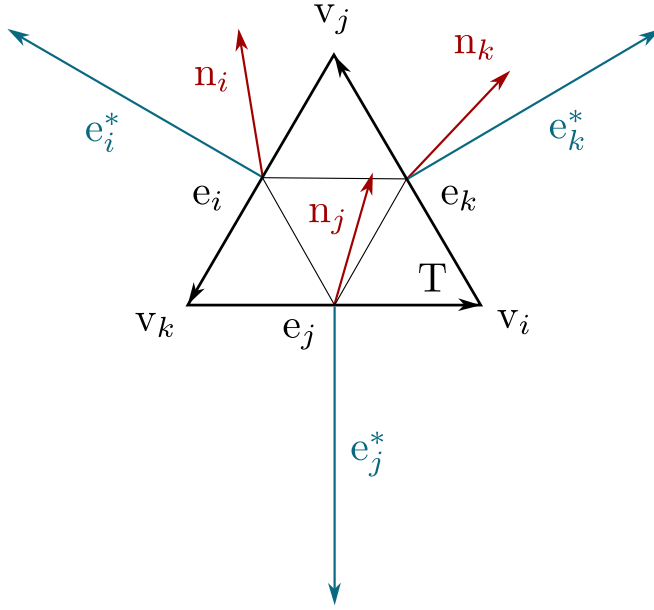
or on 3 non-parallel vectors $\{e_i, e_j, e_k\}$ through

$$Q(e_i, e_i), Q(e_j, e_j), Q(e_k, e_k).$$

In the latter case, $e_k := \alpha_i e_i + \alpha_j e_j$ is a linear combination of the remaining vectors with coefficients $\alpha_i \in \mathbb{R}$, and the mixed term $Q(e_i, e_j)$ can simply be recovered by polarisation:

$$Q(e_k, e_k) = Q(\alpha_i e_i + \alpha_j e_j, \alpha_i e_i + \alpha_j e_j) = \alpha_i^2 Q(e_i, e_i) + \alpha_j^2 Q(e_j, e_j) + 2\alpha_i \alpha_j Q(e_i, e_j).$$

A piecewise constant *discrete* quadratic form Q on a simplicial mesh can be defined in the exact same way, given that in each triangle plane, Q is a quadratic form in \mathbb{R}^2 . Distinguished directions in such a triangle plane are the triples of edges e_i or of orthogonal dual edges $e_i^* = e_i^\perp$, *i.e.*, the edges rotated clockwise by 90 degrees in the triangle plane.



In the following, let A_T denote the area of a triangle T , and let (ijk) be a cyclic permutation of indices (123) . It holds

Lemma 4.1. *Let a quadratic form Q in the plane of a non-degenerate triangle T be prescribed along the triangle edges e_i or the dual edges e_i^* by*

$$Q_i := Q(e_i, e_i) , \quad Q_i^* := Q(e_i^*, e_i^*) .$$

Then Q can be written as:

$$\begin{aligned} Q &= -\frac{1}{8A_T^2} \sum_{(ijk)} (Q_i - Q_j - Q_k) e_i^* \otimes e_i^* \\ &= -\frac{1}{8A_T^2} \sum_{(ijk)} (Q_i^* - Q_j^* - Q_k^*) e_i \otimes e_i . \end{aligned} \quad (4.1)$$

Proof. Let T be a planar triangle with vertices v_1, v_2, v_3 , oriented edges $e_i := v_k - v_j$ and dual edges e_i^* . If T is not degenerate, the edges are pairwise non-parallel, hence the dyadic products $e_i^* \otimes e_i^*$ form a basis for quadratic forms, such that Q can be written as

$$Q = \sum_{s=1}^3 \mu_s e_s^* \otimes e_s^*$$

with coefficients $\mu_i \in \mathbb{R}$ that are to be determined. Prescribing the values $Q(e_i)$ along the edges e_i leads to:

$$Q(e_i) = e_i^T Q e_i = \sum_{s=1}^3 \mu_s e_i^T (e_s^* \otimes e_s^*) e_i = \sum_{s=1}^3 \mu_s (e_i^T e_s^*)^2 \quad \text{for } i = 1, 2, 3 .$$

Let θ_{is} be the oriented angle between e_i and e_s^* , and α_{is} the oriented angle between e_i and e_s . Then it holds by elementary geometric considerations, for $i \neq s$

$$\begin{aligned} |e_i^T e_s^*| &= |e_i| |e_s^*| |\cos(\theta_{is})| = |e_i| |e_s| |\cos(\alpha_{is} - \frac{\pi}{2})| \\ &= |e_i| |e_s| |\sin(\alpha_{is})| \\ &= |e_i \times e_s| \\ &= 2A_T . \end{aligned}$$

Together with the orthogonality of e_i and e_i^* , it follows

$$\begin{aligned} Q(e_i) &= \sum_{s=1, s \neq i}^3 \mu_s (2A_T)^2 \\ \frac{1}{4A_T^2} Q(e_i) &= \mu_j + \mu_k \quad \text{for } i = 1, 2, 3 \end{aligned}$$

where the indices i, j, k cycle through (123). Solving the resulting linear system finally yields

$$\mu_i = -\frac{1}{8A_T^2} (Q(e_i) - Q(e_j) - Q(e_k)) .$$

The expression involving the evaluations on the dual edges Q_i^* follows from an analogous deduction. □

Remark. An similar approach allows to express the quadratic form as

$$Q|_T = -\frac{1}{8A_T^2} \sum_{i=1}^3 Q_i (e_j^* \otimes e_k^* + e_k^* \otimes e_j^*) .$$

4.2 Discrete fundamental forms

We will make use of the definition of discrete quadratic forms just introduced to define the discrete first and generalized second fundamental forms on a discrete shell. All we have left to do is to describe how these discrete forms should act on edges (or on dual edges, but we will settle for edges). These values will be determined by relying on finite difference approaches of the smooth expressions.

If the discrete surface K is closely inscribed to \mathcal{S} , the edge vectors e_i are a finite difference approximation of tangent vectors of the surface. As the continuous first fundamental form of a surface \mathcal{S} measures the squared length of tangent vectors, $I(v, v) = \|v\|^2$, we assign the discrete first fundamental form I along an edge the analogous value, *i.e.*, the squared length of the corresponding edge:

$$I(e_i, e_i) := \langle v_k - v_j, v_k - v_j \rangle = \|e_i\|^2 . \quad (4.2)$$

The smooth generalized second fundamental form applied to a tangent vector v yields a directional 'normal' (or rather 'directorial') curvature $II_n(v) = \langle dn(v), v \rangle$. As directors are not attached to vertices, measuring their change along edges is not possible directly. Yet, by noting that the segment which connects two edge midpoints of a triangle is parallel to the third edge and has half its length, the discrete second fundamental form can still be defined by a simple finite difference discretisation of the smooth expression. With $n_i := n(e_i)$ we obtain:

$$II_n(e_i, e_i) := 2\langle n_j - n_k, v_k - v_j \rangle = 2\langle n_j - n_k, e_i \rangle . \quad (4.3)$$

For our particular application to elastic deformations, there is a subtle reformulation of the expression for discrete quadratic forms which allows to make the implementation more efficient.

In the smooth setting, we already saw that in order to measure the change of first and second fundamental forms on a common reference surface, we need to pull back the operators of the deformed surface. For the discrete quadratic forms, we could do the same and pull back the discrete form explicitly to the undeformed configuration, leading to an unhandy expression involving two different bases $\{\bar{e}_i^* \otimes \bar{e}_i^*\}_i$ and $\{\phi^*(e_i^* \otimes e_i^*)\}_i$:

$$\bar{Q} - \phi^*Q = -\frac{1}{8A_T^2} \sum_{(ijk)} (\bar{Q}_i - \bar{Q}_j - \bar{Q}_k) \bar{e}_i^* \otimes \bar{e}_i^* - (\tilde{Q}_i - \tilde{Q}_j - \tilde{Q}_k) \phi^*(e_i^* \otimes e_i^*) \quad (4.4)$$

where

$$\bar{Q}_i = \bar{Q}(\bar{e}_i) , \quad \tilde{Q}_i := Q(e_i) .$$

A more efficient procedure is to consider the deformed fundamental forms as a quadratic forms on the *undeformed* triangle by defining directional values directly on the undeformed edges through

$$Q_i := Q(\bar{e}_i) .$$

Thereby, we only use one basis $\bar{e}_i \otimes \bar{e}_i$ for both forms without introducing any approximation.

A similarly compact expression (but with a slightly different scaling) for discrete membrane strains and shape operators has already been used in [GSH⁺04]. However, the authors use different formulas for each of these forms, such that the similarity in structure is not made entirely clear.

4.3 Consistency

In the last chapter, we already showed that our definition of the discrete shearing energy is consistent (Proposition 3.1). We will now show that by using finite difference approximations of the smooth directional evaluations of the quadratic forms, we also naturally guarantee the discrete fundamental forms and especially the corresponding energy to be consistent.

4.3.1 Notation and assumptions

Throughout this section, we will denote by h the maximum mesh size of the undeformed and deformed discrete surfaces \bar{K}, K .

We will also assume that discrete surfaces are closely inscribed (Def. 3.2) into the approximated smooth surfaces, *i.e.*, that \bar{K} is closely inscribed to $\bar{\mathcal{S}}$ and K is closely inscribed to \mathcal{S} . The normal projections from the inscribed discrete undeformed, resp. deformed, surface to the undeformed, resp. deformed, smooth surface are denoted by $\bar{\pi}$, resp. π . For ease of notation, we will denote the images $\bar{\pi}(\bar{\mathbf{x}})$, $\pi(\mathbf{x})$ of points $\bar{\mathbf{x}} \in \bar{K}$, $\mathbf{x} \in K$, by $\bar{\mathbf{x}}'$, \mathbf{x}' :

$$\begin{aligned}\bar{\mathbf{x}}' &:= \bar{\pi}(\bar{\mathbf{x}}) \\ \mathbf{x}' &:= \pi(\mathbf{x}) .\end{aligned}$$

We will further use the following assumptions:

- The undeformed and deformed smooth surfaces $\bar{\mathcal{S}}, \mathcal{S}$, are compact.
- The smooth undeformed and deformed surfaces $\bar{\mathcal{S}}, \mathcal{S}$, the smooth director fields \bar{n}, n , and the diffeomorphism ϕ describing the deformation are \mathcal{C}^∞ . The curvatures of $\bar{\mathcal{S}}$ and \mathcal{S} are uniformly bounded.
- We denote by $\{\bar{v}_i\}_i$ the vertices of the undeformed discrete triangulated surface \bar{K} . The vertices of the *deformed* discrete surface K are then given by $\{\phi(\bar{v}_i)\}_i$ and K inherits the connectivity of \bar{K} .
- The closely inscribed discrete surfaces \bar{K}, K , have vertices on their boundaries that sample the boundaries of the smooth surfaces.
- The aspect ratio of the triangles of \bar{K} is uniformly bounded.
- For both \bar{K} and K we assume that the triangulation is quasi-uniform, *i.e.*, that there exist positive constants c_1, c_2 , such that for the length h_i of every deformed or undeformed edge it holds $c_1 h_i \leq h \leq c_2 h_i$.
- Discrete directors sample the smooth director field on edge midpoints, *i.e.*, a director n_i on an edge e_i with midpoint m_i is defined as $n_i := n(\pi(m_i))$.

Notice that because ϕ is a diffeomorphism, it follows from the assumptions that the aspect ratio of the triangles of K is also bounded.

4.3.2 Consistency of membrane and bending energies

The proof of the consistency relies on elementary Taylor approximations and the following lemmas which are mostly based on results by Morvan and Thibert [MT04].

Lemma 4.2. *Let $\pi : \mathbb{K} \rightarrow \mathcal{S}$ be the piecewise differentiable normal projection as defined in Definition 3.2. Let further N be the unit normal field of \mathcal{S} . Then for the scalar function $\lambda : \mathcal{S} \rightarrow \mathbb{R}$ defined by*

$$\pi(\mathbf{x}) = \mathbf{x} + \lambda(\pi(\mathbf{x}))N(\pi(\mathbf{x}))$$

it holds per triangular element T with diameter h_T

$$\begin{aligned} (a) \quad & \|d\lambda\|_{\infty, T} = \mathcal{O}(h_T) \\ (b) \quad & \|\lambda\|_{\infty, T} = \mathcal{O}(h_T^2) \end{aligned}$$

where $\|\cdot\|_{\infty, T}$ is the maximum norm on T .

Proof. For the proof of the lemma, we will first show that there exists a positive constant c such that

$$c \leq \|d\pi\|_{\infty, T}.$$

It was shown in [HPW05] that the area distortion $A := d\psi^T d\psi$ induced by ψ can be expressed as

$$A = P \cdot Q^{-1} \cdot P$$

where P and Q can be diagonalized (not simultaneously in general) as

$$P = \begin{pmatrix} 1 - \lambda\kappa_1 & 0 \\ 0 & 1 - \lambda\kappa_2 \end{pmatrix} \quad Q = \begin{pmatrix} (\cos \alpha)^2 & 0 \\ 0 & 1 \end{pmatrix}.$$

Here κ_1, κ_2 , are the principal curvatures of the smooth surface \mathcal{S} and α is the angle between the unit normal field N of \mathcal{S} and the piecewise constant normal field N of the discrete surface. We assume α to be smaller than $\pi/3$ which holds for bounded aspect ratio and sufficiently small h .

This expression can now be used to bound $d\psi$ and consequently $d\pi$. Indeed, by looking at the eigenvalues of P, Q^{-1} , we get

$$\|d\psi^T d\psi\| \leq \max\{|1 - \lambda\kappa_1|^2, |1 - \lambda\kappa_2|^2\} \cdot \max\{1, \frac{1}{(\cos \alpha)^2}\}.$$

As $\alpha \leq \pi/3$ we have

$$\frac{1}{(\cos \alpha)^2} \leq 4.$$

Moreover, let the principal curvatures of \mathcal{S} be bounded by k , $|\kappa_i| \leq k$, and let $l := \sup_{x \in \mathcal{S}} \lambda(x) < \infty$. Then we get that

$$|1 - \lambda\kappa_i|^2 \leq |1 + lk|^2 =: C/4,$$

where C is a positive constant and $C/4$ tends to 1 as h (and therefore λ) tends to 0.

Altogether, we obtain a uniform upper bound for $\|\mathrm{d}\psi^T \mathrm{d}\psi\|$,

$$\|\mathrm{d}\psi^T \mathrm{d}\psi\| \leq C .$$

From this, it follows that $\|\mathrm{d}\psi\| \leq \sqrt{C}$ is also bounded. As π is the inverse of the bijective mapping ψ , we finally get that $\mathrm{d}\pi$ has a uniform lower bound

$$c \leq \|\mathrm{d}\pi\| .$$

(a) In order to show the first statement, we express λ alternatively by its pullback $\lambda \circ \pi$ to \mathbf{K} via π :

$$(\lambda \circ \pi)(\mathbf{x}) = \langle N(\pi(\mathbf{x})), \pi(\mathbf{x}) - \mathbf{x} \rangle .$$

Restricted to \mathbf{T} , the derivative of this pullback is directly related to the angle α between the surface normals of \mathcal{S} and \mathbf{T} . Indeed, let u be a unit tangent vector to \mathbf{T} , then it holds

$$\mathrm{d}(\lambda \circ \pi)(u) = \langle \mathrm{d}N(\mathrm{d}\pi(u)), \pi(\mathbf{x}) - \mathbf{x} \rangle + \langle N(\pi(\mathbf{x})), \mathrm{d}\pi(u) - u \rangle .$$

Using that $\mathrm{d}\pi(u)$ and $\mathrm{d}N(\mathrm{d}\pi(u))$ are tangential to \mathcal{S} whereas $\pi(\mathbf{x}) - \mathbf{x}$ and $N(\pi(\mathbf{x}))$ are normal, it follows

$$\mathrm{d}(\lambda \circ \pi)(u) = \langle N(\pi(\mathbf{x})), u \rangle$$

and consequently

$$|\mathrm{d}(\lambda \circ \pi)| \leq |\sin \alpha| .$$

It was shown in [MT04] that this angle scales like $h_{\mathbf{T}}$ in the maximum norm, hence we get that $\|\mathrm{d}(\lambda \circ \pi)\| = \|\mathrm{d}\lambda \mathrm{d}\pi\| \sim h_{\mathbf{T}}$. With $\|\mathrm{d}\lambda\| = \sup_{|u|=1} \frac{|\mathrm{d}\lambda(\mathrm{d}\pi(u))|}{|\mathrm{d}\pi|}$ and given that by the previous statement $\|\mathrm{d}\pi\|$ is uniformly bounded below, it follows that $\mathrm{d}\lambda$ also scales like $h_{\mathbf{T}}$.

(b) The second statement follows immediately by integration: if the derivative $\mathrm{d}\lambda$ grows at most at rate $h_{\mathbf{T}}$, λ can at most grow at rate $h_{\mathbf{T}}^2$. \square

Lemma 4.3. *Let \mathcal{S} and \mathbf{K} satisfy the assumptions of 4.3.1. Then, in any point $\mathbf{x} \in \mathbf{K}$*

$$\begin{aligned} \|I|_{\pi(\mathbf{x})} - I|_{\mathbf{x}}\|_M &\leq Ch^2 \\ \|II_n|_{\pi(\mathbf{x})} - II_n|_{\mathbf{x}}\|_M &\leq Ch \end{aligned}$$

where C is a positive constant depending on the properties of \mathcal{S} and the shape regularity of \mathbf{K} .

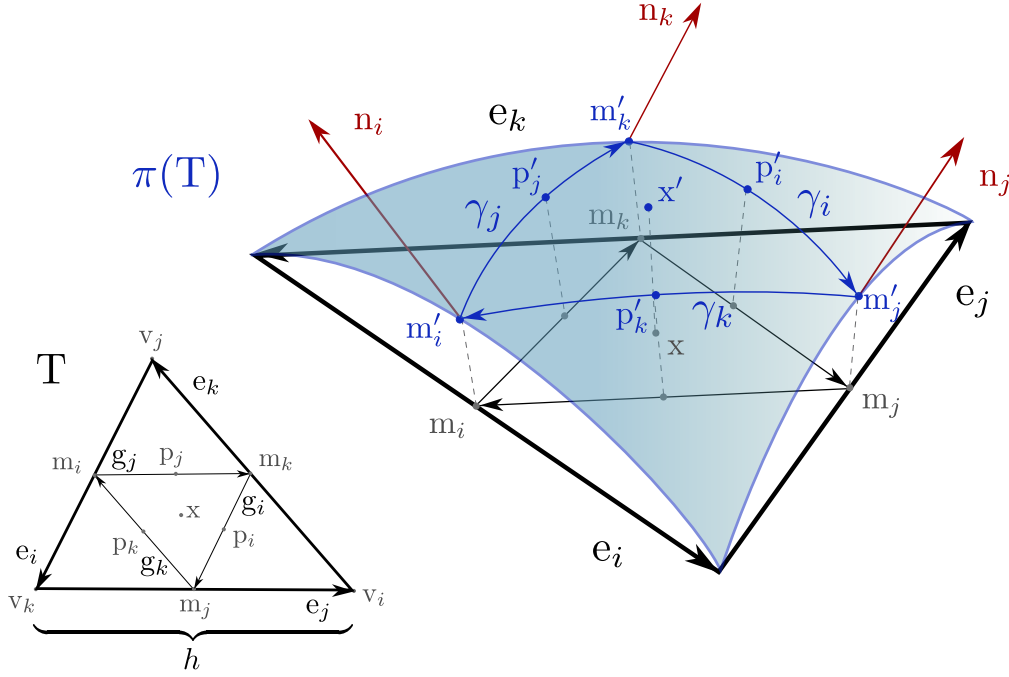


Fig. 4.1 A triangle T and its image $\pi(T)$ on the smooth surface \mathcal{S} with the corresponding notations. Gray dashed lines connect points on T with their corresponding image on \mathcal{S} .

Proof. First, we introduce several notations, illustrated by Figure 4.1. Consider a triangle T of K and its image $\pi(T) \subset \mathcal{S}$. The scalar coefficient c will denote different constants independent of h , but depending on the geometry of \mathcal{S} and K . Indices i, j, k will designate a cyclic permutation of indices 1, 2, 3.

Let g_i denote the parametrized segments connecting edge midpoints m_k, m_j , in T , such that

$$g_i : [0, h_i/2] \rightarrow K, \quad g_i(0) = m_k, \quad g_i(h_i/2) = m_j,$$

and let

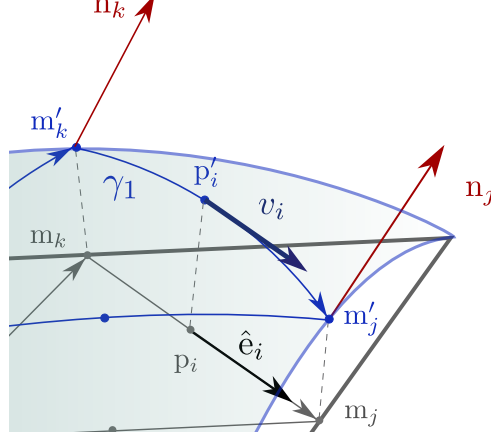
$$\gamma_i := \pi \circ g_i : [0, h_i/2] \rightarrow \mathcal{S}$$

be the normal projection of g_i on the smooth surface. Also, let $p_i := g_i(h_i/4)$ be the midpoint of g_i , and let

$$\begin{aligned} \hat{e}_i &:= g'_i(h_i/4) \\ v_i &:= \gamma'_i(h_i/4) = d\pi(\hat{e}_i). \end{aligned}$$

Notice that \hat{e}_i is a unit vector parallel to the edge vector e_i and $v_i := \gamma'_i(h_i/4)$ is a tangent vector to \mathcal{S} in p'_i .

For the proof of the statement about the second fundamental form, we will proceed in three steps.



(i) It holds $\underline{\underline{\Pi_n|_{p'_i}(v_i) = \Pi_n|_{p_i}(\hat{e}_i) + \mathcal{O}(h)}}}$.

As we consider γ_i as a mapping in \mathbb{R}^3 , we can approximate $d\pi(\hat{e}_i) = v_i$ by a central finite difference approximation

$$v_i = \frac{2}{h_i}(m'_j - m'_k) + \mathcal{O}(h^2) .$$

Similarly, for the director field n it holds

$$dn(v_i)|_{p'_i} = \frac{2}{h_i}(n(m'_j) - n(m'_k)) + \mathcal{O}(h^2) .$$

By definition we have $\Pi_n|_{p'_i}(v_i) = \langle dn(v_i)|_{p'_i}, v_i \rangle$ and obtain

$$\Pi_n|_{p'_i}(v_i) = \frac{4}{h_i^2} \langle n(m'_j) - n(m'_k), m'_k - m'_j \rangle + \mathcal{O}(h^2) ,$$

and by inserting the definition of the discrete directors $\{n_i\}_i$ it writes

$$\Pi_n|_{p'_i}(v_i) = \frac{4}{h_i^2} \langle n_j - n_k, m'_k - m'_j \rangle + \mathcal{O}(h^2) .$$

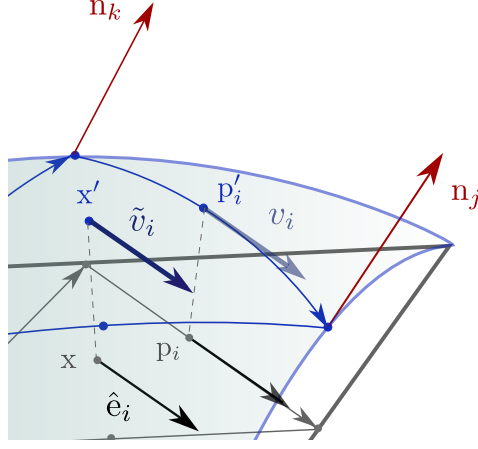
According to statement (b) of the previous lemma, $\lambda : \mathcal{S} \rightarrow \mathbb{R}$ is of order h^2 , hence $m_i = m'_i + \mathcal{O}(h^2)$. It follows

$$\begin{aligned} \Pi_n|_{p'_i}(v_i) &= \frac{4}{h_i^2} \langle n_j - n_k, m_k - m_j \rangle + \mathcal{O}(h^2) \\ &= \frac{2}{h_i^2} \langle n_j - n_k, v_k - v_j \rangle + \mathcal{O}(h^2) . \end{aligned}$$

By definition of the discrete quadratic form Π_n we finally obtain

$$\Pi_n|_{p'_i}(v_i) = \Pi_n|_{p_i}(\hat{e}_i) + \mathcal{O}(h^2) .$$

%



(ii) It holds $II_n|_{\mathbf{x}'}(\tilde{v}_i) = II_n|_{\mathbf{x}}(\hat{e}_i) + \mathcal{O}(h)$.

Let \mathbf{x} denote some arbitrary point in T . Let us keep denoting by \hat{e}_i the translation of \hat{e}_i to \mathbf{x} , and set $\tilde{v}_i := d\pi_{\mathbf{x}}(\hat{e}_i)$.

As on T $d\pi$ is smooth (because \mathcal{S} is smooth), we can consider $d\pi_{(\cdot)}(\hat{e}_i)$ as a function of the point where it is evaluated and get the approximation

$$\|\tilde{v}_i - v_i\|_{\mathbb{R}^3} = \|d\pi_{\mathbf{x}}(\hat{e}_i) - d\pi_{p_i}(\hat{e}_i)\|_{\mathbb{R}^3} \leq c\|\mathbf{x} - p_i\|_{\mathbb{R}^3} \leq \frac{c}{2}h .$$

As n is assumed smooth, the change of dn from p'_i to \mathbf{x}' is bounded by the geodesic distance from \mathbf{x}' to p'_i on \mathcal{S} , hence by h ([MT04]).

Thus, the change of dn is bounded by h and the vectors v_i, \tilde{v}_i , as well as the points \mathbf{x}', p'_i , are close to each other with respect to h . Thus it holds

$$|II_n|_{\mathbf{x}'}(\tilde{v}_i) - II_n|_{p'_i}(v_i)| = |\langle dn_{\mathbf{x}'}(\tilde{v}_i), \tilde{v}_i \rangle - \langle dn_{p'_i}(v_i), v_i \rangle| \leq a_3 h .$$

Using that II_n is constant on T and including (i) finally gives

$$\begin{aligned} |II_n|_{\mathbf{x}'}(\tilde{v}_i) - II_n|_{\mathbf{x}}(\hat{e}_i)| &\leq |II_n|_{\mathbf{x}'}(\tilde{v}_i) - II_n|_{p'_i}(v_i)| + |II_n|_{p'_i}(v_i) - II_n|_{p_i}(\hat{e}_i)| \\ &\leq ch . \end{aligned}$$

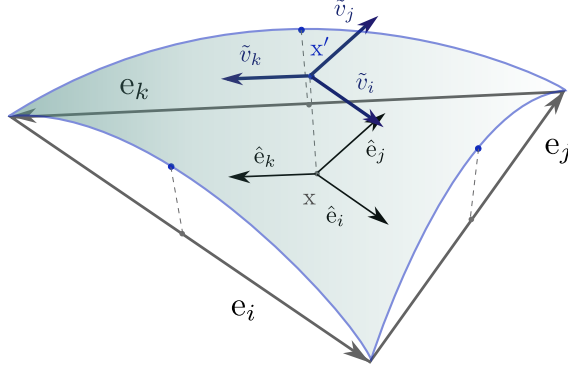
%

(iii) It follows $\|II_n|_{\mathbf{x}'}\|_M^2 - \|II_n|_{\mathbf{x}}\|_M^2 \leq Ch$.

The formula for quadratic forms derived in (4.1) holds similarly for $II_n|_{\mathbf{x}'}$ and $II_n|_{\mathbf{x}}$. Moreover, the expression still holds if the 3 directions used to evaluate the form do not form a triangle, except for the simplification of the cross product.

By use of (ii), all the corresponding components in these expressions differ by order h , hence the corresponding quadratic forms only differ by order h and we obtain the statement

$$\|II_n|_{\mathbf{x}'} - II_n|_{\mathbf{x}}\|_M \leq Ch .$$



%

One could proceed in a similar way to get the statement of the lemma for the consistency error of the first fundamental form. An alternative way is to recognize that the difference between the smooth and the discrete first fundamental forms is the metric distortion induced by the normal projection π or, equivalently, by its inverse mapping ψ .

Therefore, we can make use of the properties of the metric distortion $A = P \cdot Q^{-1} \cdot P$ already mentioned in the proof of Lemma 4.2. Indeed, λ is of order h^2 , such that for an eigenvalue of P we have $1 - \lambda\kappa_i = \mathcal{O}(1 + h^2)$. Moreover, the angle α is of order h , hence for the non-constant eigenvalue of Q we also get $(\cos \alpha)^2 = \mathcal{O}(1 + h^2)$. It follows that A approaches the identity by order h^2 in the operator norm. As we are considering a finite dimensional space, all norms are equivalent, and we get

$$\|I - \mathbf{I}\|_M \leq Ch^2 .$$

□

We can now deduce the consistency error of the membrane and bending energies with respect to the L^2 -norm.

Let ϕ^*I, ϕ^*II_n , denote the pullbacks of the fundamental forms of the deformed smooth surface to the undeformed smooth surface

$$\begin{aligned} \phi^*I(\bar{v}_i) &= I(d\phi(\bar{v}_i)) = \langle d\phi(\bar{v}_i), d\phi(\bar{v}_i) \rangle \\ \phi^*II_n(\bar{v}_i) &= II_n(d\phi(\bar{v}_i)) = \langle dn(d\phi(\bar{v}_i)), d\phi(\bar{v}_i) \rangle . \end{aligned}$$

Let the deformed edge e_i be given by

$$e_i = \phi(v_k) - \phi(v_j) ,$$

and let $m_i = \frac{1}{2}(\phi(\bar{v}_j) + \phi(\bar{v}_k))$ be its midpoint. Then we can define the pullbacks of the discrete fundamental forms by

$$\begin{aligned} \Gamma^*(\hat{e}_i) &:= \langle \hat{e}_i, \hat{e}_i \rangle \\ \Pi_n^*(\hat{e}_i) &:= 2\langle n(m_j) - n(m_k), \hat{e}_i \rangle . \end{aligned}$$

Proposition 4.1. *Let $\bar{\mathcal{S}}, \bar{\mathcal{K}}$, and \mathcal{S}, \mathcal{K} , satisfy the assumptions of 4.3.1. Then*

$$\left| \int_{\bar{\mathcal{S}}} \|\phi^* I - \bar{I}\|_M^2 d\bar{A} - \int_{\bar{\mathcal{K}}} \|\mathbf{I}^* - \bar{\mathbf{I}}\|_M^2 d\bar{A} \right| \leq \tilde{C}h^2$$

$$\left| \int_{\bar{\mathcal{S}}} \|\phi^* \mathbf{II}_n - \bar{\mathbf{II}}_n\|_M^2 d\bar{A} - \int_{\bar{\mathcal{K}}} \|\mathbf{II}_n^* - \bar{\mathbf{II}}_n\|_M^2 d\bar{A} \right| \leq Ch$$

where C is a positive constant depending on the properties of \mathcal{S} and the shape regularity of \mathcal{K} .

Proof. On the undeformed surface, we can directly apply the results of the previous lemma to get the pointwise estimate

$$\|\bar{I} - \bar{\mathbf{I}}\|_M \leq Ch^2$$

$$\|\bar{\mathbf{II}}_n - \bar{\mathbf{II}}_n\|_M \leq Ch .$$

For the deformed fundamental forms however, we have to show that for the pullbacks $\phi^* I, \phi^* \mathbf{II}_n$, of the fundamental forms of the smooth deformed surface and for the discrete fundamental forms $\mathbf{I}^*, \mathbf{II}_n^*$, we still have

$$\|\phi^* I - \mathbf{I}^*\| \leq Ch^2$$

$$\|\phi^* \mathbf{II}_n - \mathbf{II}_n^*\| \leq Ch .$$

First, by finite difference approximation, we have

$$\begin{aligned} d\phi(\bar{v}_i) &= \frac{1}{h}(\phi(\bar{v}_j) - \phi(\bar{v}_k)) + \mathcal{O}(h^2) \\ &= \hat{e}_i + \mathcal{O}(h^2) . \end{aligned} \tag{4.5}$$

Thus for the first fundamental form we immediately get

$$\begin{aligned} \phi^* I(\bar{v}_i) &= \langle \hat{e}_i, \hat{e}_i \rangle + \mathcal{O}(h^2) \\ &= \mathbf{I}^*(\hat{e}_i) + \mathcal{O}(h^2) . \end{aligned}$$

In order to get the approximation for the second fundamental form, we need to show that

$$\mathbf{m}_i' = \phi(\bar{\mathbf{m}}_i') + \mathcal{O}(h^2) . \tag{4.6}$$

Then

$$n(\phi(\bar{\mathbf{m}}_i')) = n(\mathbf{m}_i') + \mathcal{O}(h^2) = n_i + \mathcal{O}(h^2) .$$

follows because of the smoothness of n , and this eventually implies

$$dn(d\phi(\bar{v}_i)) = \frac{2}{h}(n_j - n_k) + \mathcal{O}(h^2) .$$

To prove (4.6), we first notice that $\mathbf{m}_i' = \mathbf{m}_i + \mathcal{O}(h^2)$, such that it is sufficient to show $\mathbf{m}_i = \phi(\bar{\mathbf{m}}_i') + \mathcal{O}(h^2)$. Then, we can consider the undeformed edge \bar{e}_i as a

parametrized path, $\bar{e}_i : [0, h] \rightarrow \mathbb{R}^3$, with $\bar{e}_i(0) = \bar{v}_j$, $\bar{e}_i(h) = \bar{v}_k$ and $\bar{e}_i(h/2) = \bar{m}_i$. We further define a path ξ on \mathcal{S} by

$$\xi(t) := \phi \circ \bar{\pi} \circ \bar{e}_i(t) ,$$

which is the image by ϕ of the projection of \bar{e}_i on the smooth surface $\bar{\mathcal{S}}$. This path can be used to rewrite m_i and $\phi(\bar{m}'_i)$ as

$$\begin{aligned} m_i &= \frac{1}{2}(\xi(0) + \xi(h)) \\ \phi(\bar{m}'_i) &= \xi(h/2) . \end{aligned}$$

Equation (4.6) then follows by inserting the Taylor expansion of ξ in h and in $h/2$.

Combining (4.5) and (4.6), we get

$$\phi^* II_n(\bar{v}_i) = II_n^*(\hat{e}_i) + \mathcal{O}(h^2) .$$

From the approximations of the directional evaluations of the pullback of the fundamental forms, step (ii) and (iii) of the proof of Lemma 4.3 go through and we get

$$\begin{aligned} \|\phi^* I - I^*\|_M &\leq Ch^2 \\ \|\phi^* II_n - II_n^*\|_M &\leq Ch . \end{aligned}$$

To prove the statement of the proposition, it is now sufficient to apply triangle inequalities repeatedly. For the first fundamental form, we get, in the weighted Frobenius norm $\|\cdot\|_M$,

$$\begin{aligned} \|\phi^* I - \bar{I}\|_M &= \|\phi^* I - I^* + I^* - \bar{I}\|_M \\ &= \|I^* - \bar{I}\|_M + \mathcal{O}(h^2) , \end{aligned}$$

and

$$\begin{aligned} \|I^* - \bar{I}\|_M &= \|I^* - \bar{I} + \bar{I} - \bar{I}\|_M \\ &= \|I^* - \bar{I}\|_M + \mathcal{O}(h^2) . \end{aligned}$$

Thus we obtain

$$| \|\phi^* I - \bar{I}\|_M^2 - \|I^* - \bar{I}\|_M^2 | = \mathcal{O}(h^2) .$$

The same procedure yields the estimate for the second fundamental form:

$$| \|\phi^* II_n - \bar{II}_n\|_M^2 - \|II_n - \bar{II}_n\|_M^2 | = \mathcal{O}(h) .$$

To get the statement of the proposition, we then have to integrate over the corresponding surfaces. As $|\det d\pi|$ is of order $1 + \mathcal{O}(h^2)$, we get

$$\begin{aligned} \int_{\bar{\mathcal{S}}} \|\phi^* I - \bar{I}\|_M^2 d\bar{A} - \int_{\bar{K}} \|I^* - \bar{I}\|_M^2 d\bar{A} &= \int_{\bar{K}} (\|\phi^* I - \bar{I}\|_M^2 |\det d\pi| - \|I^* - \bar{I}\|_M^2) d\bar{A} \\ &\leq Ch^2 . \end{aligned}$$

Similarly, for the second fundamental form we obtain

$$\int_{\mathcal{S}} \|\phi^* H_n - \bar{H}_{\bar{n}}\|_M^2 d\bar{A} - \int_{\bar{K}} \|\Pi_n^* - \bar{\Pi}_{\bar{n}}\|_M^2 d\bar{A} \leq Ch .$$

□

4.4 Relation to existing constant strain models

4.4.1 Geometric reformulation of the constant strain triangle

For the membrane energy, the presented discrete model recovers the widely used constant strain triangle (CST) that results from piecewise linear interpolation (M_0^1) of the positions. This relation was already mentioned in [GSH⁺04] where the membrane strains were expressed very similarly. It can be made explicit by elementary manipulations of the stiffness matrix of the M_0^1 basis functions expressed in barycentric (triangular) coordinates. As this calculation does not provide any further insight, we will omit it.

4.4.2 Connection to the triangular Morley element

In the last chapter, we noticed that it is crucial for a shearable shell model to provide reliable predictions when shearing is constrained to vanish, *i.e.*, in the Kirchhoff limit, as this behaviour is strongly related to its susceptibility to shear locking.

With our definition of shearing, imposing the Kirchhoff assumption implies that every director n_i is forced to stay orthogonal to its corresponding edge e_i and is thus left with a single degree of freedom which can be seen as a *turning angle* around the edge axis.

More precisely, on an edge e_i shared by triangles T and \tilde{T} , let α_i be the angle between the (unsheared) director n_i and the triangle normal N of T , in the plane orthogonal to the edge e_i (see Fig. 4.2). Then we can write the director n_i as

$$n_i = \cos(\alpha_i)N + \sin(\alpha_i) \hat{e}_i^* ,$$

and eventually obtain

$$\Pi_n(e_i) - \Pi_n(e_j) - \Pi_n(e_k) = -\frac{8A_T}{|e_i|} \sin(\alpha_i) .$$

Inserting this in (4.1) and using the rescaled basis $\{|\bar{e}_i|^2 (\bar{\hat{e}}_i^* \otimes \bar{\hat{e}}_i^*)\}_{i=1,2,3}$ (where \hat{e}^* denotes the rotated unit edge), we obtain the following Kirchhoff version of our second fundamental form:

$$\Pi_{\text{Kirchhoff}} := \sum_{i=1}^3 \frac{\sin(\alpha_i)}{h_i/2} \bar{\hat{e}}_i^* \otimes \bar{\hat{e}}_i^* . \quad (4.7)$$

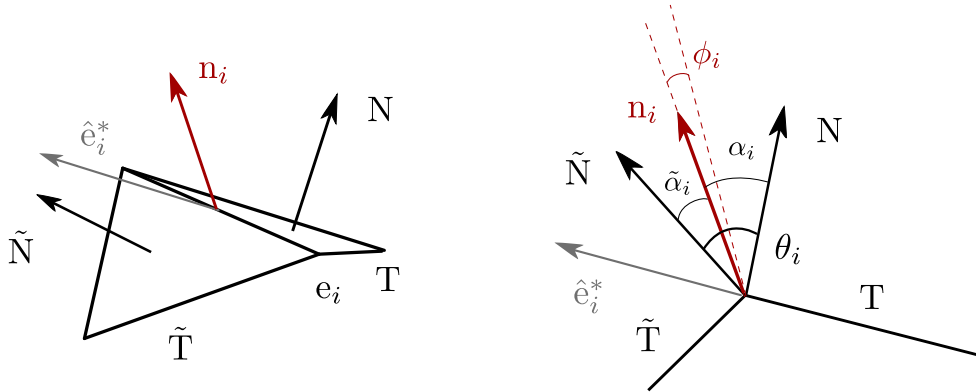


Fig. 4.2 T and \tilde{T} are neighboring triangles with common edge e_i . \hat{e}_i^* is the unit edge, rotated by 90 degrees in the plane of T . The angle θ_i is the angle between the adjacent face normals N and \tilde{N} ; $\alpha_i, \tilde{\alpha}_i$ denote the angles between the director \mathbf{n}_i and N, \tilde{N} respectively. ϕ_i is the angle between \mathbf{n}_i and the angle bisecting direction.

The height h_i of the triangle T appears through $2A_T = |e_i| \cdot h_i$.

This Kirchhoff formulation points out a close relation to the so-called Morley triangle [Mor71], which was later reintroduced as the low-order Kirchhoff plate element DKT6 [BZH01]. The non-conforming finite element space corresponding to this element can be written as

$$\mathcal{M} := \{v \in P^2(T) \mid \int_e [\nabla v \cdot \hat{e}^*] ds = 0 \quad \forall \text{ edges } e\} \quad (4.8)$$

where $[\cdot]$ denotes the difference in values (component-wise) from one element to the another across a common edge. In words, these are piecewise quadratic functions which are continuous at vertices, and whose edge tangential projection is continuous at edge midpoints. A possible set of degrees of freedom of this Kirchhoff plate element are the values of the displacement w_h of the vertices and the derivative $\nabla w_h \cdot \hat{e}_i^*$ in normal direction to the edge at edge midpoints. This derivative is a scalar value, that can be used to approximate the rotation angle α_i at the edge midpoint, and thus provides the relation to the above-mentioned Kirchhoff model.

Nonlinear versions of the Morley element for shell models (which also treat the membrane strains with CST) are the model proposed by van Keulen and Boijj [vKB96] on the finite element side, and the discrete mid-edge shape operator (MSO) derived in [GGRZ06] from the geometric view.

The shape operator MSO was numerically shown to be extremely robust to mesh structure, especially compared to other current low-order operators estimating curvature, including quadratic fit and the cotangent formula. The shell model derived in this thesis provides a shear-deformable version of this operator, and thereby generalizes it to a wider range of applications, while inheriting its robustness with respect to mesh-structure.

Lemma 4.4. *For shallow shells and for sufficiently fine mesh resolutions, the Kirchhoff limit of the discrete second fundamental form corresponds to the mid-edge shape operator.*

Proof. Let Λ denote the mid-edge shape operator on a triangle T . It is defined by means of a finite difference approximation of the change of particularly defined mid-edge normals m_i given by

$$m_i = N + (\theta_i/2 + s_i\phi_i)e_i^* .$$

As before, N is the face normal of T , θ_i is the angle between the face normals of T and of the neighbouring triangle \tilde{T} , s_i equals ± 1 , and ϕ_i designates the *free* angle between m_i and the angle bisecting direction (see Fig. 4.2). The directional evaluations of the shape operator Λ along edges are given by

$$\begin{aligned} \Lambda(e_i) &:= 2 \langle m_k - m_j, e_i \rangle \\ &= 2 ((\theta_k/2 + s_k\phi_k)e_i \cdot e_k^* - (\theta_j/2 + s_j\phi_j)e_i \cdot e_j^*) . \end{aligned}$$

If the angles θ_i and ϕ_i are small, which is for example the case for shallow shells or for sufficiently fine triangulations, the director n_i of the Cosserat model can be expressed as

$$\begin{aligned} n_i &= N + (\theta_i/2 + s_i\phi_i)e_i^* + \sin(\psi_i) e_i \\ &= m_i + \sin(\psi_i) e_i , \end{aligned}$$

where ψ_i is the signed shear angle in direction of e_i .

The values of Π_n along edges are then given by

$$\Pi_n(e_i) = \Lambda_i + 2 (\sin(\psi_j)e_i \cdot e_j - \sin(\psi_k)e_i \cdot e_k) .$$

In particular, for vanishing shear angle $\psi_i = 0$, we get $\Pi_n(e_i) = \Lambda(e_i)$, and hence the corresponding quadratic forms are equal.

□

4.4.3 The geometry of rotation-free elements

Closely related to the Morley triangle –conceptually as well as analytically– are so-called *rotation-free shell elements*. However, whereas for the Morley triangle the angle at edge midpoints is *a priori* free, rotation-free elements –as their name suggests– get rid of this rotation by prescribing the angle by the vertex positions of the neighbouring triangles, following some specific rule.

In their very enlightening investigation of various rotation-free models [GT07], Gaerdsback and Tibert point out that several of these models rely on a same procedure to generate an operator measuring two-dimensional curvature by a linear

superposition of 3 one-dimensional curvature measures. Yet, this superposition is considered by the authors as ad hoc, as "no exact relation exists" between these quantities of different dimensions. The geometric perspective of our construction not only provides a rigorous justification of this relation through (4.7). It also allows to correctly interpret the involved quantities, as it turns out that this common superposition procedure actually corresponds to the construction of a discrete second fundamental form per triangle in our geometric sense through

$$\mathbb{I}_{\text{rotation-free}} := \sum_{i=1}^3 \kappa_i \bar{\mathbf{e}}_i^* \otimes \bar{\mathbf{e}}_i^* .$$

where $\{\kappa_i\}_{i=1,2,3}$ are prescribed directional curvatures. This makes also clear that by this method, the one-dimensional curvatures $\{\kappa_i\}_{i=1,2,3}$ that are considered as normal curvatures *across* edges (e.g. by an integrated hinge angle) are effectively not used as such. A discrete second fundamental form with curvatures $\{\kappa_i\}_{i=1,2,3}$ across edges, *i.e.*, along rotated unit edges $\bar{\mathbf{e}}_i^*$ should in contrast be written as

$$\tilde{\mathbb{I}}_{\text{rotation-free}} := \sum_{i=1}^3 (\kappa_i - \kappa_j - \kappa_k) \bar{\mathbf{e}}_i \otimes \bar{\mathbf{e}}_i$$

(compare to (4.1)).

Remarks.

1. It is well known that the accuracy of such rotation-free elements (and low-order elements in general) can strongly depend on the specific shape of the mesh and the position of the mesh with respect to the considered geometry. By providing a correct intuition of what geometric entity is actually used as curvature, the insight we worked out in this last section is useful to understand for which mesh-patterns and geometries a particular definition of curvature is particularly suitable and for which it might break down.

2. It is a comfortable side effect of the uniform description of the membrane and the bending strains in terms of structure that the same code can basically be reused, which eases the implementation considerably (see Appendix).

Chapter 5

DCS: A Discrete Cosserat Shell model

The approaches to discretization preferred in different areas often have little in common.

Denis Zorin [Zor05]

In this chapter, we present the Discrete Cosserat Shell (DCS) model that proceeds from the investigations of the previous chapters. The resulting model turns out to be an enhancing geometric reformulation of a Reissner-Mindlin shell element proposed by Flores *et al.* [FOZ95], and provides in particular an alternative interpretation of the assumed strain approach of this model. The last two sections are dedicated to theoretical and numerical validations.

5.1 Discrete model

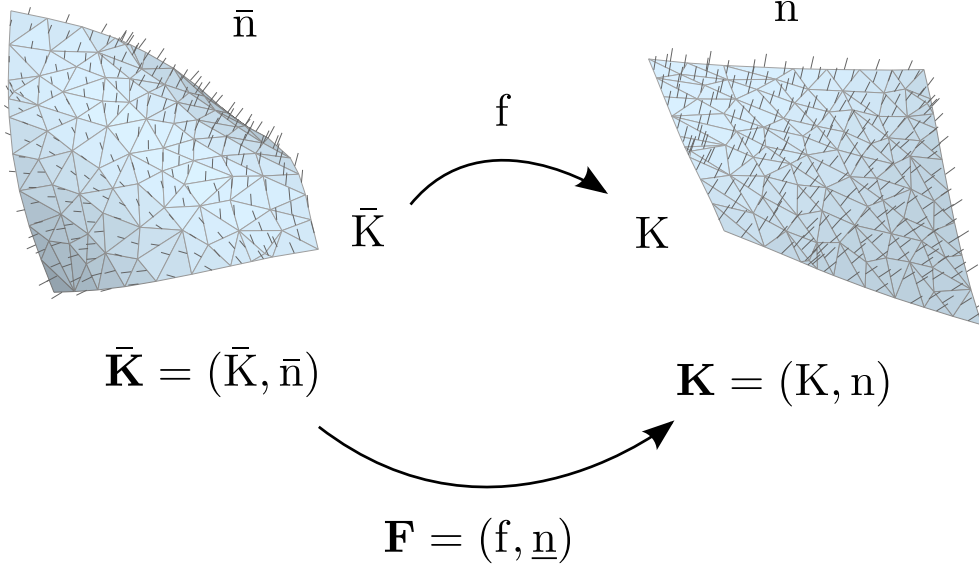
Definition 5.1. A *discrete shell* $\mathbf{K} = (\mathbf{K}, \mathbf{n}, t)$ is composed of an embedded 2-dimensional simplicial surface $\mathbf{K} = (\mathbf{V}_\mathbf{K}, \mathbf{E}_\mathbf{K}, \mathbf{T}_\mathbf{K})$ with vertices $\mathbf{V}_\mathbf{K}$, edges $\mathbf{E}_\mathbf{K}$, and triangular faces $\mathbf{T}_\mathbf{K}$, a *unit* director field \mathbf{n} based on edge midpoints, and a thickness $t \in \mathbb{R}$.

Definition 5.2. A *deformation* of a discrete initial configuration $\bar{\mathbf{K}} = (\bar{\mathbf{K}}, \bar{\mathbf{n}}, t)$ is a mapping

$$\mathbf{F} = (\mathbf{f}, \underline{\mathbf{n}}) : \bar{\mathbf{K}} \rightarrow \mathbf{K}$$

where \mathbf{f} maps each vertex to a point in \mathbb{R}^3 , and $\underline{\mathbf{n}}$ associates a unit director with each *undeformed* edge.

The deformed shell \mathbf{K} is the discrete shell whose simplicial mid-surface is defined by vertices $\mathbf{V}_\mathbf{K} = \mathbf{f}(\bar{\mathbf{V}}_\mathbf{K})$, with the same connectivity as $\bar{\mathbf{K}}$, and the director field $\underline{\mathbf{n}} = \mathbf{n}$ associated with its edges.



Just as in the smooth case, we will assume that undeformed configurations are unsheared, *i.e.*, undeformed directors are all orthogonal to their corresponding edge. As this does not completely pin down their position, we additionally assume that they all point on the same side of the mid-surface, and minimize the induced bending energy.

Remark. The proof for consistency of the last chapter is not affected by this assumption. Indeed, although the pullback $\bar{n}(\pi(m_e)) = \bar{N}(\pi(m_e))$ must not be orthogonal to the edge e , and hence the discrete director field only approximately samples the smooth director field, this approximation is still good enough given that the smooth surface normal is perpendicular to the edge up to second order [GGRZ06].

Discrete stretching and bending energies First and generalized second fundamental forms were defined as discrete quadratic forms, constant per triangle, determined by 3 edge-values as given in (4.2) and (4.3). The values for the undeformed and deformed first fundamental forms have the expressions

$$\begin{aligned} \bar{I}_{\Gamma}(\bar{\mathbf{e}}_i, \bar{\mathbf{e}}_i) &:= \langle \bar{\mathbf{v}}_k - \bar{\mathbf{v}}_j, \bar{\mathbf{v}}_k - \bar{\mathbf{v}}_j \rangle = \|\bar{\mathbf{e}}_i\|^2 \\ I_{\Gamma}(\bar{\mathbf{e}}_i, \bar{\mathbf{e}}_i) &:= \langle f(\bar{\mathbf{v}}_k) - f(\bar{\mathbf{v}}_j), f(\bar{\mathbf{v}}_k) - f(\bar{\mathbf{v}}_j) \rangle = \|\mathbf{e}_i\|^2 . \end{aligned} \quad (5.1)$$

For the generalized second fundamental forms we have

$$\begin{aligned} \bar{\Pi}_{\bar{\mathbf{n}}, \Gamma}(\bar{\mathbf{e}}_i, \bar{\mathbf{e}}_i) &:= 2\langle \bar{\mathbf{n}}_k - \bar{\mathbf{n}}_j, \bar{\mathbf{e}}_i \rangle \\ \Pi_{\mathbf{n}, \Gamma}(\bar{\mathbf{e}}_i, \bar{\mathbf{e}}_i) &:= 2\langle \mathbf{n}_k - \mathbf{n}_j, \mathbf{e}_i \rangle . \end{aligned} \quad (5.2)$$

Here, we directly define the pullback of the deformed fundamental forms on the undeformed configuration, as described in Section 4.2.

Discrete shear form The discrete shear form is a discrete one-form, again defined by values on edges. These values are the projection of the director on the discrete edge-based tangent plane as defined in (3.6):

$$s_n(e_i) = |\underline{n}_i^{\text{tan}}|^2 = \langle \underline{n}_i, \hat{e}_i \rangle^2 .$$

To obtain the actual piece-wise linear one-form s_n from these values, one simply uses a Whitney one-form interpolation scheme as described in the appendix.

We also refer to the appendix for the details of the actual implementation of the energies.

Discrete Cosserat Energy Altogether, we obtain the total elastic energy of DCS for isotropic homogeneous materials:

$$W = \frac{1}{2} \sum_{T \in T_K} \left(A_T \left(\frac{t}{4} \|\mathbf{I}_T - \bar{\mathbf{I}}_T\|_M^2 + \frac{t^3}{12} \|\mathbf{II}_{n,T} - \bar{\mathbf{II}}_{n,T}\|_M^2 \right) + t\kappa G \int_T |s_n|^2 dA \right) . \quad (5.3)$$

The sum is over triangular faces T_K , and A_T denotes, as before, the area of such a face. The material norm $\|\cdot\|_M^2$ and the shear modulus G are the same as in the remarkably similar smooth energy (2.2).

Again, this formulation can easily be extended to non-isotropic materials.

5.2 A geometric justification of assumed strains

Our discrete energy formulation can easily be translated to the FE language. As already mentioned in the last chapter, the membrane energy corresponds to the energy resulting from a piecewise linear conforming interpolation of vertex positions. The bending energy results from a piecewise linear non-conforming interpolation of the directors based on midpoints, whereas the shearing field is a lowest order Raviart-Thomas interpolation of the directors' projection onto the edges.

DCS may thus be seen as a geometric reformulation of the shell element TLLL considered by Flores *et al.* [FOZ95]. However, a doubt persists as it does not become clear how the shearing part of TLLL is exactly evaluated. What is stated explicitly though, is that the shearing energy of this element is based on an assumed strain ansatz that postulates a linear shear field with constant edge tangential components [OZF94], and relies on a very particular choice of interpolated edge values.

The assumed strain ansatz is widely used in the construction of shear-deformable triangular shell elements, as well as in other elasto-plastic simulations where numerical difficulties are ubiquitous. For Reissner-Mindlin plates, the basic idea is very simple: to make sure that shearing can be zero independently of bending

contributions, the easy way out is to write down the shearing and bending strain matrices, deduce the relation that shearing must satisfy analytically in order to be able to vanish, and replace the initial shear strain matrix by a *substitute* shear strain matrix which does satisfy these relations [OZST92].

The difference of distinct assumed strain approaches lies in the construction of this substitute matrix. The most common approach is to sample shearing only in those points where the relation is satisfied, which leads to *reduced integration*. A seemingly more subtle approach (which still often recovers a reduced integration approach) is to *define* shear strains *a priori* such that they satisfy the previously identified relations, which can again be done in different ways [OZST92, BR97, NTRNXB08].

Assumed strain approaches as well as reduced integration methods are often disputed, since, albeit practically useful and theoretically justified in many cases (for example if they correspond to an easier numerical treatment of an equivalent mixed formulation [MH90]), they are often used incautiously, lacking rigorous analysis (see, *e.g.*, [CB03, Dvo95]). In any case, the shear strain is explicitly constructed such that in the discrete setting, the bothersome locking cannot occur. Although this approach is very pragmatic, it does not directly rely on a property of the initial smooth problem and might thus be considered as ad hoc [BBR00].

For DCS, if the shearing energy is essentially equivalent to the one obtained by the particular assumed strain ansatz of TLLL, it results from very different geometric arguments. Using only the edge-tangential parts of the directors, specifically at edge midpoints, results from the additional degree of freedom in the definition of discrete tangent planes, which was in turn motivated by the insight that measuring shear in this way corresponds to using the most reliable information of the mesh *exclusively*. From this, preserving the structure of shearing as a one-form naturally suggests the Raviart-Thomas interpolation of these values.

Remark. In Chapter 3, we also observed that a different definition of normals, in particular a definition completely prescribed by the vertex positions, is likely to lead to an unsuitable bending energy when shearing is constrained to zero. Hence our evaluation of shear also makes sure that shearing can vanish independently of bending, but this is a side effect of the approach rather than the actual motivation of our definition of shear strains.

5.3 Zero-energy configurations

The linear Reissner-Mindlin plate element corresponding to DCS was shown to be free of spurious modes [OZF94]. We will give an elementary geometric proof that *in practice* the same holds for the nonlinear model DCS, as the only zero-energy

configurations apart from global isometries are configurations where directors are *flipped*, *i.e.*, rotated by 180 degrees around the edge.

Proposition 5.1. *The discrete energy (5.3) has no zero-energy configurations except for global isometries of the undeformed configuration and flipping of directors.*

Proof. It is sufficient to show the statement for a single triangle. Let \bar{v}_i and \bar{n}_i be the 3 vertices and 3 directors of an undeformed configuration of a triangle. In particular, directors are unsheared, *i.e.*, orthogonal to their corresponding edges.

Let $(v_i, \underline{n}_i)_{i=1,2,3}$ be a prospective zero-energy configuration of the triangle. Stretching energy can only be zero if the edges have the same length as in the undeformed configuration. Given that the triangle is defined by these lengths up to global isometries, it follows that any configuration with zero membrane energy is a global rotation of the triangle. Hence, let discard global isometries of the triangle and set $v_i = \bar{v}_i$.

To find the possible positions of directors $\underline{n}_i = n_i$ that lead to zero energy, it is then sufficient to look at different configurations of the directors on a fixed triangle.

As usual, let $e_i = v_k - v_j$. In order to annul shearing and bending respectively, it must hold for $\{\underline{n}_i\}_{i=1,2,3}$:

$$\begin{cases} \langle \underline{n}_i - \bar{n}_i, e_i \rangle & = 0 \\ \langle (\underline{n}_k - \bar{n}_k) - (\underline{n}_j - \bar{n}_j), e_i \rangle & = 0, \end{cases} \quad (5.4)$$

where $(ijk) = (123)$ designates a cyclic permutation of indices. Hence, we have to prove that a solution \underline{n}_i to this system satisfies $\underline{n}_i = \pm \bar{n}_i$.

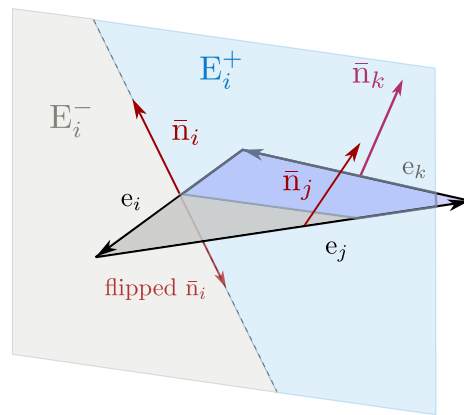


Fig. 5.1 E_i is the plane orthogonal to the edge e_i , containing \bar{n}_i . E_i^+ is the halfspace intersecting the triangle, E_i^- its complement. The bending energy is the same for $+\bar{n}_i$ or its *flipped* position $-\bar{n}_i$.

If we set $\delta \mathbf{n}_i := \underline{\mathbf{n}}_i - \bar{\mathbf{n}}_i$ as the difference of the directors, the use of $\mathbf{e}_i + \mathbf{e}_j + \mathbf{e}_k = 0$ yields

$$\begin{cases} \langle \delta \mathbf{n}_k, \mathbf{e}_i \rangle &= \langle \delta \mathbf{n}_j, \mathbf{e}_i \rangle \\ \langle \delta \mathbf{n}_k, \mathbf{e}_j \rangle &= \langle \delta \mathbf{n}_j, \mathbf{e}_k \rangle, \end{cases}$$

for the second equation. Consequently all the products $\langle \delta \mathbf{n}_i, \mathbf{e}_j \rangle$ for $i \neq j$ are equal, say to some $\alpha \in \mathbb{R}$. Taking into account the first equation of (5.4), a solution $\underline{\mathbf{n}}_i$ of the linear system needs to satisfy

$$\langle \delta \mathbf{n}_i, \mathbf{e}_j \rangle = \alpha \cdot (1 - \delta_{ij}) \quad \forall i, j = 1, 2, 3$$

where δ_{ij} is Kronecker's delta.

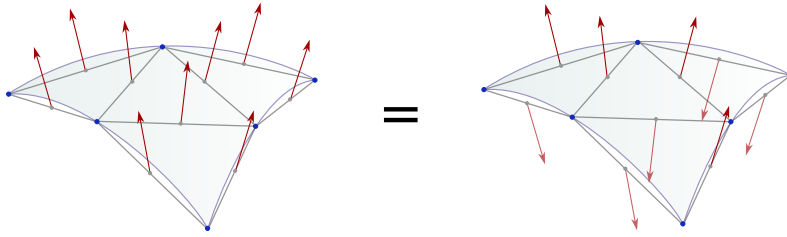
Hence $\delta \mathbf{n}_i$ is orthogonal to \mathbf{e}_i for all $i = 1, 2, 3$. By assumption on the undeformed configuration $\bar{\mathbf{n}}_i$ is orthogonal to \mathbf{e}_i , and therefore the deformed director $\underline{\mathbf{n}}_i$ is also orthogonal to \mathbf{e}_i .

Let E_i denote the plane orthogonal to \mathbf{e}_i that passes through the edge midpoint (see Fig. 5.1), which thus contains $\bar{\mathbf{n}}_i$ as well as $\underline{\mathbf{n}}_i$.

The direction of $\underline{\mathbf{n}}_i$ separates this plane in two half-spaces. Let E_i^+ denote the half-space of E_i which crosses the inside of the triangle, E_i^- its complement. Then there are 3 possibilities.

If $\delta \mathbf{n}_i$ lies in E_i^+ , then $\langle \delta \mathbf{n}_i, \mathbf{e}_j \rangle \geq 0$ and $\langle \delta \mathbf{n}_i, \mathbf{e}_k \rangle \leq 0$, such that $\alpha = 0$. By symmetry, the same holds for $\delta \mathbf{n}_i \in E_i^-$. Finally, if $\delta \mathbf{n}_i = \lambda \bar{\mathbf{n}}_i$ for some $\lambda \in \mathbb{R}$, then $\underline{\mathbf{n}}_i = \pm \bar{\mathbf{n}}_i$ because both $\underline{\mathbf{n}}_i$ and $\bar{\mathbf{n}}_i$ have unit length. □

This means that the energy is not only blind to a global change of orientation of the discrete surface, but simply rotating directors by 180 degrees *locally* does also not affect the energy.



However, for practical applications this is not an issue. To compute a deformation, we follow a principle of least energy and compute local minima of the elastic deformation energy. In particular, if we start from a configuration where all directors are on the same side of the surface, the directors will stay away from configurations that require high energy. Crossing the triangle plane in order to flip induces large bending energy, hence such a configuration will naturally be avoided as long as the step between two successive configurations is not so large that the corresponding energy well can be jumped over.

5.4 Numerical validation

As suggested by tests run with TLLL ([FOZ95]) and its underlying linear plate element ([OZF94]), DCS passes classical linear and nonlinear shell benchmark tests. Some representative results are presented here.

A note on boundary conditions In the following computations, the boundary conditions that are used are clamped and simply supported boundaries, and application of external loads and moments. To simulate simply supported boundaries, we simply fix the vertex degrees of freedom, and leave directors free. For clamped boundary conditions, we fix positional *and* director degrees of freedom. This interpretation of 'clamped' is sometimes called *soft clamped*, and in this case, shearing strains on the boundary do not need to vanish. Another variant, also called *hard clamped*, is to fix normals on the boundary *and* impose that directors and normals coincide there. A similar distinction can be made when applying moments. In our computations, we applied the moment to directors, without any further constraint on the shearing strains.

For a detailed discussion about boundary conditions for Kirchhoff and Cosserat shells, we refer to standard textbooks such as [CB03].

5.4.1 Analytic linear benchmarks

For small deformations of square and circular plates, analytic solutions for particular benchmarks are available, for Kirchhoff plates, Reissner-Mindlin plates and sometimes for the 3D model. A general method to obtain analytic solutions for arbitrary boundary conditions and more involved geometries is still a matter of research [BK04].

We tested DCS on clamped circular and square plates under uniform load. The convergence plots show the logarithm of the relative error with respect to the analytic solution of the most deflected point at full load against the logarithm of the *mesh density* ($\#$ elements) $^{-1/2}$ or the average *edge length* of the elements.

Circular plate under uniform load

For the circular plate of radius r under uniform load q , exact formulas exist for the deflections for clamped (w_c) and simply supported (w_{ss}) boundaries. If we call D the bending modulus, defined as $D := \frac{Et^3}{12(1-\nu^2)}$, these formulas correspond to [TWK59]:

Kirchhoff:

$$w_c^K = \frac{q r^4}{64 D} , \quad w_{ss}^K = \frac{(5 + \nu) q r^4}{64 D (1 + \nu)}$$

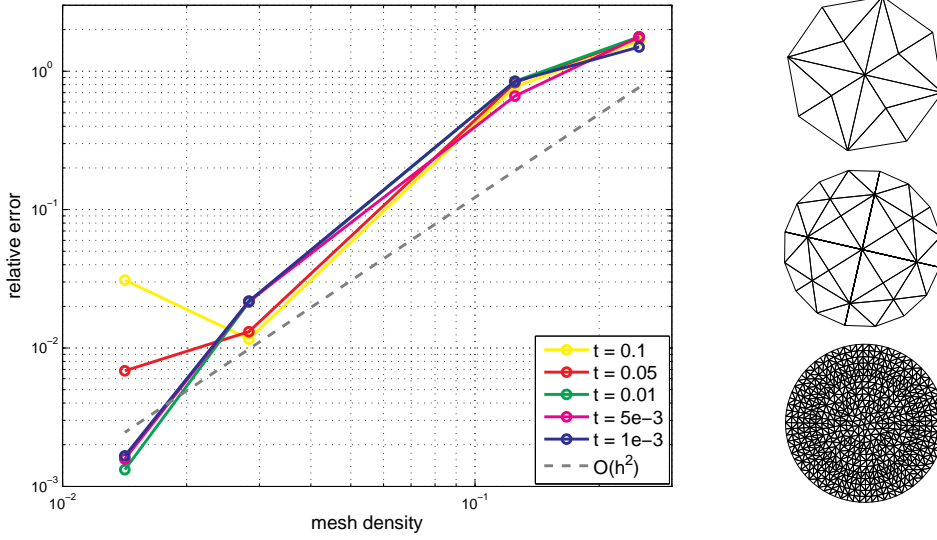


Fig. 5.2 Convergence of DCS to the analytic solution for a clamped circular plate under uniform load for various thicknesses.

Reissner-Mindlin:

$$w_c^{RM} = w_c^K \left(1 + \frac{4}{1-\nu} \left(\frac{t}{r} \right)^2 \right), \quad w_{ss}^{RM} = w_{ss}^K \left(1 + \frac{4}{3} \frac{(3+\nu)}{(1-\nu)(5+\nu)} \left(\frac{t}{r} \right)^2 \right).$$

We did the experiment for a disk of radius $r = 1$ with material parameters $E = 1.7242 \cdot 10^7, \nu = 0.3$, for thicknesses

$$\{1 \cdot 10^{-1}, 5 \cdot 10^{-2}, 1 \cdot 10^{-2}, 5 \cdot 10^{-3}, 1 \cdot 10^{-3}\}.$$

The load q was adapted to the thickness in a way to keep the expected deflection between $1 \cdot 10^{-4}$ and $1 \cdot 10^{-8}$.

The meshes are pictured next to the convergence plot in Fig. 5.2. As the general behaviour did not differ from clamped to simply supported boundary conditions, we only present the experiments for clamped boundaries.

The results support that DCS converges quadratically to the analytic deflection of the Reissner-Mindlin plate for sufficiently small thicknesses. For larger t , we can observe the theoretical convergence rate $\mathcal{O}(\max(t^2, h^2))$ as refining the mesh *increases* the error.

Square plate under uniform load

For the square plate of edge length 1 under uniform load, we used again as material parameters $E = 1.7242 \cdot 10^7, \nu = 0.3$, and the thickness values

$$\{1 \cdot 10^{-1}, 5 \cdot 10^{-2}, 1 \cdot 10^{-2}, 1 \cdot 10^{-3}\}.$$

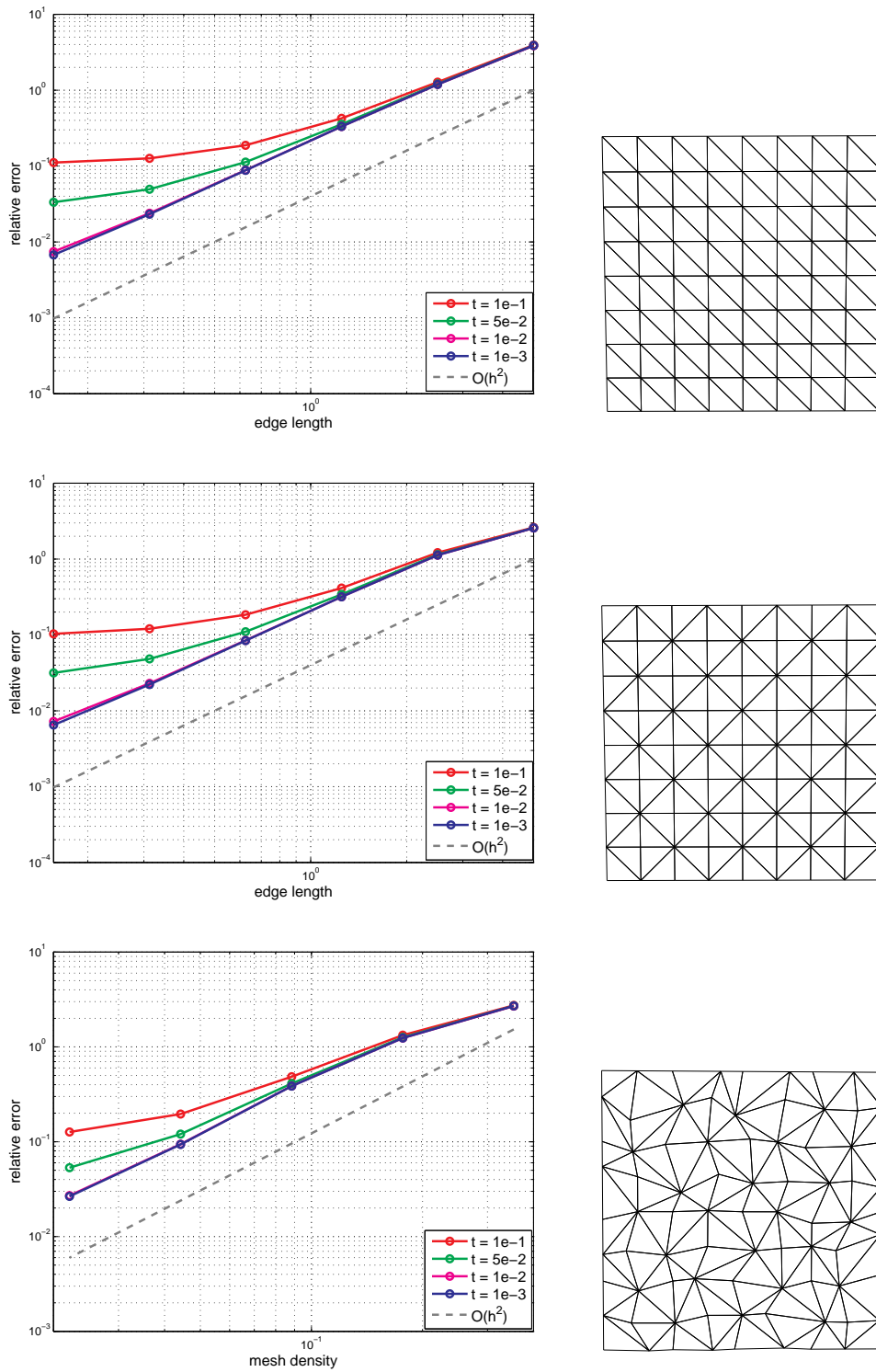


Fig. 5.3 Convergence of DCS to the analytic solution for a clamped square plate under uniform load as given in [TWK59] on a regular mesh, a cross mesh and an irregular mesh.

The applied uniform load density is such that it integrates to 1 over the whole plate. For simply supported boundaries, analytic solutions are obtained by a series extension due to Navier. For clamped boundaries, they are deduced from a clever superposition of these solutions for different loads, see [TWK59].

The presented results were obtained for clamped boundaries. We did this experiment on three different meshes (see Fig. 5.3) to inspect the dependency of DCS on mesh structure.

The general behaviour differs only slightly, which validates that DCS inherits the robustness to mesh structure from its related Kirchhoff version MSO [GSH⁺04]. Just as for the circular plate, we see a deterioration of the convergence rate when t gets larger, which illustrates again the theoretical convergence rate $\mathcal{O}(\max(h^2, t^2))$.

5.4.2 Nonlinear benchmarks

The static nonlinear test problems listed below are taken from the paper by Sze, Liu and Lo on *Popular benchmark problems for geometric nonlinear analysis of shells* [SLL04]. The reference values are the values given in the mentioned paper, which correspond to the converged solutions of the all-purpose quadrilateral shell element S4R of the finite element software *Abaqus*.

Table 5.1 below contains the relative errors in deflection of the vertices with the largest deflection, with respect to the number of degrees of freedom. The subsequent figures show the corresponding deflection curves of these particular vertices, *i.e.*, their position at different ratios P/P_{\max} of the applied load P with respect to the total load P_{\max} . The black curve represents the reference solution, the coloured curve show the values obtained with DCS on different mesh resolutions. The numbers in the legend give the number of degrees of freedoms that was solved for. It shows that even on coarse meshes, DCS behaves qualitatively correct.

Table 5.1 Relative error of the deflections simulated with DCS with respect to the converged solution of Abaqus' S4R element

Loaded cantilever			Slit annular plate			Pinched hemisphere		
DOFS	Relative error		DOFS	Relative error		DOFS	Relative error	
	z-direction	x-direction		vertex A	vertex B		vertex A	vertex B
153	1.34e-2	1.87e-2	135	4.415e-1	5.632e-1	120	7.75e-1	8.651e-1
495	3.3e-3	5.17e-3	651	1.574e-2	3.00e-1	432	6.432e-1	1.342e-1
1755	8e-4	2.13e-3	2379	1.31e-2	4.69e-2	1872	2.01e-1	1.51e-2
6579	5e-4	1.36e-3	9075	1.25e-2	1.96e-2	7200	4.2e-2	6e-4

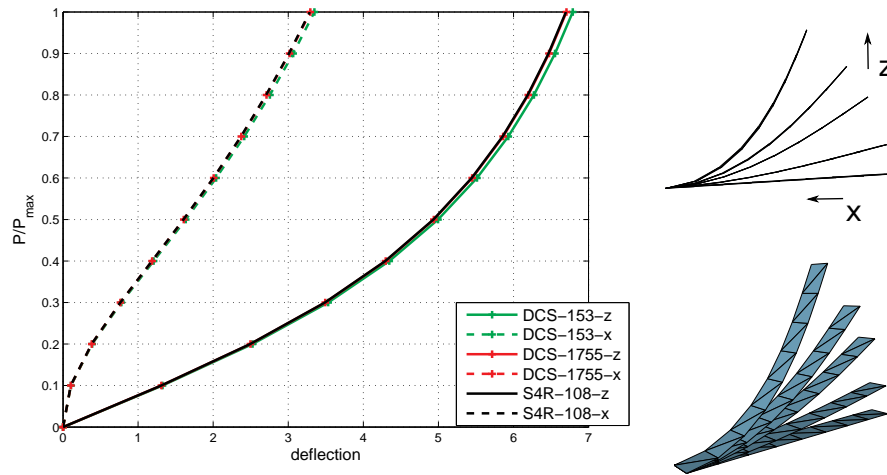


Fig. 5.4 Cantilever subjected to end shear force A cantilever of length $L = 10$, width 1 and of thickness $t = 0.1$ is clamped on one side. On the other end, we apply a total force of $P_{\max} = 4$ by uniform incrementation. The considered material parameters are $E = 1.2 \cdot 10^6$, $\nu = 0$.

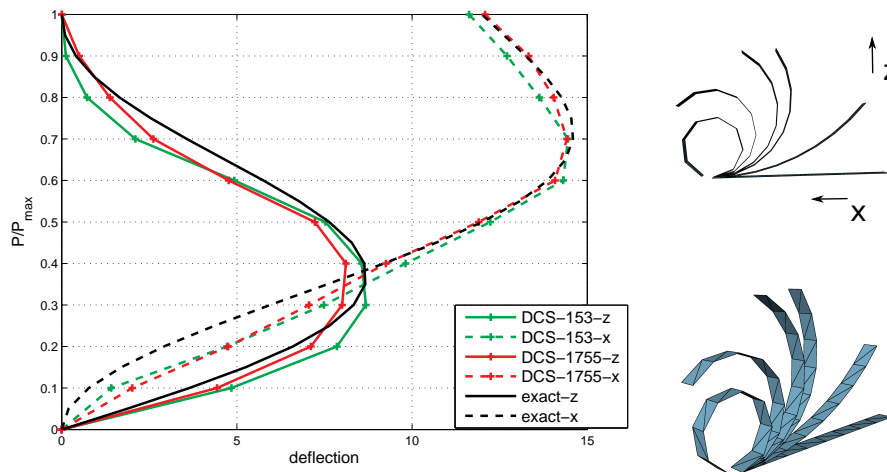


Fig. 5.5 Cantilever subjected to moment In this example, a slightly different cantilever ($L = 12$, $t = 0.1$, $E = 1.2 \cdot 10^6$, $\nu = 0$) is again clamped on one side. On the other side, we successively apply a moment such that the cantilever rolls up, forming a series of circular arcs.

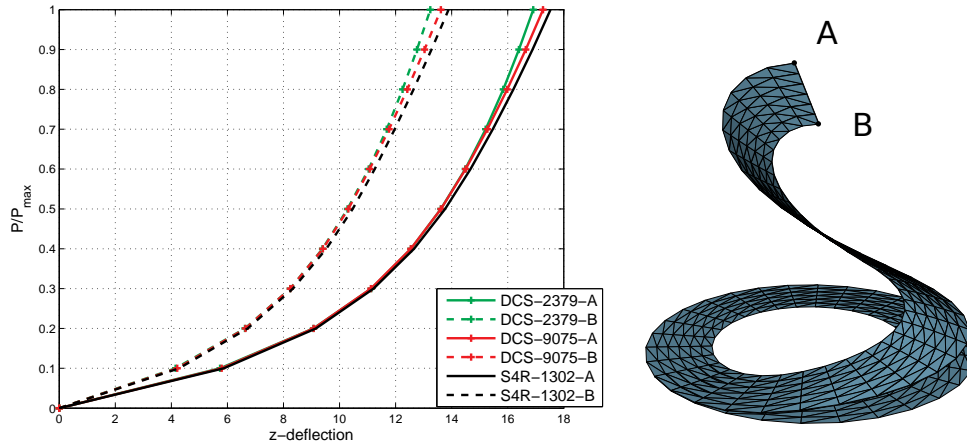


Fig. 5.6 Slit annular plate An annular plate ($E = 21 \cdot 10^6, \nu = 0$) of inner and outer radii 6 and 10, and of thickness $t = 0.03$ is cut open at some point. One side of the cut is clamped, the other side is pulled up vertically. By the geometry of the plate, this deformation activates membrane strains as well as bending strains.

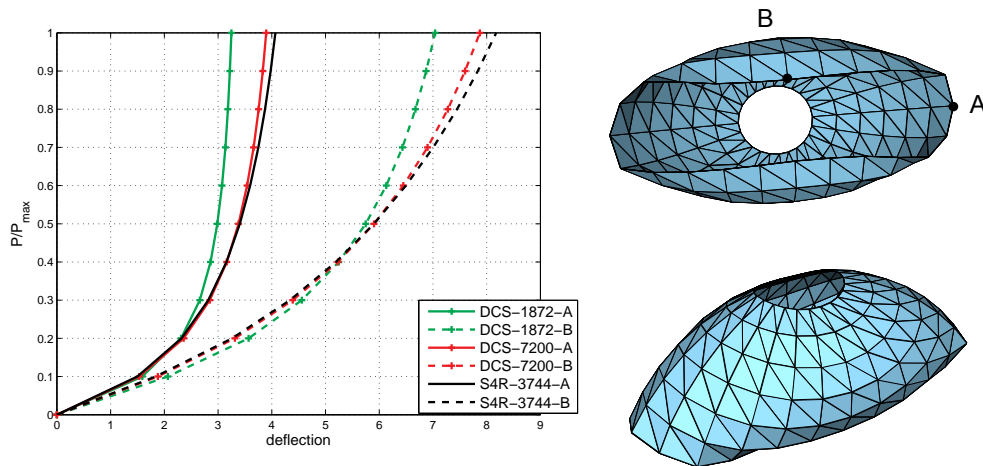


Fig. 5.7 Pinched Hemisphere On the pinched hemisphere ($E = 6.825 \cdot 10^7, \nu = 0.3$) of radius $R = 10$ and thickness $t = 0.04$, two pairs of antipodal points are simultaneously pulled outwards (A and its opposite) and pushed inwards (B and its opposite). The curves show the deflection of A and B in these respective directions.

Chapter 6

Discussion

There are very few topics in structural mechanics where so many investigations have been published.

Bischoff *et al.* [BBWR04]

The question that motivated this thesis was how far we could go in constructing a physical shell model by means of discrete geometric tools, and to see what advantages this approach can provide. This last chapter gives a critical examination of the discrete geometric model that resulted from this approach by comparing it to a selection of low-order shell models which were constructed from very different perspectives.

The second section provides a discussion on the difficulty of an objective evaluation of the quality of shell models in general, and the limits of low-order models in particular.

6.1 Comparison to existing low-order shell models

As noticed in literally any publication on plate and shell models since at least the 1970's, the massive amount of existing models makes it impossible to even roughly account for all of them. In this section, we picked those classes of models –possibly biased in favour of more geometric models– that seemed conceptually closest to the aim we had in mind, and opposed them to our model. Before doing so, we will briefly summarize the model that our geometric approach resulted in. A condensed overview of this comparison in table form is provided at the end of this section.

6.1.1 Recapitulation of DCS

DCS behaves qualitatively correct and sufficiently accurate in nonlinear benchmarks on coarse meshes, which is exactly the goal we were aiming at. Its underlying linear plate model is theoretically well understood, and in particular for small t on relatively coarse meshes, this model has optimal convergence order $\mathcal{O}(h^2)$. While we have not tackled the more challenging problem of a theoretical convergence proof for the nonlinear model, we could show that the discrete energy is consistent, and we identified the –practically benign– zero-energy modes of the model.

Moreover, by following the ideas of discrete exterior calculus and keeping in mind structure preservation in the sense of [AFW09], we managed to define the discrete energies via purely geometric arguments, avoiding assumed strains, reduced integration or other stabilization techniques. Finally, its close relation to the shear-rigid model MSO and the linear benchmarks suggest that DCS is very robust with respect to mesh structure.

6.1.2 Low-order shell FE: MITC3

A very popular class of Reissner-Mindlin plate and shell elements is based on the "mixed-interpolation of tensorial components" (MITC) approach, first proposed by Bathe *et al.* [BBF89]. The linear *plate* models of this type are built on the propositions (P1)–(P5) that we investigated in Chapter 3 for the construction of DCS. For most of these elements, theoretical analyses are available, and for example the lowest order *quadrilateral* plate element MITC4 was shown to be optimally convergent ($\mathcal{O}(h^2)$) on *regular* grids.

The MITC *shell* models are based on a degenerate solid approach rather than on a two dimensional shell formulation. The construction of these models is based on the choice of independent interpolation schemes for the different strains and an appropriate way to couple them. This coupling is done on so-called *tying points*, whose precise positioning on the element can strongly affect the predictive capability of the shell element [BLH03]. In particular, this construction seems to involve several choices without providing a good general guide to make them:

To construct the MITC triangular shell finite elements, each transverse shear strain interpolation scheme can be combined with various inplane strain interpolation schemes. As a result, we can develop many new shell finite elements, but only few elements will be effective for practical purposes. [LB04]

This also explains why different MITC shell models came up more or less one by one during the last 30 years (MITC4 in 1984 [DB84], MITC9 and MITC16 in 1993 [BB93], improved MITC9 in 2003 [BLH03], MITC6a and MITC6b in [LB04], improved MITC6a in 2007 [dVCS07]).

One of the possible low-order triangular version of this class, named MITC3, was numerically analysed in 2004 [LB04]. Similarly to DCS, shearing is evaluated at edge midpoints and (by an assumed strain approach) assumed constant along each edge. From there however, the three edge values are used to construct two linear strain fields, providing together an isotropic shear strain field over the triangle.

This element gives satisfying results in numerical nonlinear experiments and does not exhibit any spurious zero-energy modes in numerical tests. In linear benchmarks though, it shows that its convergence behaviour strongly depends on the considered mesh [LNB07]. In particular, it seems shear locking free on cross meshes, but shows locking on regular meshes when the (thickness / length)-ratio is smaller than $1 \cdot 10^{-3}$. In [LNB07], MITC3 is compared to three further 3-node triangular shell finite elements, among which it performs best in the sense that it shows the 'least' amount of locking and of mesh dependence.

On the theoretical side, no convergence or consistency results seem to be available for any triangular MITC *shell* element yet, in particular not for MITC3.

6.1.3 Discrete geometric models

Physically based models have recently become popular in computer graphics applications, such that various discrete geometric methods for the simulation of thin-walled structures are already in use in this field. The most popular might be the discrete shell model, proposed in [GHDS03], which is based on using hinge angles for the bending strains. However, the predictive reliability of this model is known to be extremely mesh dependent, as even in standard benchmarks it does not converge for some mesh patterns [GGRZ06].

An improvement to this problem was brought by the already mentioned MSO model. The main difference between MSO and DCS is that, as a shear-deformable model, DCS is physically more accurate for moderately thick shells. For engineering applications, this difference in accuracy for a given material can be crucial. For computer graphic applications however, the precise material and thereby material constants are mostly not available, and the main concern is to have *qualitatively* plausible deformations.

Numerical tests on thick and thin shells of different bending and shearing stiffness suggest that purely in terms of deformation behaviour, using a shear-deformable model rather than a shear-rigid model does not make a significant difference, at least not for homogeneous material with relatively simple boundary conditions. More interesting effects might however be achievable for special boundary conditions and inhomogeneous/anisotropic material, and even more likely by stepping back from the physical model and varying bending and shearing stiffnesses independently.

6.1.4 Mimetic discretisation

Recently, *mimetic finite differences* and *mimetic discretisation* [BLS05] approaches have been proposed in the engineering community as a technique to treat partial differential equations on general polygonal meshes. Just as for the discrete geometric approach, the discrete problem is formulated essentially in terms of the degrees of freedom. This technique has been successfully applied to several different physical applications, including electromagnetism, linear diffusion and continuum mechanics.

While we are not aware of any mimetic models suitable for geometrically non-linear shell deformations, Beirão da Veiga and Mora proposed a mimetic Reissner-Mindlin *plate* model for polygonal meshes [BdVM11], including non-convex polygons. For this discretisation, the authors start again from the familiar 'locking-free' conditions for Reissner-Mindlin plates as described in Chapter 3, in particular assuring a discrete Helmholtz decomposition of their finite dimensional function spaces.

These finite spaces are eventually determined by nodal values for the scalar displacements w_h , by nodal values and edge-tangential values for the rotation field θ_h , and by edge-tangential values only for the shearing γ_h . In particular, in the specific case of a triangular mesh, they obtain as finite-dimensional function spaces $W_h = M_0^1$ and $\Gamma_h = RT_0$, similarly to DCS, but for rotations Θ_h they recover the Morley space \mathcal{M} as seen in (4.8). They prove their element to converge linearly, and uniformly with respect to thickness.

6.1.5 Isogeometric shells

Another relatively recent tool for shell analysis is based on isogeometric analysis which was introduced by Hughes et al. [HCB05] in 2005. The main advantage of this approach is its foundation on NURBS-basis functions which are also used in many commercial computer-aided design (CAD) software tools. Particularly for industrial applications, this allows to cycle through design and analysis phases without the tedious conversion from one representation to another. In perspective of the applications which motivated this thesis, like automotive design and digital mock-up, this seems a major advantage.

Moreover, the global support of the basis functions makes it very easy to achieve global C^1 -continuity, which is a major problem in shell analysis, such that isogeometric analysis seems particularly well-suited for these applications. Unfortunately, the large support comes with various drawbacks. Not only it involves more degrees of freedom, but it also requires technical effort to handle local events, in particular local refinement [VGJS11]. Moreover, the regularity of the NURBS function only holds patch-wise. When different patches are connected, in general not even C^0 -continuity can be assured without altering at least one of the patches [BCC⁺10].

For the special case of shell analysis, isogeometric models have been proposed by Kiendl et al. [KBLW09] for Kirchhoff, and by Benson et al. [BBHH10] for Reissner-Mindlin shell modelling. Both models show very good numerical results. However, both models tend to favor the use of higher-order polynomials on coarser meshes to get the most efficient and accurate outcome. Especially in the shear-deformable model, locking is not avoided explicitly (in particular no reduced integration is used), but bypassed by the use of higher-order basis functions.

An isogeometric model for linear Reissner-Mindlin *plate* analysis which seems more closely related to DCS, was recently developed by Beirão da Veiga *et al.* [BdVBL⁺12]. This model uses the capacity of spline basis functions to approximate differential forms "in the spirit of [AFW09]". Specifically, the regularity of the spline function spaces adequately mimics the structure of the de Rham complex, and by treating all the variables of the model –not only shearing– as differential forms, the others are able to find discrete spaces for deflections W_h and rotations Θ_h which directly satisfy

$$\text{grad } W_h \subset \Theta_h .$$

Optimal convergence of this method is proven theoretically and illustrated numerically for spline spaces up from degree $p = 2$.

6.1.6 Subdivision shells

Subdivision surfaces were initially used in computer graphic applications for smooth rendering of surfaces. When used for analysis, they are closely related to the isogeometric approach, as they can be seen as a generalization of spline surfaces, essentially relying on the refinability of B-spline functions [ZS00].

They were first introduced for Kirchhoff shell analysis by Cirak et al. [COS00] and recently extended to shear-deformable shells [CLB11]. In the latter model, bending is measured by second derivatives, just as in the shear-rigid model, and shearing is measured independently. By separating bending and shearing, the unfavourable correlation between these energies which produces locking is *a priori* avoided, and the model thus seems equally suitable for both thin and thick shells.

This separation of bending and shearing might seem slanted, as it leads to a shell model that carries the difficulties of both the Kirchhoff approach *and* the Cosserat shell. However, in contrast to finite elements, for subdivision shells –just as for NURBS– the inter-element regularity required for second derivatives is very easily obtained, such that the C^1 -continuity is not a challenge. Decoupling bending and shearing then solves the shear locking problem in a very simple manner. However, a complete independence of bending and shearing is physically unjustified, and does not correspond to any theoretical model deduced from 3D or 2D kinematics.

Table 6.1 Schematical comparison of the considered shear-deformable plate and shell models The first column states if the model is suitable for the linearised ‘plate’ setting only, or if it can also be used for geometrically non-linear ‘shell’ deformations. The column ‘mesh-dependence’ indicates whether the model depends strongly (-) or little (+) on the mesh structure. By p_{pos} and p_{dir} we denote the polynomial degree per triangle or patch of the functions used to approximate the positions and the directors respectively.

	suitable for		mesh-dependence	Shear locking shows	Comments
	plates	shells			
Discrete Differential Geometry					
DCS	x	x	+	for large t ($p_{pos} = 1, p_{dir} = 1$)	no practical spurious zero-energy modes
Finite elements					
Triangular shell [LB04]	x	x	-	for small t ($p_{pos} = 1, p_{dir} = 1$)	numerically no spurious zero-energy modes
Mimetic discretisation					
Reissner-Mindlin plate [BdVM11]	x		+	no ($p_{pos} = 1, p_{dir} = 2$)	defined on polygonal meshes; convergence order $\mathcal{O}(h)$;
Isogeometric analysis					
Reissner-Mindlin shell [BHH10]	x	x	+	for $p_{pos} < 3$	no reduced integration
Reissner-Mindlin plate [BdVBL+12]	x		unspecified	not for $p_{pos} \geq 3, p_{dir} \geq 2$	optimal convergence order for $p_{pos} \geq 3, p_{dir} \geq 2$
Subdivision surfaces					
Shear-deformable subdivision shells [CLB11]	x	x	+	no	unphysical decoupling of bending and shearing

6.2 Limitations

While working on this thesis, two uncomfortable questions kept coming up. The first is:

What is a fair evaluation of nonlinear shell models?

The second can be formulated provocatively as:

In view of the progress in terms of fast computation, is it necessary to reduce the number of degrees of freedom to a strict, possibly excessive minimum?

This concluding section proposes a discussion of these concerns.

6.2.1 How to evaluate?

As depicted in Chapter 5, we evaluated the DCS model by linear as well as nonlinear benchmarks, as it is usual for testing shell elements. Already for the linear tests, it was not completely clear what a fair comparison would be. Analytic solutions are usually given in terms of a formula depending on the thickness, the material parameters and the load, but the transition from the linear to the nonlinear regime is not sharp, such that the choice of these parameters also affects whether the reference value is to be expected or not.

In the nonlinear setting, reference benchmarks are usually provided by established elements, that were tested against yet older elements or results, and in the end it is not clear whether the initial reference solutions refer to 3D solutions, to shearable or unshearable shell models. The practical purpose of a shell model is to give a satisfying approximation of the 'real' three dimensional problem, such that it seems tempting to compete with reference 3D values. However, this comparison is clearly unfair, as even the best discrete model and the highest resolution cannot overcome modelling errors, which are inherent in a 2D shell model. For a proper evaluation, it thus seems essential to have reliable evidence about the material and geometry parameters for which the different model assumptions become neglectable. This would allow to know in which cases shear-rigid and shear-deformable shells should coincide, and in which both shell models should coincide with the 3D model. Such thresholds do not seem to be available in the literature.

If the reference model and the test parameters are chosen, the next question arises: what norm should be used to measure the error? In engineering literature, nonlinear shell models are mostly evaluated by comparing the deflection of some distinguished point to an established reference. This is also the method we adopted. However, there are many different and seemingly equally justified techniques taking into account one or several criteria among displacements, strains, stresses and energies, sometimes even taking into account whether the discrete model is based on a mixed formulation or not (see e.g. [CB03] for an overview).

Finally, the question remains what particular geometries and meshes should be tested. In computer graphics applications, robustness with respect to mesh dependence is very important as the considered meshes are often created by meshing algorithms that often provide relatively random Delaunay triangulations. Therefore, the models presented in this community are usually tested for meshes of different quality and regularity.

For engineering literature, the dependence on the mesh is rather secondary, as most often the geometries are meshed for the very purpose of the analysis, and this is usually done as uniformly as possible. In these cases however, it seems important that the model behaves similarly well on different types of geometries and for different boundary conditions and strain regimes [CB03].

In the end, we decided to mainly followed the engineering criteria for our benchmarks, as the validity of benchmarks seems to strongly depend on what is trusted from experience in the target community.

6.2.2 Low-order for efficiency?

The main constraint in the construction of the presented model was to build a shell model in the framework of discrete differential geometry. This was not out of dogmatic beliefs, but on account of the numerous discrete models which, by their relatively simple geometric structure, had already shown to give very valuable insights in several physical applications. And indeed, also in the case of shell simulation and shear locking our investigations unveiled new insights.

From a purely practical aspect, the discrete geometric point of view however restricts the model to low-order approximations, as it relies on dealing with the basic combinatorial entities of the mesh only. It is well known in FE analysis that some physical models, including shells and fluid simulations, become sensitively more difficult when they are treated with too few degrees of freedom. For instance, the difficulties of Kirchhoff and Cosserat shells, namely the C^1 -continuity and shear locking, both become less of a challenge when using slightly higher order discretisations. For the issue of shear locking, this also shows in the comparative Table 6.1 at the end of this chapter.

Still, even in practical engineering applications it is very common to stick with low-order approximations and deal with the adherent difficulties. Historically, the main argument for this focus is that low-order models are easier to implement and seemingly faster to compute. However, it strongly depends on the considered problem and the expected accuracy whether the trade-off between precision and resolution favours using a low-order model on a high-resolved mesh or a high-order model on a coarse mesh. For a very insightful investigation of this problem for plates we refer to [AP02], [Sur94].

Moreover, given the the extreme progress in terms of computational power, it appears questionable if searching for the absolute minimum of degrees of free-

dom for the sake of fast computations is still a valid argument. Especially recent achievements in the computer graphics community, where fast simulations of elasto-plastic deformations, even with 3D models, are rather common [MDM⁺02, CPSS10, MTPS08, WRK⁺10] suggests that being able to use models with moderately many degrees of freedom in real-time simulations seems more of a challenge on the implementation side. While such fast models do not aim at the precision available in finite element models, making use of some of their tools and model simplifications used to speed up computations might lead to an appropriate compromise between fast computation and a more comfortable way to accuracy.

Hence, while keeping in mind that higher order approaches can introduce theoretical challenges on their own (such as sensitivity to mesh distortion and oscillations near boundaries and singularities [RWRA09, HCP11]), it might be worthwhile to concede discrete shell models more degrees of freedom without giving up the aim of computational efficiency.

Appendix

Quick implementation guide

This appendix relates very concisely the different energies determining the model, in a formulation suitable for a quick implementation.

The canonical starting point for discrete geometric models in general is a half-edge mesh data structure, that allows to easily assign values and variables to the different simplicial entities of the mesh, and provides enough connectivity information to allow to easily loop over adjacent vertices, faces and edges (OpenMesh is a possible open source candidate). In this data structure, we first have to assign the variables that is solved for, which are the positions of the vertices, *i.e.*, a 3-vector per vertex, and the position of the directors, *i.e.*, a 3-vector per edge. It is then easy to assign each triangle the corresponding energy, only using the local variables of the triangle, and the global energy is assembled by summing up the triangle-wise energies.

Membrane and bending energies per triangle

We describe how to easily implement the norm of a quadratic form as given in Section 4.1. Membrane and bending energies of DCS then only differ with respect to some particular coefficients given below.

Notice that the code can be used virtually unchanged for alternative definitions of first and second fundamental forms.

Let P be a quadratic form, written on a triangle T as

$$P_T = -\frac{1}{8A_T^2} \sum_{i=1}^3 (P_i - P_j - P_k)(\bar{e}_i^* \otimes \bar{e}_i^*) \quad (6.1)$$

where $P_i = P(e_i)$ are the directional values depending on the variables of the problem (vertex positions and directors), and \bar{e}_i^* the orthogonal dual edges of the undeformed configuration. As usual, A_T denotes the area of the considered triangle.

The energy associated with P is then determined by its norm

$$W^{P_T} = M (\nu \operatorname{tr}(P_T)^2 + (1 - \nu) \operatorname{tr}((P_T)^2))$$

where M is a coefficient depending on the material and ν is the Poisson ratio.

As we want to measure the change of a fundamental form Q from the undeformed configuration to the deformed configuration, we set $\bar{Q}_i := \bar{Q}(\bar{e}_i)$ and $Q_i := Q(\bar{e}_i)$, and denote by δQ the quadratic form defined by values

$$\delta Q_i := Q_i - \bar{Q}_i .$$

Substituting P by δQ in (6.1) and inserting the resulting expression in the formula for the energy $W^{\delta Q}(T)$, we get

$$W^{\delta Q} = M \frac{1}{(16A_T^2)^2} \sum_{\substack{i,o=1 \\ (ijk),(opq)}}^3 (\delta Q_i - \delta Q_j - \delta Q_k)(\delta Q_o - \delta Q_p - \delta Q_q) q_{io}$$

where

$$q_{io} := \nu \operatorname{tr}(\bar{e}_i^* \otimes e_i^*) \operatorname{tr}(\bar{e}_o^* \otimes \bar{e}_o^*) + (1 - \nu) \operatorname{tr}(e_i^* \otimes e_i^* \cdot \bar{e}_o^* \otimes \bar{e}_o^*) .$$

With $\operatorname{tr}(\bar{e}_i^* \otimes \bar{e}_i^*) = \bar{e}_i^* \cdot \bar{e}_i^* = \bar{e}_i \cdot \bar{e}_i$, q_{io} simplifies to:

$$q_{io} = \nu(\bar{e}_i \cdot \bar{e}_i)(\bar{e}_o \cdot \bar{e}_o) + (1 - \nu)(\bar{e}_i \cdot \bar{e}_o)^2 .$$

From this, the only thing that needs to be adapted to the particular quadratic form we are dealing with, are the values δQ_i and the material coefficient M .

For the **DCS membrane energy**:

$$\begin{aligned} \delta Q_i^m &= (\bar{e}_i \cdot \bar{e}_i - e_i \cdot e_i) \\ M^m &= \frac{Et}{(1 - \nu^2)} \end{aligned}$$

For the **DCS bending energy**:

$$\begin{aligned} \delta Q_i^b &= 2 ((\bar{n}_k - \bar{n}_j) \cdot \bar{e}_i - (n_k - n_j) \cdot e_i) \\ M^b &= \frac{Et^3}{12(1 - \nu^2)} \end{aligned}$$

The barred quantities refer to the undeformed configuration and stay unchanged. In particular, they will drop when taking derivatives.

Remark. If we use the alternative formulation

$$P(T) = -\frac{1}{8A_T^2} \sum_{i=1}^3 P_i(\bar{e}_j^* \otimes \bar{e}_k^* + \bar{e}_k^* \otimes \bar{e}_j^*) ,$$

the deduction of an implementation-ready formulation goes through in a similar way.

Shearing per triangle

The shearing energy is a discrete one-form, prescribed by one value per edge. To measure the energy per triangle for a given configuration, we have to integrate the corresponding linear function over the triangle T .

Let s be the discrete shear-form on the triangle, determined by the edge values

$$s_i := \mathbf{n}_i \cdot \hat{\mathbf{e}}_i = \mathbf{n}_i \cdot \frac{(\mathbf{v}_k - \mathbf{v}_j)}{\|\mathbf{v}_k - \mathbf{v}_j\|} .$$

In terms of the basis functions $\{\psi_i\}_i$ for Whitney one-forms [Bos88], which take value 1 on edge e_i respectively, and 0 on the remaining edges, the discrete shear form s_n is simply given by

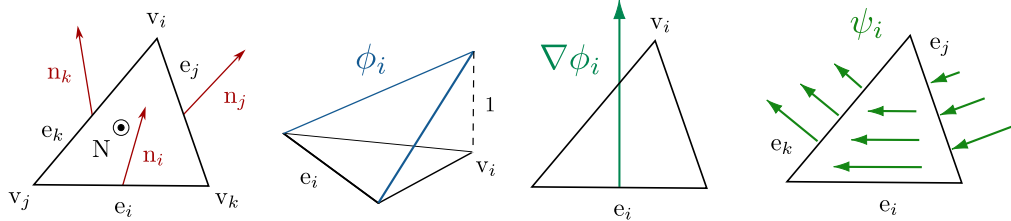
$$s_n = \sum_i s_i \psi_i .$$

In particular, the **DCS shearing energy** writes

$$W^s(T) := t\kappa G \int_T \langle s, s \rangle dA = \frac{t}{4} \kappa G \sum_i s_i^2 \int_T \langle \psi_i, \psi_i \rangle dA + 2 \sum_{i \neq j} s_i s_j \int_T \langle \psi_i, \psi_j \rangle dA \quad (6.2)$$

with the material coefficient $m_s = \frac{E}{2(1+\nu)}$ and the shear correction factor $\kappa = \frac{5}{6}$.

We will present a concise derivation of the L^2 -norms of the Whitney basis functions in terms of geometric entities of the triangle.



The basis functions ψ_i can be expressed in terms of Whitney zero-forms ϕ_i , which are nothing else than the usual Lagrange M^1 basis functions, as

$$\psi_i = \phi_k d\phi_j - \phi_j d\phi_k .$$

The derivatives of these in turn have a very simple expression when written as vector fields, namely

$$\nabla \phi_i = \frac{1}{2A_T} \mathbf{N} \times \mathbf{e}_i ,$$

where \mathbf{N} is the triangle's unit normal (see, e.g., [BKP+10]). In particular

$$|\nabla \phi_i|^2 = \frac{|\mathbf{e}_i|^2}{4A_T^2}$$

and

$$\langle \nabla \phi_j, \nabla \phi_k \rangle = \frac{|\mathbf{e}_j||\mathbf{e}_k|}{4A_{\text{T}}^2} \cos(\mathbf{e}_j, \mathbf{e}_k) .$$

Using the familiar L^2 -norms of the hat functions ϕ_i

$$\int_{\text{T}} |\phi_i|^2 dA = \frac{A_{\text{T}}}{6} , \quad \int_{\text{T}} \langle \phi_i, \phi_j \rangle dA = \frac{A_{\text{T}}}{12}$$

and setting $l_i := \|\mathbf{e}_i\|$, $\alpha_{jk} := \cos(\mathbf{e}_j, \mathbf{e}_k)$, the L^2 inner products of the Whitney basis functions eventually simplify to

$$\begin{aligned} \int_{\text{T}} \langle \psi_i, \psi_i \rangle dA &= \frac{1}{24A_{\text{T}}^2} \left(l_j^2 + l_k^2 + \frac{1}{2} l_j l_k \alpha_{jk} \right) \\ \int_{\text{T}} \langle \psi_i, \psi_j \rangle dA &= \frac{1}{48A_{\text{T}}^2} (l_j l_k \alpha_{jk} - 2l_j l_i \alpha_{ji} - l_k^2 + l_i l_k \alpha_{ki}) . \end{aligned}$$

These values can then be introduced into (6.2).

Notice that in the case of small membrane strains, the deformation is almost isometric, meaning that the shape of each single triangle stays almost unaltered with respect to the undeformed configuration. In that case, it is sufficient to precompute only once the values for A_{T} , $\{l_i\}_i$, $\{\alpha_{ij}\}_{i,j}$, and for the above integrals.

Constraint on length of directors

Throughout the theoretical description of our model, we assumed that directors had unit length, which is consistent with the model assumption that no transverse through-the-thickness strains can occur. For the implementation however, we used a Newton's method in order to minimize the discrete energy, such that we use the gradient and the Hessian of the discrete Cosserat energy. One possible way to make sure that the directors keep unit length during the Newton steps is to take the derivatives of the directors on the unit sphere. As a simplifying alternative to this cumbersome procedure, we suggest to use the usual derivatives in \mathbb{R}^3 and introduce an additional energy, meant to encounter stretching of the directors, without affecting on the numerical efficiency or stability.

This energy is edge-based and has the simple form

$$W^l(\mathbf{e}_i) = M^m (1 - \mathbf{n}_i \cdot \mathbf{n}_i)^2$$

where M^m is the membrane stiffness already used to penalize in-plane stretching, and hence encodes the resistance of the material to change of length in any direction if the material is isotropic.

Simulation

Once the energies are defined, the deformation is determined by the lowest possible energy configurations, meaning that the energy needs to be minimized. To do so, there are several possibilities, like minimization algorithms and Newton-like methods, merely requiring some linear algebra and/or optimization libraries. For our implementation, we chose to rely on the classical Newton's method and decided to use the C++-libraries PETSc and TAO. Depending on what sort of Newton algorithm one uses, first and second derivatives of the energy are required. The provided expressions for the energy make it comfortable to compute the analytic derivatives, thereby allowing for a very efficient computation. Automatic differentiation tools are also an option, although they are usually slower.

List of notations

Smooth setting

$\bar{\mathcal{S}}, \mathcal{S}$	undeformed, deformed shell configuration
$\bar{\mathcal{S}}, \mathcal{S}$	undeformed, deformed mid-surface
\bar{n}, n	undeformed, deformed director field
\underline{n}	pullback of the deformed director field
I, II_n, III_n	first fundamental form, and generalized second and third fundamental forms
σ_n	shear form
Φ	deformation of a shell
ϕ	deformation of the mid surface
\mathcal{W}	elastic deformation energy
ω	$\ II_n\ _{\text{Frob}}^2$, bending energy density
dA	volume element
N	unit normal field

Discrete setting

$\bar{\mathbf{K}}, \mathbf{K}$	undeformed, deformed shell configuration
$\bar{\mathbf{K}}, \mathbf{K}$	undeformed, deformed mid surface
\bar{n}, n	undeformed, deformed director field
n^{tan}	projection of the discrete director to the discrete tangent plane
\underline{n}	pullback of the deformed director field
I, II_n	first and generalized second fundamental forms
s_n	shear form
\mathbf{F}	deformation of a discrete shell
f	deformation of the discrete mid surface
W	discrete deformation energy
w	$\ II_n\ _{\text{Frob}}^2$, discrete bending energy density
dA	volume element
N	triangle normals or averaged triangle normals

Function spaces

M^0	piecewise constant functions
M_0^1	piecewise linear continuous functions
M_{nc}^1	piecewise linear non-conforming functions (Crouzeix-Raviart)
RT_0	rotated lowest order Raviart-Thomas space
\mathcal{M}	discrete Morley space

Reissner-Mindlin plate

W, W_h	continuous, discrete scalar displacements
Θ, Θ_h	continuous, discrete rotation field
Γ, Γ_h	continuous, discrete shear vector field

Q, Q_h	rot-part in the smooth and continuous Helmholtz decomposition of Γ, Γ_h
R	Reduction operator
<i>Material parameters</i>	
E, ν	Young's (elastic) modulus and Poisson ratio
G	shear modulus: $\frac{E}{2(1+\nu)}$
D	bending modulus: $\frac{Et^3}{12(1-\nu^2)}$
κ	shear correction factor, usually $\frac{5}{6}$

Bibliography

- [AADL11] Gabriel Acosta, Thomas Apel, Ricardo G. Durán, and Ariel L. Lombardi, *Error estimates for raviart-thomas interpolation of any order on anisotropic tetrahedra*, Math. Comput. **80** (2011), no. 273, 141–163.
- [AF89] D. N. Arnold and R. S. Falk, *A uniformly accurate FEM for the Reissner-Mindlin plate*, SIAM Journal Numer. Anal. **26** (1989), no. 6, 1276–1290.
- [AF97] D. N. Arnold and R. S. Falk, *Analysis of a linear-linear finite element for the Reissner-Mindlin plate model*, Math. Models Methods Appl. Sci. **7** (1997), no. 2, 217–238.
- [AFW09] D. N. Arnold, R. S. Falk, and R. Winther, *Geometric decompositions and local bases for spaces of finite element differential forms*, Comput. Meth. Appl. Mech. Engrg. **198** (2009), no. 21-26, 1660–1672.
- [AP02] M. Ainsworth and K. Pinchedez, *The hp-MITC finite element method for the Reissner-Mindlin plate problem*, Jour. Comput. Appl. Math. **148** (2002), no. 2, 429 – 462.
- [AT95] F. Auricchio and R. L. Taylor, *A triangular thick plate finite element with an exact thin limit*, Finite Elem. Anal. Des. **19** (1995), no. 1-2, 57–68.
- [BB93] M. L. Bucalem and K.-J. Bathe, *Higher-order MITC general shell elements*, Int. Jour. for Num. Meth. in Eng. **36** (1993), no. 21, 3729–3754.
- [BBF89] F. Brezzi, K.-J. Bathe, and M. Fortin, *Mixed-interpolated elements for Reissner-Mindlin plates*, Int. Jour. for Num. Meth. in Eng. **28** (1989), no. 8, 1787–1801.
- [BBHH10] D. J. Benson, Y. Bazilevs, M. C. Hsu, and T. J. R. Hughes, *Isogeometric shell analysis: the Reissner-Mindlin shell*, Comput. Meth. Appl. Mech. Engrg. **199** (2010), no. 5-8, 276–289.

- [BBR00] K.-U. Bletzinger, M. Bischoff, and E. Ramm, *A unified approach for shear-locking-free triangular and rectangular shell finite elements*, *Computers & Structures* **75** (2000), no. 3, 321–334.
- [BBWR04] M. Bischoff, K.-U. Bletzinger, W. A. Wall, and E. Ramm, *Models and finite elements for thin-walled structures*, *Encyclopedia of Computational Mechanics*, vol. 2, John Wiley & Sons, Ltd, 2004.
- [BCC⁺10] Y. Bazilevs, V. M. Calo, J. A. Cottrell, J. A. Evans, T. J. R. Hughes, S. Lipton, M. A. Scott, and T. W. Sederberg, *Isogeometric analysis using T-splines*, *Comput. Meth. Appl. Mech. Engrg.* **199** (2010), no. 5-8, 229–263.
- [BDS93] I. Babuska, J. M. D’Harcourt, and C. Schwab, *Optimal shear correction factors in hierarchical plate modelling*, *Mathematical Modelling and Scientific Computing* **1** (1993), no. 1, 1–30.
- [BdVBL⁺12] L. Beirão da Veiga, A. Buffa, C. Lovadina, M. Martinelli, and G. Sangalli, *An isogeometric method for the Reissner–Mindlin plate bending problem*, *Comput. Meth. Appl. Mech. Engrg.* **209-212** (2012), 45–53.
- [BdVM11] L. Beirão da Veiga and D. Mora, *A mimetic discretization of the Reissner–Mindlin plate bending problem*, *Numerische Mathematik* **117** (2011), 425–462, 10.1007/s00211-010-0358-8.
- [Ber09] V. L. Berdichevsky, *Variational principles of continuum mechanics. I, II*, *Interaction of Mechanics and Mathematics*, Springer-Verlag, Berlin, 2009.
- [BFS91] F. Brezzi, M. Fortin, and R. Stenberg, *Error analysis of mixed-interpolated elements for Reissner–Mindlin plates*, *Math. Models Methods Appl. Sci.* **1** (1991), no. 2, 125–151.
- [BK04] K. Bhaskar and B. Kaushik, *Simple and exact series solutions for flexure of orthotropic rectangular plates with any combination of clamped and simply supported edges*, *Composite Structures* (2004), no. 63, 63–68.
- [BKP⁺10] Mario Botsch, Leif Kobbelt, Mark Pauly, Pierre Alliez, and Bruno Levy, *Polygon mesh processing*, AK Peters, 2010.
- [BLH03] K.-J. Bathe, P.-S. Lee, and J.-F. Hiller, *Towards improving the MITC9 shell element*, *Computers & Structures* **81** (2003), 477–489.
- [BLS05] F. Brezzi, K. Lipnikov, and M. Shashkov, *Convergence of mimetic finite difference method for diffusion problems on polyhedral meshes*, *SIAM J. Numer. Anal.* **43** (2005), 1872–1896.

- [Bob08] A.I. Bobenko, *Discrete differential geometry*, Oberwolfach seminars, Birkhäuser, 2008.
- [Bos88] A. Bossavit, *Mixed finite elements and the complex of Whitney forms*, The mathematics of finite elements and applications, VI (Uxbridge, 1987), Academic Press, London, 1988, pp. 137–144.
- [BR97] M. Bischoff and E. Ramm, *Shear deformable shell elements for large strains and rotations*, Int. Jour. for Num. Meth. in Eng. **40** (1997), no. 23, 4427–4449.
- [Bra01] D. Braess, *Finite elements. Theory, Fast Solvers and Applications in Solid Mechanics*, Cambridge University Press, 2001.
- [BWR⁺08] M. Bergou, M. Wardetzky, S. Robinson, B. Audoly, and E. Grinspun, *Discrete Elastic Rods*, ACM Transactions on Graphics **27** (2008), no. 3.
- [BZH01] J. L. Batoz, C. L. Zheng, and F. Hammadi, *Formulation and evaluation of new triangular, quadrilateral, pentagonal and hexagonal discrete Kirchhoff plate/shell elements*, Int. Jour. for Num. Meth. in Eng. **52** (2001), no. 5-6, 615–630.
- [CB03] D. Chapelle and K.-J. Bathe, *The Finite Element Analysis of Shells –Fundamentals*, Springer-Verlag, 2003.
- [CC96] E. Cosserat and F. Cosserat, *Sur la théorie de l'élasticité. premier mémoire.*, Annales de la faculté des sciences de Toulouse, 1, 10 no. 3–4, 1896, pp. I1–I116.
- [CDS10] K. Crane, M. Desbrun, and P. Schröder, *Trivial Connections on Discrete Surfaces*, Computer Graphics Forum **29** (2010), no. 5, 1525–1533.
- [Cia05] P.G. Ciarlet, *An Introduction to Differential Geometry with Applications to Elasticity*, Journal of Elasticity **78–79** (2005), no. 1–3, 1–215.
- [CL96] P. Ciarlet and V. Lods, *Asymptotic analysis of linearly elastic shells. i - iii.*, Arch. Ration. Mech. Anal. **136** (1996), 119–200.
- [CLB11] F. Cirak, Q. Long, and P.B. Bornemann, *Shear-flexible subdivision shells*, International Journal for Numerical Methods in Engineering (2011), In print.
- [COS00] F. Cirak, M. Ortiz, and P. Schröder, *Subdivision surfaces: A new paradigm for thin-shell finite-element analysis*, Int. Jour. for Num. Meth. in Eng. **47** (2000), 2039–2072.

- [CPSS10] I. Chao, U. Pinkall, P. Sanan, and P. Schröder, *A simple geometric model for elastic deformations*, ACM Trans. Graph. **29** (2010), no. 4, 38:1–38:6.
- [CR73] M. Crouzeix and P.-A. Raviart, *Conforming and non-conforming finite element methods for the stationary Stokes equations*, RAIRO Analyse numérique **7 R-3** (1973), 33–76.
- [DAT10] S.B. Dong, C. Alpdogan, and E. Taciroglu, *Much ado about shear correction factors in Timoshenko beam theory*, Int. Jour. of Solids and Structures **47** (2010), no. 13, 1651 – 1665.
- [DB84] E. N. Dvorkin and K.-J. Bathe, *A continuum mechanics based four-node shell element for general non-linear analysis*, Engineering Computations **1** (1984), no. 1, 77–88.
- [DHLM05] M. Desbrun, A. N. Hirani, M. Leok, and J. E. Marsden, *Discrete exterior calculus*, arXiv:math.DG/0508341.
- [dVCS07] L. Beirão da Veiga, D. Chapelle, and I. Paris Suarez, *Towards improving the MITC6 triangular shell element*, Computers & Structures **85** (2007), no. 21–22, 1589 – 1610.
- [Dvo95] E. N. Dvorkin, *Nonlinear analysis of shells using the MITC formulation*, Arch. of Comp. Meth. in Eng. **2** (1995), no. 2, 1–50.
- [Fal08] R. S. Falk, *Finite elements for the Reissner–Mindlin plate*, Mixed Finite Elements, Compatibility Conditions, and Applications (2008), 195–232.
- [FJM02] G. Friesecke, R. D. James, and S. Müller, *A theorem on geometric rigidity and the derivation of nonlinear plate theory from three-dimensional elasticity*, Comm. Pure Appl. Math. **55** (2002), no. 11, 1461–1506.
- [FJM06] ———, *A hierarchy of plate models derived from nonlinear elasticity by Γ -convergence*, Arch. Ration. Mech. Anal. **180** (2006), no. 2, 183–236.
- [FOZ95] F. G. Flores, E. Oñate, and F. Zarate, *New assumed strain triangles for nonlinear shell analysis*, Comput. Mech. **17** (1995), no. 1-2, 107–114.
- [GGRZ06] E. Grinspun, Y. Gingold, J. Reisman, and D. Zorin, *Computing discrete shape operators on general meshes*, EUROGRAPHICS 2006 **25** (2006), no. 3.
- [GHDS03] E. Grinspun, A. N. Hirani, M. Desbrun, and P. Schröder, *Discrete shells*, Siggraph/Eurographics Sympos. Comput. Anim., 2003, pp. 62–67.

- [GKN93] A.L. Goldenveizer, J.D. Kaplunov, and E.V. Nolde, *On Timoshenko-Reissner type theories of plates and shells*, Int. Jour. of Solids and Structures **30** (1993), no. 5, 675 – 694.
- [GSH⁺04] Y. Gingold, A. Secord, J.Y. Han, E. Grinspun, and D.Zorin, *A discrete model for inelastic deformation of thin shells*, 2004, Preprint.
- [GT07] M. Gärdsback and G. Tibert, *A comparison of rotation-free triangular shell elements for unstructured meshes*, Comput. Meth. Appl. Mech. Engrg. **196** (2007), 5001 – 5015.
- [HCB05] T. J. R. Hughes, J. A. Cottrell, and Y. Bazilevs, *Isogeometric analysis: CAD, finite elements, NURBS, exact geometry and mesh refinement*, Comput. Meth. Appl. Mech. Engrg. **194** (2005), no. 39-41, 4135–4195.
- [HCP11] A. Huerta, E. Casoni, and J. Peraire, *A simple shock-capturing technique for high-order discontinuous Galerkin methods*, Int. Jour. for Num. Meth. in Fluids (2011), n/a–n/a.
- [HPW05] K. Hildebrandt, K. Polthier, and M. Wardetzky, *On the convergence of metric and geometric properties of polyhedral surfaces*, GEOMETRIAE DEDICATA **123** (2005), 89–112.
- [JLLO09] P. Jung, S. Leyendecker, J. Linn, and M. Ortiz, *Discrete lagrangian mechanics and geometrically exact Cosserat rods*, Tech. Report 160, Mathematik, 2009.
- [KBLW09] J. Kiendl, K.-U. Bletzinger, J. Linhard, and R. Wüchner, *Isogeometric shell analysis with Kirchhoff-Love elements*, Comput. Meth. Appl. Mech. Engrg. **198** (2009), no. 49-52, 3902–3914.
- [Koi71] W.T. Koiter, *On the mathematical foundation of shell theory*, Act. Con Int. Math. (1971), no. 3, 123–130.
- [LB04] P.-S. Lee and K.-J. Bathe, *Development of MITC isotropic triangular shell finite elements*, Computers & Structures **82** (2004), no. 11-12, 945 – 962.
- [LMW04] M. Leok, J. E. Marsden, and A. Weinstein, *A discrete theory of connections on principal bundles*, (preprint, [arXiv:math.DG/0508338](https://arxiv.org/abs/math/0508338)), 2004.
- [LNB07] P.-S. Lee, H.-C. Noh, and K.-J. Bathe, *Insight into 3-node triangular shell finite elements: the effects of element isotropy and mesh patterns*, Computers & Structures **85** (2007), no. 7-8, 404 – 418.
- [Lov04] C. Lovadina, *A low-order nonconforming finite element for Reissner–Mindlin plates*, SIAM J. Numer. Anal. **42** (2004).

- [LR96] H. Le Dret and A. Raoult, *The membrane shell model in nonlinear elasticity: A variational asymptotic derivation*, Journal of Nonlinear Science **6** (1996), no. 1, 59–84.
- [LR00] ———, *Variational convergence for nonlinear shell models with directors and related semicontinuity and relaxation results*, Arch. Ration. Mech. Anal. **154** (2000), no. 2, 101–134.
- [Mar08] C. Mardare, *On the derivation of nonlinear shell models from three-dimensional elasticity*, Rev. Roumaine Math. Pures Appl. **53** (2008), no. 5-6, 499–522.
- [MDM⁺02] M. Müller, J. Dorsey, L. McMillan, R. Jagnow, and B. Cutler, *Stable real-time deformations*, Proceedings of the 2002 ACM SIGGRAPH/Eurographics symposium on Computer animation (New York, NY, USA), SCA '02, ACM, 2002, pp. 49–54.
- [MH90] D. S. Malkus and T. J. R. Hughes, *Mixed finite element methods—reduced and selective integration techniques: a unification of concepts*, Comput. Meth. Appl. Mech. Engrg. (1990), 63–81.
- [Mor71] L.S.D. Morley, *On the constant moment plate bending element*, Journal of Strain Analysis. **6** (1971), no. 10.
- [MT04] J.-M. Morvan and B. Thibert, *Approximation of the normal vector field and the area of a smooth surface*, Discrete Comput. Geom. **32** (2004), no. 3, 383–400.
- [MTPS08] J. Mezger, B. Thomaszewski, S. Pabst, and W. Straßer, *Interactive Physically-based Shape Editing*, Computer Aided Geometric Design, 10 2008.
- [MW00] D. S. Meek and D. J. Walton, *On surface normal and gaussian curvature approximations given data sampled from a smooth surface*, Comput. Aided Geom. Des. **17** (2000), no. 6, 521–543.
- [NJ09] P. Neff and J. Jeong, *A new paradigm: the linear isotropic Cosserat model with conformally invariant curvature energy*, ZAMM - Zeitschrift für Angewandte Mathematik und Mechanik **89** (2009), no. 2, 107–122.
- [Nov03] S. P. Novikov, *Discrete connections on the triangulated manifolds and difference linear equations*, 2003, (preprint, [arXiv:math-ph/0303035v2](https://arxiv.org/abs/math-ph/0303035v2)).
- [NTRNXB08] N. Nguyen-Thanh, T. Rabczuk, H. Nguyen-Xuan, and S. P.A. Bordas, *A smoothed finite element method for shell analysis*, Comput. Meth. Appl. Mech. Engrg. **198** (2008), no. 2, 165–177.
- [Ogd97] R.W. Ogden, *Non-linear elastic deformations*, Dover books on physics, Dover Publications, 1997.

- [OZF94] E. Oñate, F. Zarate, and F. Flores, *A simple triangular element for thick and thin plate and shell analysis*, Int. Jour. for Num. Meth. in Eng. **37** (1994), 2569–2582.
- [OZST92] E. Oñate, O.C. Zienkiewicz, B. Suarez, and R.L. Taylor, *A general methodology for deriving shear constrained Reissner-Mindlin plate elements*, Int. Jour. for Num. Meth. in Eng. **33** (1992), 345–367.
- [PB92] P. Peisker and D. Braess, *Uniform convergence of mixed-interpolated elements for Reissner-Mindlin plates*, RAIRO - Modélisation mathématique et analyse numérique et **26** (1992), no. 5, 557–574.
- [Pet06] P. Petersen, *Riemannian geometry*, Graduate Texts in Mathematics, Springer, 2006.
- [PPGT06] R. Paroni, P. Podio-Guidugli, and G. Tomassetti, *The Reissner-Mindlin plate theory via Γ -convergence*, C.R. Acad. Sci. Paris (2006), no. 343, 437–440.
- [RGZ07] J. Reisman, E. Grinspun, and D. Zorin, *A note on the triangle-centered quadratic interpolation discretization of the shape operator*, 2007, Preprint.
- [RWRA09] S. S. Ramesh, C.M. Wang, J.N. Reddy, and K.K. Ang, *A higher-order plate element for accurate prediction of interlaminar stresses in laminated composite plates*, Composite Structures **91** (2009), no. 3, 337 – 357.
- [SF89] J.C. Simo and D.D. Fox, *On a stress resultant geometrically exact shell model – Part I: Formulation and optimal parametrization*, Comput. Meth. Appl. Mech. Engrg. **72** (1989), 267–304.
- [SLL04] K. Y. Sze, X. H. Liu, and S. H. Lo, *Popular benchmark problems for geometric nonlinear analysis of shells*, Finite Elements in Analysis and Design **40** (2004), 1551–1569.
- [Spi98] M. Spivak, *Calculus on manifolds*, Perseus Books, 1998.
- [SRR69] S. Srinivas, A. K. Rao, and C. V. Joga Rao, *Flexure of simply supported thick homogeneous and laminated rectangular plates*, ZAMM - Zeitschrift für Angewandte Mathematik und Mechanik **49** (1969), no. 8, 449–458.
- [Ste81] J. Steiner, *Ueber parallele Flächen.*, Jacob Steiner’s gesammelte Werke (Karl Weierstrass, ed.), 1881, pp. 173–176.
- [Sur94] M. Suri, *Analytic and computational assessment of locking in the hp finite element method*, Comput. Meth. Appl. Mech. Engrg. **133** (1994), 347–371.

- [TWK59] S. Timoshenko and S. Woinowsky-Krieger, *Theory of plates and shells*, McGraw-Hill classic textbook reissue series, McGraw-Hill, 1959.
- [VGJS11] A. V. Vuong, C. Giannelli, B. Jüttler, and B. Simeon, *A hierarchical approach to adaptive local refinement in isogeometric analysis*, *Comput. Meth. Appl. Mech. Engrg.* **200** (2011), 3554–3567.
- [vKB96] F. van Keulen and J. Booij, *Refined consistent formulation of a curved triangular finite rotation shell element*, *Int. Jour. for Num. Meth. in Eng.* **39** (1996), 2803–2820.
- [Whi57] H. Whitney, *Geometric Integration Theory*, Princeton Univ. Press, 1957.
- [WRK⁺10] M. Wicke, D.l Ritchie, B. M. Klingner, S. Burke, J. R. Shewchuk, and J. F. O’Brien, *Dynamic local remeshing for elastoplastic simulation*, *ACM Trans. Graph.* **29** (2010), 49:1–49:11.
- [YSMK00] H. T. Y. Yang, S. Saigal, A. Masud, and R. K. Kapania, *A survey of recent shell finite elements*, *Int. Jour. for Num. Meth. in Eng.* **47** (2000), no. 1-3, 101–127.
- [Zor05] D. Zorin, *Curvature-based energy for simulation and variational modeling*, *Proc. of the Int. Conference on Shape Modeling and Applications SMI’05 (Los Alamitos, CA, USA)*, IEEE Computer Society, 2005, pp. 198–206.
- [ZS00] Denis Zorin and Peter Schröder, *Subdivision for Modeling and Animation*, Tech. report, SIGGRAPH 2000, 2000, Course Notes.
- [ZT00] O. C. Zienkiewicz and R. L. Taylor, *The finite element method. Vol. 2*, 5th ed., Butterworth-Heinemann, Oxford, 2000, Solid mechanics.

Curriculum vitae

Personal

Name Clarisse Ablavi Weischedel
Date of birth 07.01.1986
Place of birth Lomé (Togo)
Place of residence Göttingen

Academic

since March 2012 **Research Assistant**
Georg-August-Universität Göttingen
Institute for Numerical and Applied Mathematics
Group: Discrete Differential Geometry
Advisor: Prof. Dr. Max Wardetzky

2009 - 2012 **Ph.D. scholarship**
Fraunhofer Institute for Industrial Mathematics
Kaiserslautern
Department: Mathematical Methods for Dynamics and Durability

2008 **Diplom** (MSc equivalent) in **Mathematics** (minor in Philosophy)
Universität Hamburg
Topic: Compact Riemannian manifolds with
non-compact holonomy group
Advisor: Prof. Dr. Vicente Cortés Suárez

2003 **Baccalauréat français**, série S (scientifique)
Lycée français de Lomé (Togo), affiliated to
Académie de Nantes (France)